

Seconda Università degli Studi di Napoli

Dottorato di ricerca in Ingegneria Elettronica

Ciclo XXVI

Campi Elettromagnetici

SHARAD Data Inversion and Calibration over Mars

Ing. Luigi Castaldo

Coordinatore

Prof. Giovanni Leone

Tutori

Dott. Raffaele Solimene

Dott. Giovanni Alberti

ANNO ACCADEMICO 2012-2013



D^{III} SUN

Dipartimento di Ingegneria Industriale e dell'Informazione



PREFACE

The present PhD thesis is the description of part of the research activity done during the period of work at the Second University of Naples, mostly pursued at CO.RI.S.T.A. of Naples, Italy and during a short term internship at the Institute of Electronic Systems, in the Warsaw University of Technology, Poland. The decision to pursue the Ph.D. came out not as a natural process after the graduation, but from several other working and life experiences. It was a mature process which leads to understand the higher education for my scientific learning and interest's growth was also important for cultural and social education. I got a specialist education and moreover I got a more structured way of thinking in order to solve both theoretical and practical problems. The interaction with people from different country and culture, with different formation and opinion, made me understanding even more how it is important to appreciate and share the knowledge coming out from different experience. The possibility to cooperate as a SHARAD Science Team was a great advantage to have a closer connection with the instruments and specialists from different fields and environments. The present work is focused on the elaboration and interpretation of SHARAD data, radar sounder currently in orbit around Mars. This instrument has greatly contributed to explore Mars surface and sub-surface also in view of future human exploration of the planet. The research work done deals with the estimation of dielectric parameters of the soil and subsoil and with the detection and interpretation of subsurface morphologies in order to understand the formation of the Martian landscape.

ABSTRACT

In this work, aspects of electromagnetic vector wave propagation and scattering from Mars surface and subsurface are considered in relation to the investigation of Synthetic Aperture Sounder. The work is focused on the elaboration and interpretation of SHARAD data, the radar sounder currently in orbit around Mars on the spacecraft Mars Reconnaissance Orbiter. Cerberus Palus is a thoroughly studied region of Mars, characterized by evident platy textures that were interpreted either as evidence for a frozen sea close to Mars' equator or as being resultant of lava, mud or ice-flows coming from Cerberus Fossae through Athabasca Valles. Radargrams provided by radar sounder SHARAD clearly show the presence of subsurface layers in the area. By exploiting the great amount of available data, an accurate quantitative analysis, aimed to estimate electromagnetic properties of surface and subsurface layers, has been performed in terms of permittivity and attenuation. To this aim, an electromagnetic approach has been used, taking into account effects of scattering due to surface roughness, for avoiding overestimated results. This has been done by using theory of electromagnetic scattering from fractal surfaces and by estimating needed parameters from topographic data provided by Mars Orbiter Laser Altimeter (MOLA) which was one of five instruments on board the Mars Global Surveyor (MGS) spacecraft. Three distinct geologic formations have been analyzed, namely a part of Zephyria Planum, the Cerberus plains and the bedrock beneath the plains. The retrieved electromagnetic parameters have been also modeled as a mixture of volcanic rocks with either ice or air. A deep analysis of inversion has been extended to the whole Mars surface, by exploiting the full coverage of SHARAD data and by modelling the relationship between surface scattering and signal power received by the instrument.

Keywords: *Synthetic Aperture Sounder, Sharad, Mars, Inversion Scattering Models, Cerberus Palus, Mars mapping.*

RIASSUNTO

In questo lavoro, sono analizzati gli spetti della propagazione delle onde elettromagnetiche e dello scattering degli strati superficiali e sottosuperficiali di Marte, in relazione ad un Sounder ad Apertura Sintetica. Il lavoro si concentra sulla elaborazione e l'interpretazione dei dati di SHARAD, un radar sounder attualmente in orbita intorno a Marte a bordo del satellite Mars Reconnaissance Orbiter. Cerberus Palus è una regione studiata a fondo di Marte, caratterizzata da evidenti zone piane che sono state interpretate sia come prova di un mare ghiacciato vicino all'equatore di Marte che come il risultato di flussi di lava, fango o ghiaccio provenienti dalla Cerberus Fossae attraverso Athabasca Valles. I Radargrammi forniti dal radar sounder Sharad mostrano chiaramente la presenza di strati nel sottosuolo della zona considerata. Sfruttando la grande quantità di dati disponibili, è stato effettuato una analisi quantitativa accurata finalizzata per stimare le proprietà elettromagnetiche degli strati superficiali e sottosuperficiali, in termini di permittività e attenuazione. A questo scopo, è stato usato un approccio elettromagnetico, tenendo conto degli effetti di dispersione a causa di rugosità superficiale, onde evitare risultati sovrastimati. Questo è stato fatto utilizzando la teoria della diffusione elettromagnetica da superfici frattali e stimando i parametri necessari da dati topografici forniti dal Mars Orbiter Laser Altimeter (MOLA), che è stato uno dei cinque strumenti a bordo del satellite Mars Global Surveyor (MGS). Tre formazioni geologiche distinte sono state analizzate, e cioè una parte di Zephyria Planum, la pianura Cerberus e il substrato roccioso sottostante pianura. I parametri elettromagnetici recuperati sono stati modellati come mistura di rocce vulcaniche sia con ghiaccio che con aria. Un'analisi profonda di inversione è stata estesa a tutta la superficie di Marte, sfruttando la copertura completa dei dati SHARAD e modellando la relazione tra rugosità delle superfici e la potenza del segnale ricevuto dallo strumento.

Parole chiave: *Sounder ad Apertura Sintetica, Sharad, Marte, Modelli di inversion di scattering, Cerberus Palus, Mappe di Marte.*

CONTENTS

CHAPTER I: INTRODUCTION	1
I.1 HISTORY.....	2
I.2 MISSIONS.....	3
I.3 PLANET GEOLOGY.....	5
I.4 RECENT EXPLORATIONS.....	8
I.5 MRO MISSION.....	11
<i>I.5.1 Instruments on board.....</i>	<i>12</i>
I.6 PLANETARY RADAR SOUNDERS	14
CHAPTER II: SHARAD AND MOLA	17
II.1 SHARAD PLANETARY RADAR SOUNDER	17
<i>II.1.1 System Performances.....</i>	<i>23</i>
<i>II.1.2 SHARAD Operative and receiving phase.....</i>	<i>32</i>
<i>II.1.3 The SHARAD data.....</i>	<i>36</i>
<i>II.1.4 Level 1a data: Experiment Data Record (EDR).....</i>	<i>37</i>
<i>II.1.5 Level 1b data: Reduced Data Record (RDR).....</i>	<i>40</i>
II.2 MOLA	42
II.3 SHARAD DATA ACQUISITION.....	43
<i>II.3.1 Mola Data Product.....</i>	<i>45</i>
CHAPTER III: INVERSION MODELS OF CERBERUS PALUS.....	49
III.1 SCATTERING FORM NATURAL SURFACES: FRACTAL GEOMETRY	49
<i>III.1.1 The scattering.....</i>	<i>50</i>

III.2	CERBERUS PALUS	54
III.2.1	<i>Structure and Geology of the region</i>	55
III.3	SHARAD BACKSCATTERING	56
III.4	MATHEMATICAL MODEL	58
III.5	FRACTAL PARAMETER EVALUATION	64
III.6	INVERSION RESULTS	67
III.7	DISCUSSION OF RESULTS	77
III.8	6. CONCLUSIONS REGARDING CERBERUS PLAINS	82
CHAPTER IV:	MARS DATA MAPPING	85
IV.1	MAPPING: INTRODUCTION	85
IV.2	SHARAD DATA SIGNAL DESCRIPTION	87
IV.3	SHARAD DATA SIGNAL CORRECTION	89
IV.3.1	<i>Orbitographic phenomena</i>	89
IV.3.2	<i>Technical Issues</i>	89
IV.3.3	<i>Geometry</i>	90
IV.4	REFERENCE AREA	90
IV.5	CONSTANT EXTRACTION	92
IV.6	DATA CALIBRATION	94
IV.7	DISCUSSION RESULTS	95
IV.8	CONCLUSIONS RELATED TO THE OBTAINED MAPS	98
CHAPTER V:	SYNOPSIS AND OUTLOOK	101
V.1	TECHNOLOGICAL APPROACH	101
V.2	CERBERUS PALUS	102

V.3	MARS MAPPING PROCEDURE	104
V.4	FUTURE WORKS.....	105
V.5	SHORT FORM BIOGRAPHY LUIGI CASTALDO OCTOBER 2013	106
V.6	PUBLICATIONS	114
	BIBLIOGRAPHY	117

LIST OF FIGURES

FIGURE I-1 MARS PLANET RECONSTRUCTION IN WHITE THE EVIDENCE OF WATER ICE (PICTURE BY NASA)	1
FIGURE I-2 M.R.O. SATELLITE LAUNCH - AUG. 12, 2005 CAPE CANAVERAL FLORIDA (PICTURE BY NASA)	12
FIGURE II-1 SHARAD FLATTENABLE FOLDABLE TUBE (FFT) ANTENNA PACKAGE (PICTURE BY NASA)	20
FIGURE II-2 FIGURE II-3: THE SHARAD INSTRUMENT ON THE MARS RECONNAISSANCE ORBITER (PICTURE BY NASA)	20
FIGURE II-4: DOPPLER SHIFT OF A TARGET	21
FIGURE II-5 SHARAD PRINCIPLES OF OPERATION	23
FIGURE II-6 RANGE RESOLUTION FOR DIFFERENT SCENARIOS	24
FIGURE II-7 PERCENTAGE OF THE MARTIAN SURFACE FOR WHICH S FALL WITHIN PRESCRIBED RANGES.....	28
FIGURE II-8 PULSE LIMITED GEOMETRY VERTICAL VIEW.....	30
FIGURE II-9 PULSE LIMITED GEOMETRY TOP VIEW	30
FIGURE II-10: POSITIONING OF THE LISTENING WINDOW OF THE RADAR IN CASE OF PRF=700.28 Hz	35
FIGURE II-11 GROUND TRACK COVERAGE UP TO JUNE 2, 2012 (OBSERVATION 27431_01 – RM145_b)	44
FIGURE II-12 NORTH POLE GROUND TRACK COVERAGE (LEFT SIDE) AND SOUTH POLE GROUND TRACK COVERAGE (RIGHT SIDE).....	45
FIGURE II-13 MARS TOPOGRAPHY FROM MOLA [58]. TOPOGRAPHY IS SHOWN AS COLOR CODED ELEVATION DRAPED OVER SHADED RELIEF. THE PROJECTION AT MID-LATITUDES IS MERCATOR AND AT HIGH LATITUDES IS POLAR STEREOGRAPHIC. ON MARS APPROXIMATELY 1° IS 59 KM.	47
FIGURE III-1 LOCATION ON A MAP OF CERBERUS PALUS (144.5°- 152.5°E, 1°N - 8.9°N)	54
FIGURE III-2 A GENERAL STRATIGRAPHY OF THE AREA [67]	56
FIGURE III-3 LEVEL 1B IMAGE OF R 0207401 001 SS19 700 WHICH SHOWS THE FIRST LAYER BACKSCATTERING AND A SUBSURFACE LAYER.....	56

FIGURE III-4 ADOPTED ELECTROMAGNETIC MODEL FOR SHARAD DATA INVERSION 60

FIGURE III-5 MOLA DIGITAL ELEVATION MODEL (DEM) OF THE AREA UNDER STUDY. GREY BOXES REPRESENT ZONES WHERE FRACTAL PARAMETERS HAVE BEEN ESTIMATED (ZP IS ZEPHYRIA PLANUM, CP IS CERBERUS PALUS). . 64

FIGURE III-6 TYPICAL RADARGRAM OF THE AREA UNDER STUDY WITH A SCHEMATIC INDICATION OF CONSIDERED SURFACE AND SUBSURFACE INTERFACES. 67

FIGURE III-7 TYPICAL RADARGRAM IMAGE OF THE AREA UNDER STUDY (OBSERVATION NO. 589803): DOTTED RED LINE REPRESENTS THE DELAY COMPENSATED SUBSURFACE OVER CERBERUS PALUS AREA, WHITE BOXES ARE THE ZONES WITH DIFFERENT DEPTH WHERE ATTENUATION VALUE HAS BEEN ESTIMATED. ON THE LEFT SIDE ARE INDICATED GEOLOGICAL A AND B UNITS 68

FIGURE III-8 ZP AREA: (A) LOGARITHMIC VALUES OF POWER RATIO (SUBSURFACE/SURFACE) AS A FUNCTION OF SUBSURFACE INTERFACE DEPTH AND ITS LINEAR FITS (RED LINE CORRESPONDS TO NOMINAL FIT, BLACK LINES CORRESPOND TO VARIATION OF FITTING PARAMETERS). COLORS REPRESENT POWER RATIO VALUES DENSITY. POWER RATIO VALUES HAVE BEEN TAKEN FROM ZONE I AND ZONE II OF FIGURE III-5 BY USING THE PRODUCTS AND THE PARAMETRIC VALUES OF TABLE 2; (B) SUBSURFACE RELATIVE DIELECTRIC CONSTANT AS A FUNCTION OF THE GEOMETRIC FACTOR (SUBSURFACE/SURFACE). RED LINE HAS BEEN OBTAINED BY USING THE NOMINAL FITTING PARAMETER VALUE (THE C PARAMETER OF EQUATION (III-18)); BLACK LINES CORRESPOND TO VARIATION OF THE FITTING PARAMETER. STAR REPRESENTS THE NOMINAL VALUE OBTAINED FROM THE FITTING PROCEDURE (DIELECTRIC CONSTANT OF $\epsilon_{ss}=3.14$)..... 70

FIGURE III-9 CTX IMAGE P03_002081_1866_XN_06N206W OVER THE STUDY AREA. TRACE OF RADARGRAM 05898 (FIGURE III-6) IS SHOWN AS BLACK LINE. WITHIN THIS VERY FLAT AREA, WE CAN DISTINGUISH THE CONTACTS BETWEEN A AND B UNITS, THAT CAN BE ALSO OBSERVED ALONG THE RADARGRAM SHOWN IN FIGURE III-7 73

FIGURE III-10 CP AREA: (A) LOGARITHMIC VALUES OF POWER RATIO (SUBSURFACE/SURFACE) AS A FUNCTION OF SUBSURFACE INTERFACE DEPTH AND ITS LINEAR FITS (RED LINE CORRESPONDS TO NOMINAL FIT, BLACK LINES CORRESPOND TO $\pm 3 \sigma$ VARIATION OF FITTING PARAMETERS). COLORS REPRESENT POWER RATIO VALUES DENSITY. POWER RATIO VALUES HAVE BEEN EVALUATED BY USING THE PRODUCTS AND THE PARAMETRIC VALUES OF TABLE 5; (B) SUBSURFACE RELATIVE DIELECTRIC CONSTANT AS A FUNCTION OF THE GEOMETRIC FACTOR (SUBSURFACE/SURFACE). RED LINE HAS BEEN OBTAINED BY USING THE NOMINAL FITTING PARAMETER VALUE (THE C PARAMETER OF EQUATION (III-18)); BLACK LINES CORRESPOND TO $\pm 3 \sigma$ VARIATION OF THE FITTING PARAMETER. STAR REPRESENTS THE NOMINAL VALUE OBTAINED FROM THE FITTING PROCEDURE ($\epsilon_{ss} = 10.1$). 75

FIGURE III-11 RESULTS FROM POLDER-VAN SANTEN MODEL ON ZP AREA. PERMITTIVITY AND ATTENUATION VALUES FOR THE EFFECTIVE MATERIAL (HOSTING + INTRUSION) ARE THOSE REPORTED IN TABLE 6. VOLUME FRACTION OF INTRUSION MATERIAL AS A FUNCTION OF RELATIVE PERMITTIVITY (ON THE LEFT) AND LOSS TANGENT (ON THE RIGHT) OF HOSTING MATERIAL FOR ICE-FILLED (BLUE AREA) AND EMPTY PORES (GREEN AREA). WATER ICE HAS A RELATIVE PERMITTIVITY OF 3.1 AND A LOSS TANGENT OF 9×10^{-6} 79

FIGURE III-12 – RESULTS FROM POLDER-VAN SANTEN MODEL ON CP AREA. PERMITTIVITY AND ATTENUATION VALUES FOR THE EFFECTIVE MATERIAL (HOSTING + INTRUSION) ARE THOSE REPORTED IN TABLE 6. VOLUME FRACTION OF INTRUSION MATERIAL AS A FUNCTION OF RELATIVE PERMITTIVITY (ON THE LEFT) AND LOSS TANGENT (ON THE RIGHT) OF HOSTING MATERIAL FOR ICE-FILLED (BLUE AREA) AND EMPTY PORES (GREEN AREA). WATER ICE HAS A RELATIVE PERMITTIVITY OF 3.1 AND A LOSS TANGENT OF 9×10^{-6} 81

FIGURE IV-1 SURFACE POWER ECHO IN LINEAR SCALE EXTRACTED BY THE AUTOMATIC ROUTINE FROM THE OBSERVATION 0659501 001 SS19 700A, LOW-PASS FILTERED AND WEIGHTED WITH LINEAR LEAST SQUARES WITH A 2ND DEGREE POLYNOMIAL MODEL..... 88

FIGURE IV-2 MARS HURST CALCULATED ON MARS MOLA DATA 93

FIGURE IV-3 MARS TOPOTHESY CALCULATED ON MARS MOLA DATA 93

FIGURE IV-4 OCCURRENCES OF THE DIELECTRIC CONSTANT IN THE CALIBRATION AREA AFTER CALIBRATION 96

FIGURE IV-5 MAP OF MARS DIELECTRIC CONSTANT 97

FIGURE IV-6 MAP OF THE SHARAD RDR DATA SURFACE EXTRACTED POWER (LINEARLY SCALED)..... 97

FIGURE IV-7 MAP OF THE DIELECTRIC CONSTANT OF ARGYRE PLANITIA 98

LIST OF TABLES

TABLE 1 ENGINEERING PARAMETERS OF SHARAD.....	19
TABLE 2 INTEGRATION TIME FOR SELECTED VALUES OF H AND V_{sc}	26
TABLE 3 FRACTAL PARAMETER EVALUATION RESULTS	66
TABLE 4 ZEPHYRIA PLANUM AREA: PRODUCTS AND PARAMETERS USED FOR INVERSION PROCEDURE (SYMBOLS ARE THOSE INVOLVED IN EQUATIONS (III-21) AND (III-22)).....	71
TABLE 5 CERBERUS PALUS AREA: PRODUCTS AND PARAMETERS USED FOR INVERSION PROCEDURE (SYMBOLS ARE THOSE INVOLVED IN EQUATIONS (III-21) AND (III-22)).....	74
TABLE 6 SUMMARY OF INVERSION RESULTS	76

CHAPTER I: INTRODUCTION

In last four decades the knowledge of Mars through the data returned by scientific mission reached a level of details that was not foreseeable during the past. However, the evolution of this planet is still puzzling. It takes its name from the Roman's God of war, distant rusty orb in the sky, a source of ramble speculation for centuries. Could it be home for antagonist civilization? Mars is the wider studied planet of the Solar system; this intriguing planetary neighbor still activates us and could be a potential base for future colonization and keeping biological secrets. It can be the keys of our future and our past. If human beings will eve lives in another planet in the Solar System, this is the most likely candidate.

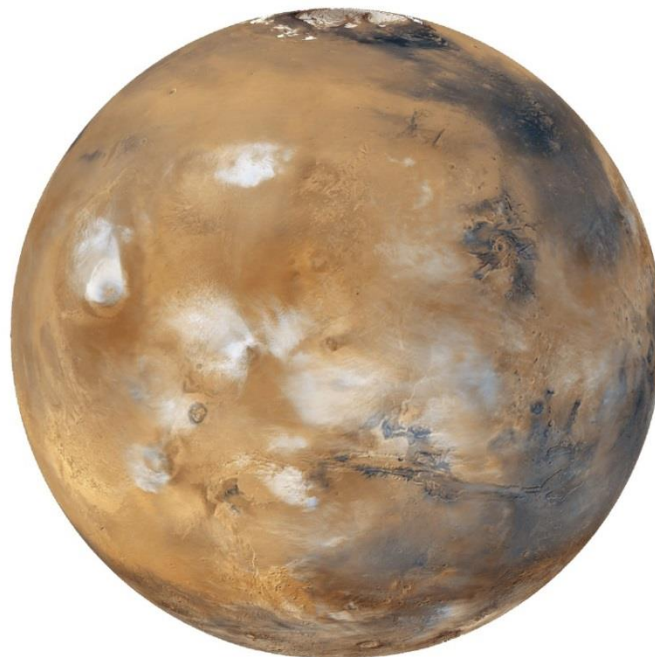


Figure I-1 MARS Planet reconstruction in white the evidence of water ice (picture by NASA)

I.1 History

The Romans associated this distant world with hostility and unrest because of his bloody like color and because of his distinctive movement in the sky. The Red Planet occasionally appears to be moving backwards crossing the sky, a behavior that confounded the observers for centuries, but in 1514 close studies of the planetary movements led Polish Astronomers Nicolò Copernicus to a revolutionary understanding of the Solar System. For much of the world history people thought to be in the center of the universe, so Copernicus founded that the explanation was the planet are orbiting around the Sun, so he could explain when Mars passes our orbits it appear that goes backwards in our sky. By the time of Copernicus's observation, Mars and the Earth has been passing each other in the respective orbits for some 4.5 billion years, time enough for the two planet to be evolved in two different worlds. The astronomers pointed the first ground-based telescopes towards Mars in 1610 despite the development of the technology the first blurred images became closer to the eyes of Earth observers. The history of these observations are marked by the oppositions of Mars, when the planet is closest to Earth and hence is most easily visible, which occur every couple of years. Even more notable are the perihelic oppositions of Mars which occurs approximately every 16 years, and are distinguished because Mars is close to perihelion making it even closer to Earth [1]. In 1877, (a perihelic opposition of Mars occurred on September 5) the director of Milano Observatory and Italian astronomer, Giovanni Schiaparelli published the first detailed map of Mars. It was the most detailed map of Mars ever published, he sketched the Martian surface and named its geological features becoming a standard reference in planetary cartography. Among the different features that he observed, there were the famous “canali”. The word, erroneously translated into English as “canals” instead of “channels”, led to widespread speculation over whether the

“canals” were constructed by intelligent beings [2]. Some of his observations were associated with real features: as an example, a light spot in the southern hemisphere, that he called Nix Olympia it is now known as Olympus Month and it is the highest pick known in the Solar System, a dorming Volcano that rises about 24 Km (15 miles) above the Martian Surface. He also noticed the existence of variable polar caps and the presence of the atmosphere, but supported a thesis of the existence of a hydraulic system of channels, that un-fortunately does not exist.

I.2 Missions

The first big step in the understanding of Mars was obtained when the space era started with the successful mission on the Moon. In 1964 the National Aeronautic and Space Administration NASA lunched a small exploration spacecraft for the Red Planet its name was Mariner 4. The spacecraft passed Mars at a distance of 9,868 kilometers recording and transmitting to Earth the first close-up picture of Mars. Mariner 4 had a television camera its mission was to flight pass Mars and send back pictures. At the time of Mariner 4, the detector that creates the image was a vacuum tube resembling a small CRT (cathode-ray tube), called a vidicon [3]. It could only make one pass. In 22 pictures, Mariner’s TV camera scanned about one percent of the Martian surface, the mission completed successfully the first fly-by of Mars It was sending back blurred pictures revealing ancient craters of varying size like the ones on the Moon, deserts apparently dead. It was a huge let down and big delusion. The enthusiasm for exploring Mars was only tempered. In 1969 NASA launched two twin spacecraft performing the first “dual mission” to Mars in order to have the guarantee that at least one was able to survive. The twin space-craft were Mariner 6 and 7. The two spacecraft were made to study the surface and

atmosphere of Mars during close flybys. In total they send back to Earth 198 photos covering about 20 percent of the planet's surface, showing the dark features long seen from Earth, but none of the canals observed by Schiaparelli. In 1971 NASA programmed again a "Dual Mission", but unfortunately Mariner 8 failure made it impossible. Mariner 9 mapped 70% of the Martian surface and studied the Martian atmosphere. Mariner 9 was engineered to orbit around Mars and became the first artificial satellite of the Red Planet. Mars was almost totally obscured by dust storms, which lasted for a month. After the storms Mariner 9 start to return spectacular images, it discovers the Tharsis region which homes to the largest volcanoes in the Solar System, centered near the equator in the western hemisphere, it includes the three enormous shield volcanoes Arsia Mons. The tallest volcano on the planet Olympus Mounts which is located off the western edge of the plateau. Mariner 9 discovered that on Eastern part of Mars a Grand Canyon stretching 4.800 kilometers across its surface, roughly parallel to the equator called "Valleys Marineris" in honor of the mission. The mission provided the about 100 percent of the planet's surface coverage from pictures and made the first close-up photographs of the Martian natural satellites: Deimos and Phobos. In 1975 NASA decided to launch two spacecraft, Viking 1 and Viking 2, each one consisting of an orbiter and a lander. The primary mission goals were to gather high resolution images of the Martian surface, characterize the structure and composition of the atmosphere and surface, and search for evidence of life. Viking 1 was launched on August 20, 1975. The landing component was equipped with robotic test instruments. It reached the Mars surface On July 20, 1976 at Chryse Planitia. Viking 2 was launched on September 9, 1975 and entered Mars orbit on August 7, 1976. The Viking 2 Lander touched down at Utopia Planitia on September 3, 1976. The two landers where exactly the same the only difference was the area of Landing. Viking 1 near the equator and Viking 2 far enough to the Nord to see frost in

winter both carried out the same experiments, and analyzed soil samples without significant results for life. Mars looked like a cold, dry, dead, place. High above the Martian surface the Viking orbiters managed to capture a mystifying image, while flying over a region of Mars called Sidonia the orbiter snapped an image of a land formation under cross lining, startlingly the formation resample a human face and as a joke NASA scientists show the photo to the press remarking about the face they founded on Mars. Under more even light condition the Martian formation doesn't look like a face at all, just a jumble of hills. With no divinity evidence of biology resulting from the Viking experiments interest of returning to the Red Planet quieted for several years.

I.3 Planet Geology

Mars appeared after this intense period of investigation characterized by an extended crustal dichotomy. The problem of Martian dichotomy was not solved in that period, but only posed. The Martian dichotomy is a global feature separating the cratered southern highlands and smooth northern lowlands. Parts of the boundary are defined by steep slopes with elevation differences of 2-6 km. Older theories foreseen the presence of a giant impact [4], or impacts. Arguments against are that the geology of the northern lowlands (Vasteras Borealis) is not consistent with a one impact hypothesis [5]. Moreover, the lowlands are not radial in shape [6], and there is no evidence of a crater rim. To achieve this results was needed the use of laser altimeter, that permitted to define the Martian topography. The Mars Orbiter Laser Altimeter (MOLA), an instrument on the Mars Global Surveyor spacecraft, has measured the topography, surface roughness, and 1.064-m reflectivity of Mars and the heights of volatile and dust clouds [7]. Another possible explanation was that the northern plains were generated by the erosion of an ancient shallow ocean.

Topographic profiles across the Mars dichotomy are not consistent with ancient coast [8]. Possible shoreline slopes are not orientated in the correct direction. Therefore these shorelines were most likely created by compressive tectonic stress. The differences between the Northern and Southern hemisphere's can be interpreted using analogues to Earth's plate tectonics. This could be the Tharsis origin. Therefore, the interpretation of this dichotomy is related to the thermal history of the planet. The Northern Hemisphere is also characterized by an extended volcanism, by the sign of a past extended tectonic activity, which was generating the largest rift in the solar System named "Valles Marineris". The extended volcanism produced large volcanoes, arranged in sequences. The volcanic features on Mars are very similar in shape, to those found on Earth, but their dimension is incomparable. Martian volcanism extended for a large timespan and the volcanoes were generated on terrains of variable ages. Numerous volcanic landforms can be found in the older cratered highlands and in the younger volcanic plains surrounding them. However, the most impressive volcanic landforms are associated with the extensive, hotspot-related up-lifts of Tharsis and Elysium plateaus. The large scale of the Tharsis shield volcanoes suggests that they formed from massive eruptions of fluid basalt over prolonged periods of time. The largest volcano on Mars is called Olympus Mons of relief from the summit to the plains surrounding it abrupt basalt scarp, it is one of the four giant shield volcanoes associated with Tharsis uplifted region. Other smaller volcanoes are Tholi and Peterae characterized by smaller volcanic vents. Moreover there is Tholus volcano, which is an isolated mountain with a central crater and Patera volcano, dominated by an irregular caldera with gentle slopes. The formation of large volcanic edifices has produced also a large tectonic activity. This was probably produced by mantle processes such as solid state mantle convection and gravity and topography can explain the observing distribution and strain of radial and concentric tectonic features [9]. The Tharsis

load appears to have produced a flexural moat around it, which shows up most dramatically as a negative gravity ring. Valles Marineris underwent a complex evolution, due to erosion processes. The Valles Marineris walls in the Tharsis region of Mars have a relief up to 11 km in the central parts of a 4000 km long system of troughs that lie just south of the Martian equator. The present configuration of the Valles Marineris walls has been attributed to erosional scarp retreat [10] and has been recognized two major types of walls [11]: spur and gully morphology, landslide scars, and small-scale talus slopes. Gullying probably implies some kind of vertical erosion and longitudinal waste transport by fluids or viscous interstitial material, probably ice [10], related to the widening of the Central Valles Marineris troughs during the late Hesperian [11], and to the emplacement of interior layered deposits. The relative age of different parts of the Martian surface was estimated through crater counting, as older surfaces have a higher crater density. Three broad epochs have been identified in the planet's geologic timescale, which were named after places on Mars that belong to those time periods. The precise timing of these periods is not known because there are several competing models describing the rate of meteor fall on Mars [12], so the dates are approximate. From oldest to youngest, these periods are the Noachian epoch (named after Noachis Terra), in which the oldest extant surfaces of Mars formed between 4.6 and 3.5 billion years ago; the Hesperian epoch (named after Hesperia Planum), marked by the formation of extensive lava plains 3.5 to 1.8 billion years ago; and the Amazonian epoch (named after Amazonis Planitia), from 1.8 billion years ago to present. The North Polar Caps are unquestionably the first planetary features visible during an approach to Mars through space, they are made of two permanent polar ice. During a pole's winter, it is called dry and frozen Carbon Dioxide, the atmosphere is very thin, it is all Carbon dioxide, it condensed in thick ice slabs of CO₂, it lies in continuous darkness, chilling the surface and causing 25-30% of the atmosphere to condense out [13]. The frozen

CO₂ during the exposure to the Sun light sublimates arising winds that sweep the poles faster to about 400 km/h transporting a large amount of dust and vapors, rising to large cirrus clouds. The polar Caps present spiral troughs which can be originated by solar heating and sublimation of ice [14]. Viking Orbiters caused a revolution in our ideas about water on Mars by discovering many geological forms that are typically formed from large amounts of water [1]. Mars may have had conditions for retaining a large amount of liquid water to flow across its surfaces. The images show that floods of water broke through dams, carved deep valleys, eroded grooves into bedrock, and traveled thousands of kilometers, the amount of water involved was almost unthinkable it estimates for some channel flows run to ten thousand times the flow of the Mississippi River [15](Carr 1996). Mars lost part of its atmosphere by impact erosion and hydrodynamic escape [15]. Mars today it is wrapped in a thin atmosphere formed of 1.6% argon, 3% nitrogen, 95% carbon dioxide [16]. The pressure on the surface varies from around 30 Pa on Olympus Mons's peak to over 1,155 Pa in the depths of Hellas Planitia, with a mean surface level pressure of 600 Pa, compared to Earth's sea level average of 101.3 KPa [1].

I.4 Recent Explorations

The Mars Global Surveyor (MGS) was and delivered in 1996 by NASA's Jet Propulsion Laboratory; in 1997 the spacecraft reached Mars and was operating until November 2006. One gully on a crater wall that was imaged in 2001 was found to have filled with light-colored material when it was re-imaged in 2005. A similar new light-colored deposit appears in a 2004 image of crater gullies previously imaged in 1999. The discover that liquid water episodically flows over the surface of the planet even today, through release from subterranean reservoirs along sun facing scarps and cliffs was one very important discover for

the mission[17]. MGS also detected patches of residual magnetization in the Martian crust [18]; implying Mars once had a magnetic field similar to the Earth today which is shielding from the solar wind. Without such shielding the radiative environment at the surface of the Earth would be too hard for life. MGS find in Eberswalde crater a fossilized and exhumed delta, which was formed most likely by the flow of water from the past [19]. Following to MGS, Mars Odyssey was launched on April 7, 2001, and arrived at Mars on October 24, 2001. This mission was made to search for evidence of past or present water and volcanic activity, it was equipped with gamma ray spectrometer which found the upper layers of Martian soil poleward of 55° of latitude contain up to 50% water ice by weight [20]. The sensor could not analyze deep in the surface and was not possible to state how deep could be the ice fills, total amount of water could be buried in the soil can be equivalent to a global layer 0.5 to 1.5 km deep[20]. On June 2nd 2003 the European Space Agency (ESA) launched its first mission to Mars: Mars Express. It consists of two parts the Mars Express Orbiter and a lander called the Beagle 2, designed to perform exobiology and geochemistry research. The Orbiter was successfully performing scientific measurements since early 2004, while the lander failed. Mars Express Orbiter was performing high resolution imaging and mineralogical mapping of the surface, radar sounding of the subsurface structure, precise determination of the atmospheric circulation and composition, and study of the interaction of the atmosphere with the interplanetary medium. The OMEGA spectrometer on board Mars Express achieved the first direct identification and mapping of both carbon dioxide and water ice in the Martian high southern latitudes, which since the early mapping observation of the permanent ice caps on the Martian poles, the southern cap was thought to be constituted of carbon dioxide ice, it was showing that this south polar cap contains perennial water ice in extended areas [21]. The MARSIS subsurface sounding radar on Mars Express could penetrate to depths of more

than 3.7 kilometers. It was found from the radar echoes that a composition of nearly pure water ice down to the bottom of the deposits, as MARSIS was able to map the thickness of the layered deposits over the entire south polar area [22]. Perhaps the most important discovery made by Mars Express is the detection of methane in the atmosphere by the PFS spectrometer [23]. There are only a few processes thought to be able to produce methane on Mars. Volcanism is one possibility, but there has been no detection of ongoing volcanic activity on Mars. Another potential source could be a reaction of olivine rock with groundwater and subsurface heat (serpentinization), but it is unclear if the necessary temperatures can be reached in the Martian subsurface. The third possibility is subterranean microbial life. The determination of the origin of methane has become the new key driver of scientific exploration, ESA's ExoMars (whose launch is planned for 2018) will carry instruments to detect and analyze Martian methane [1]. Briefly following Mars Express, NASA's twin Mars Exploration Rovers Spirit and Opportunity launched toward Mars on June 10 and July 7, 2003, landing on Mars January 4 and January 25, 2004. Spirit landing sites was at Gusev Crater, a possible former lake in a giant impact crater, the rover has not been communicating with Earth since March 22, 2010. Opportunity is still driving on the surface of Mars; the landing site was Meridiani Planum, where mineral deposits (hematite) suggest Mars had a water deposit in the past. On November 26, 2011 the Mars Science Laboratory (MSL), named Curiosity, a NASA rover was launched, it landed on Mars Aug. 6, 2012. Few hours after landing the rover have begun to send images from the surface. The duration of the mission is expected to at least one Martian year (about 2 Earth years) and the purpose will be to investigate the past and present ability of Mars to support life.

I.5 MRO Mission

Mars Reconnaissance Orbiter is a mission of NASA launched on August 12, 2005, (Figure I-2) and attained Martian orbit on March 10, 2006. In November 2006, after five months of aero braking, it entered its final orbit, the probe has reached the final orbit, which is almost perfectly circular at an altitude between 250 and 316 km and began its science activity, which still continues today. Among the NASA's strategies for the exploration of Mars MRO's scientific goal is to search for evidence that water persisted on the surface of Mars for a long period of time: while other Mars missions have shown that water flowed across the surface in Mars' history, it is still unclear whether water was ever around long enough to provide a habitat for life. MRO is an orbiter with high resolution instruments. The tools of the MRO allow NASA to choose the place with less risk and greater benefits from the scientific point of view. Another important goal for MRO is to provide support to lander missions in the form of high resolution observations of the surface for the detection of landing sites. The purpose of the MRO mission is global mapping of the surface (in visible and near infrared), investigation of the subsurface, identification of future landing sites for spacecraft and future communications and navigation support to Martian missions.



Figure I-2 M.R.O. Satellite launch - Aug. 12, 2005 Cape Canaveral Florida (picture by NASA)

I.5.1 Instruments on board

Six scientific instruments are included on the orbiter: three cameras, two spectrometers and radar are included on the orbiter including two complementary tools that will use data from the orbiter to provide scientific data. Three experimental technologies are inserted in the orbiter, so that it is used also to check the operation of new technical solutions.

I.5.1.1 Cameras

- The High Resolution Imaging Science Experiment (**HiRISE**) is a reflecting telescope of 0.5 m, the largest ever used in a space mission. It has a resolving power of 0.3 m height of 300 km. Can receive color images in the bands of red, green, and blue, and infrared. To facilitate the mapping and identification of possible

landing sites HiRISE produce stereoscopic images where the topographic information will be shown with a definition of 0.25 meters.

- The Context Imager (**CTX**) will provide monochromatic images 40 km wide with a resolution of 8 meters. The CTX is designed to work in conjunction with other image tools to provide the context of the maps that are detected by the other instruments.
- The Mars Color Imager (**MARCI**) split images of Mars in 5 bands of the visible and ultraviolet 2. MARCI will produce global maps of the planet to study the daily changes, seasonal and annual climate, the tool will also provide the information daily weather on the planet.

I.5.1.2 Spectrometers

- The Mars Climate Sounder (**MCS**) is a 9-channel spectrometer operating in the visible and infrared; a channel operates at 0.3-3 micrometers and the other eight operating between 12 and 50 micrometers. These channels have been chosen to measure temperature, pressure, water vapor and level of the powders. The instrument will observe the horizon of Mars by dividing it into vertical strips and analyzing them separately. Each strip is 5 km thick. These measurements will be combined to create daily maps of the Martian time. These maps show the variations of temperature, pressure, humidity and density.
- The Compact Reconnaissance Imaging Spectrometer for Mars (**CRISM**) instrument is a visible and near infrared (VNIR) spectrometer that is used to produce detailed maps of the surface mineralogy of Mars. It operates from 370 to 3920 nm, measures

the spectrum in 544 channels (each 6.55 nm wide), and has a resolution of 18 m at an altitude of 300 km (190 mi). CRISM is being used to identify minerals and chemicals indicative of the past or present existence of water on the surface of Mars. These materials include iron, oxides, phyllosilicates, and carbonates, which have characteristic patterns in their visible-infrared energy.

I.5.1.3 Radar

The Radar Shallow Subsurface Radar (**SHARAD**) was designed to study the interior of Martian subsurface; the detailed instrument description will be addressed in the next section.

I.5.1.4 Complementary tools

- Analysis of the gravitational field: changes in the gravitational field of Mars can be derived from the change in the speed of the MRO. The speed of the MRO will be determined using the Doppler shift of the radio signal that the probe will send to Earth.
- Analysis of the atmospheric density: sensitive accelerometers installed on board the Orbiter have been used to identify variations in the atmospheric density during the aerobreaking.

I.6 Planetary radar sounders

Radar sounders also called soil penetration radar (or GPR for Ground penetrating radar) are used in many areas such as glaciology, archeology, civil engineering and mining and oil exploration. These instruments emit signals electromagnetic at low frequencies of a few MHz to tens of GHz. In these frequency ranges, geophysical soils have the distinction of being more or less transparent, allowing the signal to penetrate deeply before being reflected by dielectric discontinuities

in the basement and so detect even imaged, objects and buried interfaces. It is a method of non-destructive survey of which the sensitivity depends on the dielectric environmental parameters surveyed and dimensioning the radar signal. The basic laws of electromagnetism are established by James Clerk Maxwell in 1864. From the early twentieth century, the electromagnetic waves are used as air carriers of information (TSF: wireless transmission), and as mine detection by the armed forces. Stern Weber, in the early 30s, operates for the first time their penetrating properties to estimate the thickness of an Austrian glacier [24], [25]. Strangely, this mode use is almost forgotten for twenty years, until a plane the U. S. Air Force crashed in Greenland in 1950 [26]. The pilot had misjudged altitude in interpreting the radar from the bottom of the glacier as that derived from the surface. The renewed interest for geophysical use of subsurface then brings NASA to install the instrument Alse (Apollo lunar sounder experiment) on the orbiter Apollo 17 mission to test this technology in an interplanetary environment [27]. Today, more than a thousand of different models are developed by GPR private companies [26]. They are used on the floor, or transported by air assets for missions of local or regional surveys. No GPR terrestrial applications were on board of a satellite platform till recent days, despite the advantages of geographic coverage areas. This is mainly due to the small percentage of interesting layers which reduces the profitability of the investment, or yet due to propagation problems related to land cover that which are not meet on other planets. Surprisingly, despite the growth of space exploration by unmanned spacecraft for nearly forty years, the radar Alse sounder has not led to other similar projects. Finally, motivated by the presence gradually certified of numerous glacial terrain periglacial and the possibility of aquifers is the Mars exploration that takes the idea of subsurface radar. The instrument Marsis (March advanced radar for subsurface and ionospheric sounding) [28] on board Mars Express (ESA European space agency), followed

closely by SHARAD (shallow radar) [29] on Mars reconnaissance orbiter (NASA), which signs the real advent of radar sounders planets. The fields of application of instruments planetary radars show very large [30]. In addition to imaging of interfaces in the basement, they can help constrain the composition and density of the surveyed soils.

CHAPTER II: SHARAD AND MOLA

SHARAD is a synthetic-aperture, orbital sounding radar, carried by NASA's Mars Reconnaissance Orbiter [29]. It works by transmitting a low-frequency radar pulse that is capable of penetrating below the surface, and is reflected by any dielectric discontinuity present in the subsurface. SHARAD is capable of a vertical resolution of 15 m (in free space) or less, depending on the dielectric constant of the material being sounded, operating at a central frequency of 20 MHz and transmitting a 10 MHz bandwidth. SHARAD data consist of radar echoes acquired along the ground track of the spacecraft during observations. Mars Orbiter Laser Altimeter (MOLA) was one of five instruments on board the Mars Global Surveyor (MGS) spacecraft, which operated in Mars orbit from September 1997 to November 2006. However, the MOLA instrument transmitted altimetry data only until June, 2001.

II.1 SHARAD Planetary radar sounder

SHARAD is the sounder radar placed on the MRO orbiter. It penetrates the surface and it is used for exploring the Martian subsurface. The radar Engineering Parameters are depicted in Table 1[31], [32]. SHARAD uses a Synthetic Aperture Technique in order to reduce the antenna footprint and increase the resolution, without the need of a larger antenna. Synthetic Aperture Radar (SAR) is a remote-sensing technology which uses the motion of the aircraft or spacecraft carrying the radar to synthesize an antenna aperture larger than the physical antenna to yield a high-spatial resolution imaging capability [33]. SAR systems can thus obtain high-spatial resolution geophysical measurements

of the Planets over wide surface areas, under all-weather, day/night conditions. The most obvious way to increase the resolution on SHARAD would have been reducing the antenna footprint by increasing its directivity. Due to the low operating carrier frequency of 20 MHz this way was not feasible while increasing the antenna gain would have required a much larger antenna with a complex deployment system. The antenna chosen for SHARAD is a dipole consisting of two fiberglass tubes, each arm 5 m long, a metal wire inside them represents the active part of the antenna. The antenna tubes, based on the fiber foldable tube (FFT) technology, were folded into five segments, the deployment relayed only on the material elasticity to extend to the desired position once released. Figure II-1 shows the folded antenna while Figure II-2 shows the SHARAD Instrument on the Mars Reconnaissance Orbiter

Table 1 Engineering parameters of SHARAD

Parameters	Value
Nominal orbit altitude	255-320 Km
Extended orbit altitude	230-407 Km
Topographic Margin	-20/+10 Km
Centre Frequency	20 MHz
Chirp Bandwidth(B)	10 MHz
Pulse width	85 microsecond
Receive window width	135 microsecond
PRF(nominal)	700.28 Hz
PRF(low orbit)	775.19 Hz
PRF(high orbit)	670.22 HZ
Power Standby	13W
Power Acquisition	28W

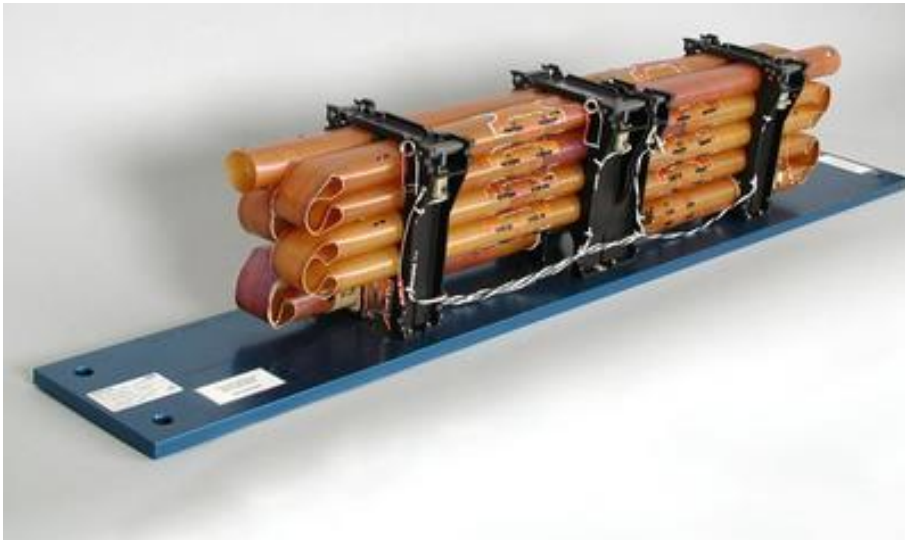


Figure II-1 SHARAD Flattenable Foldable Tube (FFT) antenna Package (picture by NASA)



Figure II-2 Figure II-3: The SHARAD Instrument on the Mars Reconnaissance Orbiter (picture by NASA)

The synthetic aperture principles note that the echo exhibits a Doppler frequency shift proportional to the transmit frequency and to the radial component of the relative velocity (for $\vartheta \ll 1$):

$$f_D = \frac{2v}{\lambda} \sin \vartheta \approx \frac{2v}{\lambda} \vartheta \quad \text{II-1}$$

The target which are at 90° to the spacecraft velocity has a zero Doppler shift ($\vartheta = 0$) while closing and receding targets have positive and negative Doppler shift, respectively. The Figure II-4 shows the Doppler shift of a target with the Doppler crossing the zero point at which the target is orthogonal to the spacecraft velocity vector.

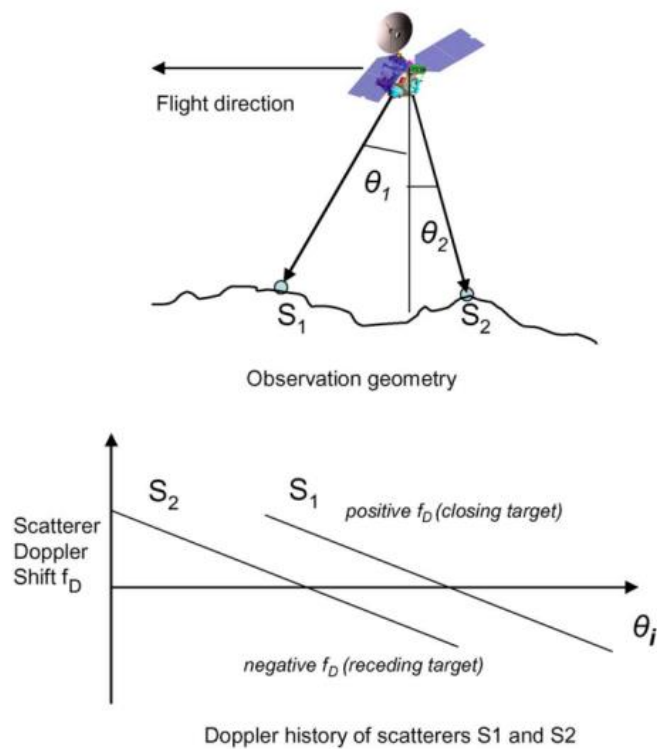


Figure II-4: Doppler shift of a target

The knowledge of the ideal Doppler history of each elementary scatterer history can be correlated with the real one to extract its azimuth position; this procedure significantly reduces the clutter echo energy, but does not eliminate the effect of surface echoes coming from the side of the track, which can mistakenly lead to the detection of fake subsurface echoes. One way to avoid to discriminate mistaken subsurface echoes it is to use an accurate surface simulator[34] which predicts the presence of surface clutter echoes of the , the corresponding fake subsurface echoes can be neglected because interpreted as clutter. A frequency modulated chirp has been adopted (signal in which the frequency varies linearly) to increase the resolution in depth. This technique provides the capability of using long pulses without compromise the range resolution, which is proportional to the pulse bandwidth. The processed signal-to-noise ratio (SNR) is proportional to the total pulse energy-long pulses then allow one to achieve the same detection capabilities with lower peak power [35],[36], [37]. From Table 1 is possible to see that SHARAD adopt a chirp bandwidth $B=10$ MHz corresponding to a time resolution of 100 ns equivalent to a range resolution of 15 m in case of free space and roundtrip [38], the resolution change with the velocity of propagation in the medium which is proportional to $\sqrt{\epsilon}$ of the medium. The range compression is performed on ground giving the possibility to employ different processing technique and to achieve in the future with new technique to different processing quality, the resulting sinc function has the main lobe amplitude equal to $1/B$ i.e. 6 dB without weighting in the compression process. The weighting function gives the control of range side lobes which is a very critical aspect of the radar sounders design because the weak subsurface echo can be hidden by the side lobes of the surface return. SHARAD ground processing uses a modified Hamming window that is capable of offering strong side lobe reduction at the expense of a main lobe widening.

II.1.1 System Performances

SHARAD is chirp radar for planetary missions, it has low power availability and the resolution is a function of the transmitted bandwidth. Following will be described the main parameters of the instruments.

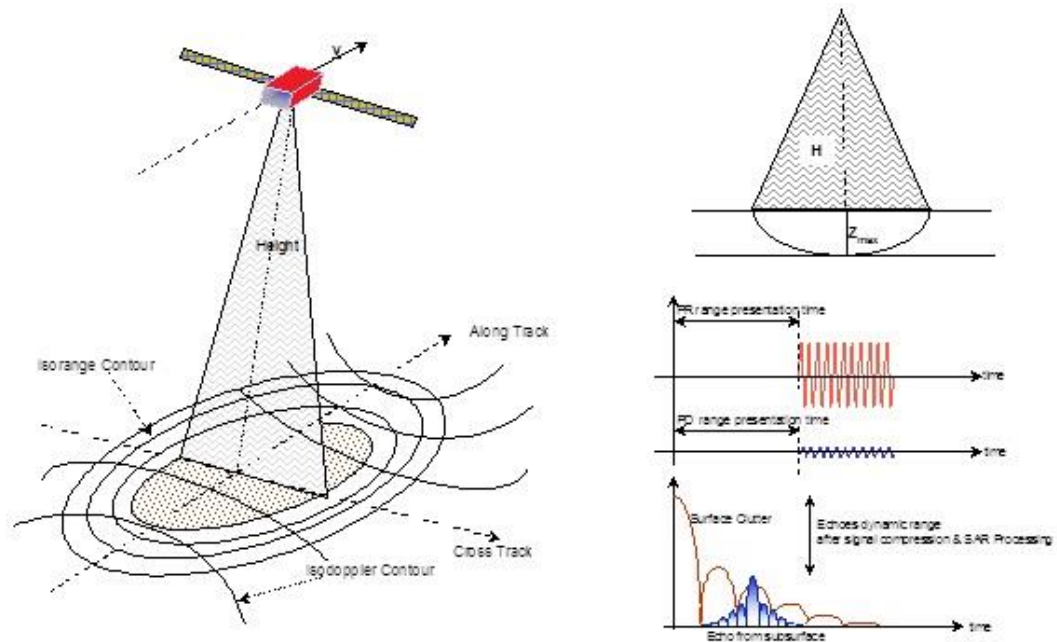


Figure II-5 SHARAD Principles of Operation

II.1.1.1 Vertical Resolution

In terrestrial dry rocks, values of dielectric constant ϵ usually range between 4 and 10, decreasing for increasing porosity; for water ice, $\epsilon \approx 3$, for CO₂ ice $\epsilon \approx 3$ [39].

$$\Delta z = c / (2 B \sqrt{\epsilon})$$

II-2

Where B is the transmitted bandwidth [40].

In order to achieve a vertical resolution of 10 m, a chirp bandwidth between 5 and 10 MHz is required, depending on the material.

Figure II-6 shows the features of Subsurface Range Resolution as function of the dielectric constant and bandwidth.

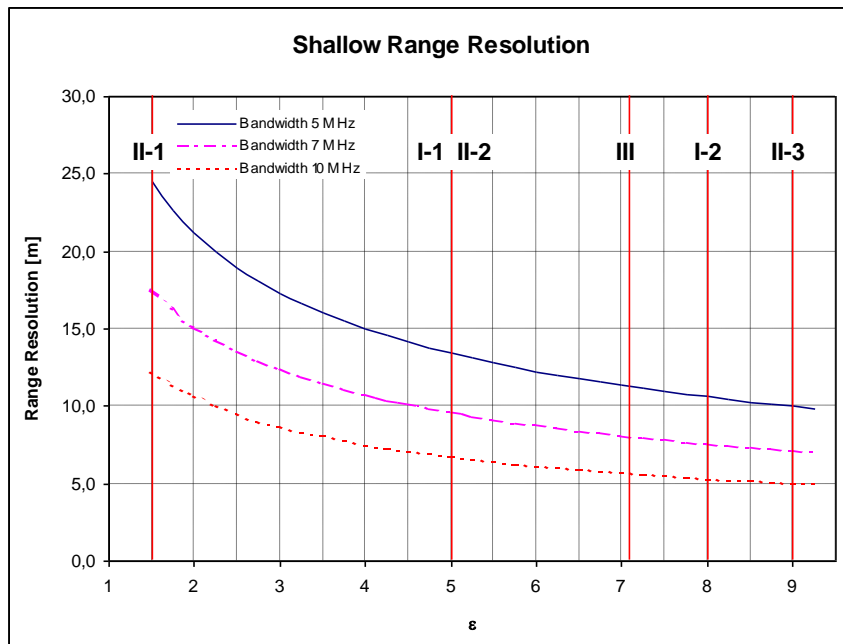


Figure II-6 Range Resolution for different scenarios

In the Figure II-6 except for the II-1 basaltic category, it can be seen that a bandwidth of 7 MHz provides resolutions better than 10 meters for all the other prospected scenarios.

II.1.1.2 Cross-Track Resolution

The SHARAD Pulse-limited resolution is of about 6 Km for 10 MHz bandwidth and can be calculated from the following equation [35], [36], [37]:

$$r=2\sqrt{(c H/B)} \tag{II-3}$$

where H is the spacecraft altitude and c the speed of light.

A higher frequency provides better resolution, but improvement is slow for the square root dependence. In case of back-scattering from specular surface, (R.M.S. rough surface height $< \lambda/4$ [39]), resolution, which depends on the carrier frequency, is given by [41]:

$$r = \sqrt{H \lambda / 2} \quad \text{II-4}$$

Which gives the Fresnel zone size, in case of SHARAD (II-4) gives $r \approx 1.5 \text{ Km}$

II.1.1.3 Along-Track Resolution

Horizontal resolution in the along-track direction can be improved by means of synthetic aperture processing, i.e. by the coherent summing of a number of echoes: resolution of an antenna having size of the length travelled by the spacecraft during the integration time (L_s) is achieved. The PRF has to be selected equal to echo Doppler bandwidth in order to adequately sample the response of the synthetic aperture [42]. Considering a Synthetic Length of 7.5 Km (indeed an integration time of about 2.2 seconds):

$$r_{az} = \frac{\lambda H}{2L_s} \approx 300\text{m} \quad \text{II-5}$$

An along-track resolution from 300 m to 1000 m is considered to be compliant with measurement requirements. To cope with the required resolution range the resulting coherent integration time can be calculated as in Table 2 for the minimum and maximum value of H and V_{sc} which is the speed of the spacecraft.

Table 2 integration time for selected values of H and V_{sc}

$1.6s < T_{int} < 2.9s$	$r_{az} = 300m$
$0.5s < T_{int} < 0.8s$	$r_{az} = 1000m$
$H_{min} \approx 230km$	$H_{max} \approx 400km$
$V_{sc\ min} \approx 3440m/s$	$V_{sc\ max} \approx 3360m/s$

For continuous coverage (no gaps) a suitable number of synthetic profiles shall be computed [43]:

$$N = T_{int} \cdot V_{sc} / r_{az}$$

32 (worst case).

II-6

In presence of specular surfaces Doppler processing may be applied on a limited number of echoes (about four); therefore also along track resolution will be limited by the Fresnel Zone size. Horizontal resolutions have been computed for a reference satellite altitude of 300 Km and a carrier frequency of 20 MHz

II.1.1.4 PRF selection

Regarding the PRF it is worth to note that its value cannot be uniquely selected on the basis of swath extent. Doppler bandwidth shall be correctly sampled. An incorrect PRF selection may entail performance degradation for values lower than the optimal or, if a two much higher value is selected, undesired increase of computational power demand on board and data volume to be transferred on ground. Synthetic aperture processing requires additionally that aliasing in the observed Doppler spectrum must be avoided. Supposing an isotropic antenna pattern in the along track direction, and considering the clutter formulation of the fractal equation[44] In the two special cases of H (the Hurst coefficient) equal to 1 to get the models of geometrical optics and $\frac{1}{2}$ the Hagfors model [45], as a references models for the subsurface and the surface clutter. It is possible to

determine the off nadir observation angle beyond which the off nadir surface clutter returns are 30 dB or more lower nadir surface echo:

$$\frac{\sigma_0(0)}{\sigma_0(\theta)} \Big|_{dB} = 15 \log_{10} \left(\cos^4(\theta) + \frac{\sin^2(\theta)}{4\pi^2 s_\lambda^4} \right) > 30 \quad \text{II-7}$$

with $H=1/2$ [45].

$$\frac{\sigma_0(0)}{\sigma_0(\theta)} \Big|_{dB} = 10 \log_{10} \left(\cos^4(\theta) e^{\frac{tg^2(\theta)}{2s^2(\lambda)}} \right) > 30 \quad \text{for} \quad \text{II-8}$$

with $H=1$ [46].

The Doppler bandwidth to be observed and thus sampled by the system will then be the one enveloped by twice the calculated angle [43]:

$$PRF \geq 2 \frac{2V_{sc}}{\lambda} \sin \theta \quad \text{II-9}$$

Where V_{sc} is the spacecraft velocity (3.4 Km/s) and λ is the center frequency wavelength of 15 m. Depending on the R.M.S. slope of the region under observation a proper value of the PRF is to be selected.

The Pulse Repetition Interval contains the radar returns (ambiguity rank = 0) if:

$$PRI \geq \frac{2 \cdot H}{c} + \frac{2 \cdot \sqrt{\epsilon} \cdot z}{c} \quad \text{II-10}$$

A 400 Km worst case altitude requires for the PRF to be less than 366 Hz for a penetration depth of 3 Km in a basaltic material having dielectric constant equal to 9. The following figure highlights that, in order to explore at least the 35% of the Martian surface, the Pulse Repetition Frequency has to be drawn by equations (II-7) and (II-8) for an r.m.s. slope of 0.06 (-1.22 on the X-axes of the graphic).

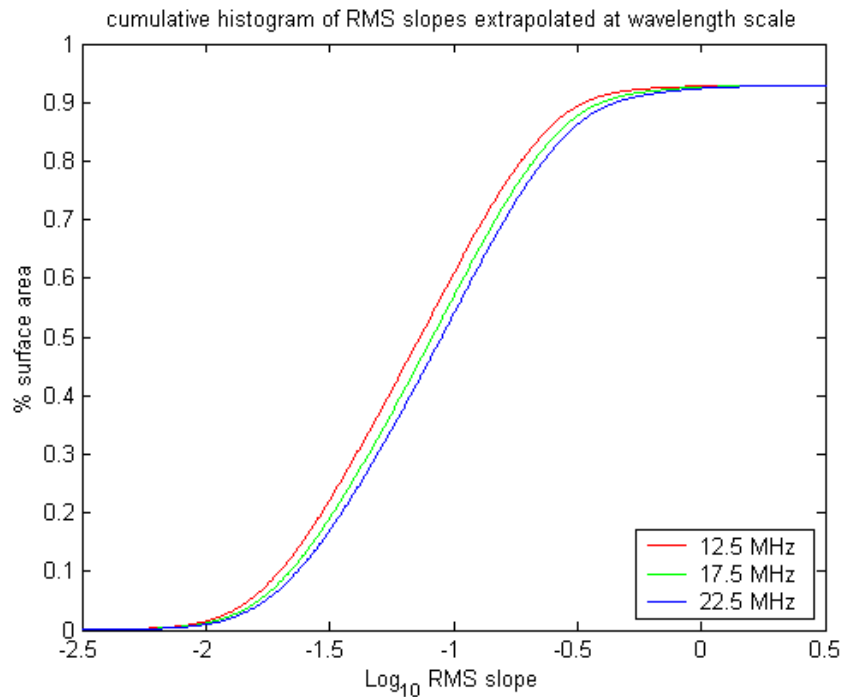


Figure II-7 Percentage of the Martian surface for which s fall within prescribed ranges

Therefore, according to the above considerations, a PRF of 200 Hz is to be selected. Otherwise, coverage of 28% of the Martian Surface requires a PRF of 150 Hz. The $\sigma_0(0)/\sigma_0(\theta)$ ratio has been computed also for Clutter Returns ranging between 20 dB and 45 dB and consequently the PRF have been achieved for the two models (Hagfors and Geometric Optic) and for different wavelength-scale r.m.s. slope.

II.1.1.5 Surface Clutter and Penetration Depth

Surface return echoes can be considered as surface clutter, because the subsurface discontinuity detection could be reduced from the surface back-scattering: thus the back-scattering coefficient can be related to the penetration depth z [43]:

$$\theta = \sqrt{\frac{2z\sqrt{\varepsilon}}{H}} \quad \text{II-11}$$

If surface and subsurface interfaces have the same roughness, the signal-to-clutter (S/C) ratio is:

$$\left. \frac{S}{C} \right|_{Hagfors} \cong R_{12}^2|_{dB} - \alpha_{dB/m} z - \Gamma_s|_{dB} + (1 - R_{01}^2)^2|_{dB} - 10 \log \left(\exp \left(- \frac{2\sqrt{\varepsilon} z}{2Hs^2(\lambda)} \right) \right) \quad \text{II-12}$$

With $H=1$ [46]

$$\left. \frac{S}{C} \right|_{G.O.} \cong R_{12}^2|_{dB} - \alpha_{dB/m} z - \Gamma_s|_{dB} + (1 - R_{01}^2)^2|_{dB} + 15 \log \left(1 + \frac{2\sqrt{\varepsilon} z}{4\pi^2 s^4(\lambda)H} \right) \quad \text{II-13}$$

With for $H=\frac{1}{2}$ [45].

The last term of the above equations can be considered as an improvement factor (IF) of the signal-to-clutter ratio, due to the decrease of the surface clutter for off-nadir observations: this term can be neglected in the worst case of very rough surfaces, no matter what the Hurst exponent is. The Clutter Cancellation improvement can be achieved by means of Doppler processing and, if need, by means of a second receiving channel. Figure II-8 and Figure II-9 presents the Pulse Limited Geometry applicable for the SHARAD Radar Sounder: in the Figure II-9 the circular crowns sliced by the Doppler processing are shown.

$$IF = \frac{R_{AZ} \sqrt{2H\Delta_Z}}{R_{AZ} \left(\sqrt{2Hn\Delta_Z} - \sqrt{2H(n-1)\Delta_Z} \right)} = \frac{1}{\sqrt{n} - \sqrt{n-1}} \quad \text{II-14}$$

$$\text{where } \Delta_Z = \frac{c}{2B\sqrt{\epsilon}} \text{ and } n = \frac{z}{\Delta_Z}$$

II.1.1.6 Surface Signal to Noise Ratio

A preliminary sizing of the radar sounder requires the evaluation of the link budget with sounding assumptions for its relevant parameters which will guide the design of the SHARAD instrument.

The single-look signal-to-noise ratio for non-coherent surface back-scattering is given [48]:

$$\frac{S}{N} = \frac{P_p G^2 \lambda^2 \sigma^0 A}{(4\pi)^3 R^4 K T F L} \tau N = \frac{P_p G^2 \lambda^3 \sigma^0}{(4\pi)^3 R^3 K T_G} \sqrt{2R\Delta} \frac{B_D \tau}{v_0} = \frac{P_p G^2 \lambda^3 \sigma^0 \sqrt{2\Delta} B_D \tau}{(4\pi)^3 R^{2.5} K T_G v_0} \quad \text{II-15}$$

$$\text{where } A \tau N = R_{AZ} 2\sqrt{2R\Delta} \tau \frac{L_S}{v_0} B_D = \frac{\lambda R}{v_0} \sqrt{2R\Delta} B_D \tau ,$$

To evaluate the above radar equation it is assumed that, 10 Watts peak power can be radiated by the antenna. A 10 MHz bandwidth for the radar pulse, entailing a 15 meters resolution in free space is used. An average altitude of 300 Km is considered as intermediate value between the extremes of the orbit which are 230 Km and 400 Km respectively. A 6% duty cycle is sustainable by the radar assuming roughly a 300 microseconds pulse and a Pulse Repetition Frequency of approximately 200 Hz. A synthetic aperture of 7.5 Km has been taken into account in the following budgets: it provides a Doppler processing gain of about 14 db. The noise term is due to Galactic and extra-galactic noise.

II.1.2 SHARAD Operative and receiving phase

SHARAD is designed to remain in a state of minimal power (Stand-By) with only the electronics functioning. During the modality operation SHARAD do not respond to commands direct the spacecraft, but continue to operate according to a sequence of commands previously loaded. All controls necessary for the operation of SHARAD are sent to the satellite and then passed to the radar, operating from the center of the ground that, during the upload, provides instructions to the instrument, by means of the OST (Operational Sequence Table), the PT (Parameter Table) and ODT (Orbital Data Table).The OST contains instructions on the radar operation to perform. After loading the OST and fired, and the instrument starts to work in Automatic reading the various entries in the file that was provided. Each line defines a single OST operating mode for the instrument, its duration and requirements necessary for the proper functioning. The PT contains all the operating parameters and engineering of SHARAD. Each parameter is identified by an identifier and associated a value.

The parameters contained in the PT can be associated with three categories main:

- Instrument Configuration Parameters, which are data, do not need to be update (i.e. constants like speed of light).
- Instrument Calibration Parameters, which after the first test are controlled by the operations center instruments so that no longer need any update (i.e. the parameters for the calculation of the closed-loop tracking).
- Instrument Operating Parameters, which must be updated before each execution of a measuring sequence.

The Orbital Data Table (ODT) contains the flight parameters of the satellite (refer to its orbit) required for the correct calculation of the position of the window reception of the received signals. These data therefore, that in actual fact concern the position and speed of the satellite are not generated on board but still sent by the command of land, and each includes two ODT values for Step (i.e. the time interval between two lines of the same ODT) and for the definition of the starting point of each line (Start ODT).

The expected ground penetration of the instrument is 1 km, but it depends on the nature of the soil. The along-track resolution for the synthetic aperture radar processing in ranges it varies from 300 to 1000 m. The nominal PRF (Pulse repetition frequency) is as shows table 1 about 700 Hz. It has been selected in a way that is at least twice the maximum expected Doppler shift of the echo with respect NY Quist criterion. The PRF is low enough to allocate all the expected radar-to-surface range variation due to the orbit altitude range plus topographic margin. The receive window is dynamically positioned according to priori knowledge of the spacecraft orbit and surface topography (programmed by the mission planning). Two extra PRFs are also selectable by command to allow operation during an extended mission, in which the spacecraft could be outside the orbit range designed for the primary mission. The halved PRF mode is available for both. It is also possible to operate the instrument with a halved PRF. This feature has been introduced to avoid possible range ambiguities that can occur from far off-nadir scatterers (around 40° –50° off-nadir angle) in the presence of particularly difficult topographies (at the expense of a 3-dB reduction of the SNR). The received signals are captured in a receive window of 135 μsec positioned for each PRF. This window duration takes into account:

- Length of the transmitted pulse: +85 μsec .
- Time window for the echo of the subsurface: +20 μsec .

- Error margin for reception window positioning: $+ / - 10 \mu\text{sec}$ –
- Delay margin due to the Mars ionosphere: $+5 \mu\text{sec}$.

The Figure II-10 shows the area for positioning the window reception when the PRF = 700.28 Hz. For the correct positioning of the receive window is necessary to know with spacecraft relative precision the distance spacecraft-surface, this is the tracking operation. SHARAD adopt two different techniques:

- The Open-loop tracking instead uses a priori knowledge of the distance of the satellite from the ground. When the radar using that type of function, using two different sets of data: one referring to the elevation profile along the predicted Martian ground-track of the satellite (profile obtained by the MOLA data present on M.G.S. Orbiter) and the other with the prediction of the orbit kept form the spacecraft. Those data are contained in the Parametric Table (PT) and in the Orbital Data Table (O.D.T).
- The Closed-loop tracking in which the information for the positioning of the listening window are generated independently by instrument through an algorithm for calculation of the tracking. The initial data for this algorithm are always provided by the ODT and the PT; through them it is calculated the round trip time of a pulse. The measurement is taken as reference while a filter controls the positioning of the listening window compared to that value.

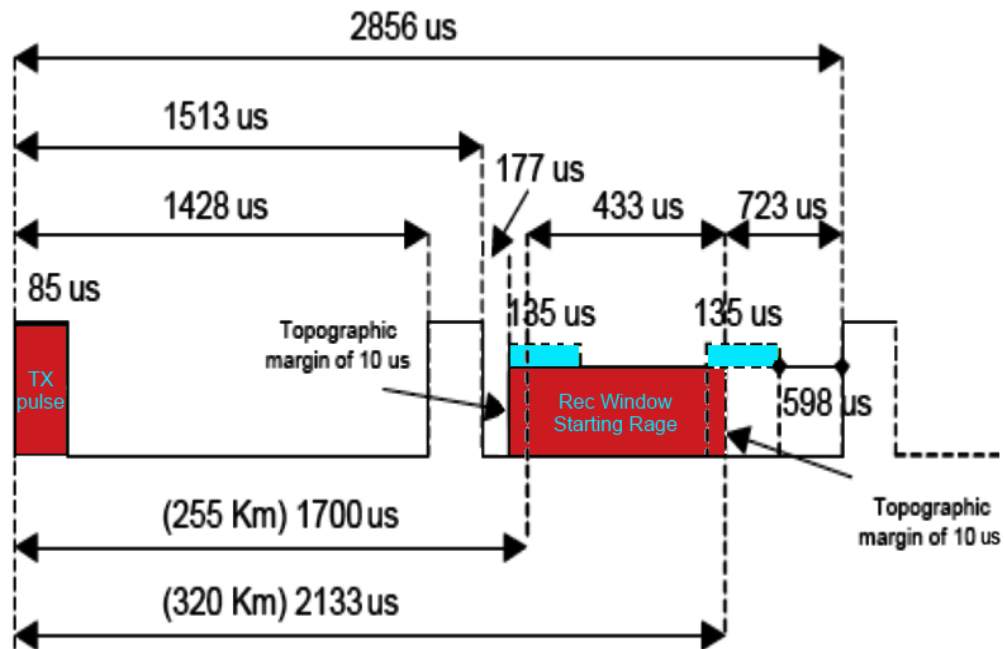


Figure II-10: Positioning of the listening window of the radar in case of PRF=700.28 Hz

The high fidelity of the signal reconstruction, in terms of linearity and amplitude/phase distortions (which, in turn, affects the side lobes of the compressed signal) is obtained mainly by avoiding any upconversion or down-conversion process in the system, and by reducing the analog electronics to a minimum. The transmit chirp is synthesized directly at the transmit frequency (15–25 MHz) by a digital signal generator and then amplified at the required power level before being sent to the matching network and the antenna. In the receiver, no analog conversion to baseband is used. Thanks to the large data storage and download capabilities of the MRO spacecraft, SHARAD has no need to perform range compression and synthetic beam formation onboard to reduce the final data rate. The availability of raw or close-to-raw data on the ground gives the user the capability to apply different types of optimized processing to

the acquired data, both now and in the future when improved processing techniques may be available. It also allows the range compression to be performed on-ground, using as reference for the correlation not a theoretical chirp but rather an optimized one derived from the calibration performed both on-ground and in-flight to account (and to compensate) for the instrument's non idealities.

II.1.3 The SHARAD data

SHARAD can operate in four different Operative (or Measurement) Modes corresponding to the different actions that the instrument may perform under the guidance of OST entries. Telemetry is always generated during Operative Modes and monitoring is active. In case of other error or anomalies during Operative Modes processing, an automatic transition is performed to Safe/Idle State.

- SUBSURFACE SOUNDING (SS) MODE SHARAD shall perform scientific measurements by transmitting radar pulses and collecting, processing and formatting received echoes. P.R.I. and duration are variable.
- RECEIVE ONLY (RO) MODE is used to perform passive measurements mainly during the on-orbit phase.
- CALIBRATION MODE is used to perform instrument calibrations during the on-orbit phase
- TEST MODE is a debug mode used to generate a stream of science data simulating an instrument operative mode, to exercise all internal functions of the instrument.

The Data produced using the last two Operative Modes have no scientific value and will not be used to produce EDR data products. The procedures for the

processing of data on the orbiter are limited to the minimum to avoid overloading of the onboard software/hardware. The data processing performed on board is limited, to simplify instrument operations: Phase compensation of the transmitted chirp to correct for radial motion of the spacecraft; conversion of the analog signal into a digital stream of echo samples; tracking of the echo position in time for the correct opening of the receiver; pre-summing and compression of echoes. The collected data is compressed to reduce the amount of memory required, packaged and then sent to the ground. All operations that deform and control the data, and the whole chain of processing (compression in range and azimuth) necessary to obtain the Radar images are executed on the ground through different software tools installed at the operational center of the instrument. The data, once the telemetry are received, are tested checking the information integrity of the data, the right execution of commands and presence of malfunctions of the radar, as well as acquired, are read and structured in specific files. The scientific data are formatted according to the standard dictated by the PDS (Planetary Data System) called Level 1A product, also known as EDR (Experiment Data Record). Such products then undergo further processing of SAR type that allows the generation data RDR (Reduced Data Format), i.e. the level 1B.

II.1.4 Level 1a data: Experiment Data Record (EDR)

The Experiment Data Record (Level 1A data) contains the data acquired by SHARAD with all auxiliary information necessary to place the data in space and time. In order to produce the EDR, the scientific data collected by the radar are sorted in time and cataloged according to the different operating modes of the SHARAD. Depending on the operating scenario, different levels of pre-summing can be selected, i.e.: pre-summing 1 (no presumming), 2, 4, 8, 16, 28, 32. When

pre-summing "N" is selected, the samples from N sequential PRIs are summed sample-by-sample, thus reducing the data rate by a factor N. The result of the sum of N echoes is referred to as a data block [49]. The selection of the operation mode of the radar is essential because the pre-summing is changing and a different calibration of the data may be needed. The packets of data duplicates are removed while those corrupt are replaced by a null value that indicates the absence of the required data. In particular, the processing at level 1A consists of the following operations:

- Deformatting of data packets.
- Sorting data over time.
- Cataloguing data based on the operating mode of the instrument to time of shooting.
- Test data quality.
- Creation of auxiliary data for the location of those in the scientific space and time.
- Generation of output formats such according the rules dictated by the PDS node.

The inputs for the creation of Experiment Data Record data are sent to the ground, from the MRO antenna. These data are following:

- The telemetry scientific SHARAD in the form of Raw Instrument Science Products, sent to the Earth after the compression.
- The files containing the information on the engineering tool.
- The telemetry of the spacecraft and all the ancillary information on the satellite about the trajectory, orbit and orientation.

- The value of the coefficients of the MRO clock edge to be converted in the format of Coordinated Universal Time (UTC) by the NAIF (Navigation and Ancillary Information Facility), one the nodes of the PDS.

The data stored within a single EDR are an aggregation of Data Blocks (set of scientific data formed by returning echoes of one or more P.R.I.) and are named Data Take, connected continuously in space and time, and characterized by the same operation mode i.e. a single OST command. The EDR Data are divided in three files:

- A binary file containing the scientific instrument telemetry called Science Telemetry file. Each row (i.e. record), is formed by an initial part containing information as the value of OST command corresponding to the processed data, the time and the parameters used to process the Data Block, scientific data formed by 3600 sample. The sample's length can vary from two to eight bits and consequently varying it will vary also the record length, note that the records defined by the same OST value keep the same sample length.
- A binary file called Auxiliary Data file. Each record of this file contains the information generated on the ground of the navigation satellite data in correspondence with the relevant records of the Data Block written in the Telemetry file. Most of these values are expressed as real numbers in the format of eight or four bytes.
- A file in ASCII (American Standard Code for Information Interchange), named label, which describes the contents of the data reported in the two binary files. This document is written in accordance with the PDS standards and describes both observations in which the data were acquired and the file format where such data were recorded.

II.1.5 Level 1b data: Reduced Data Record (RDR)

The Reduced Data Record (Level 1B Data) is consisting of the data of Level 1A on which has been performed some operations. The backscattered Echoes have been Doppler filtered and Range compressed and has been included in the data the necessary information for the space and time localization. The data obtained are formatted as PDS standard requires known as ISO Level II 27.3. In order to realize the data processing, a specific Software tool, Level 1B (L1B) Tool has been designed and implemented from the CO.RI.STA within the program SHARAD Ground Data System managed by the A.S.I. (Italian Space Agency). The read the EDR data and perform the processing operations:

- Range Compression
- Azimuth compression (also called Doppler processing),
- Ionospheric effects correction.

According to the standards two separate files are created:

- The first file has a binary format containing the processed data, the scientific data auxiliary, the engineering parameters and geometric information used to locate the observations in space and time.
- The second file is, as in the case of EDR, a label ASCII, its content is the description of the first one.

In order to obtain the desired spatial resolution both in depth and along track (ground track) the echoes of the SHARAD need to be properly processed once sent to Earth. The echoes of the SHARAD need to be properly processed once sent to Earth In order to obtain the desired spatial resolution both in depth and along track (ground track).

The processor of Level 1B performs an estimation of the parameters Doppler above before starting the chain of azimuth processing by of statistical techniques based on maps of the planet and on data collected from the same M.O.L.A. The algorithm for this task is called Chirp Scaling Algorithm, the can provide a maximum resolution, depending on precisely the Doppler parameters estimated up to 300 meters [41].

II.1.5.1 Level 1b data: Ionospheric effects correction

The propagation of the electromagnetic signals towards the Martian Ground crosses the Martian Atmosphere. The signals meet the ionospheric distortion of the transmitted waveform, caused by the ionospheric plasma. While Earth's ionosphere has four layers, the Martian ionosphere is a single layer of ionized gas that extends from about 100 km to several hundred kilometers above the surface from Viking Lander 2 direct measurements [50]. The indices of refraction of the ionosphere is frequency dependent, and introduces a variation of the group velocity within the chirp transmitted from the lowest frequency to higher, causing degradation of the signal/noise ratio (SNR). The studies on Martian ionosphere were numerous with the creation of models mathematicians that would provide both the composition is precisely the effects on radar signals [51]. Even today many of the theories developed are based on the developed in 1931 by S. Chapman [52] that dictated the formulas for predicting of a layer of the ionosphere, hypothesized to simple composition and its performance during the day. The refraction index varies dramatically depending on time of day and solar weather, as charged particles from the solar wind interact with the Mars's magnetic field. The variation of the ionosphere during the day is due to the fact that the Ionosphere is ionized by solar radiation and its effects are therefore more evident during the day time than night time. It is therefore needed to a correction during the processing of the data collected by SHARAD during the

Martian day. The choice of a deterministic correction of the signal distorted due to the ionosphere, however, would have required knowledge of the physical structure of it, which was not possible for the suite of scientific instruments transported on board of the orbiter and neither was obtainable from previous missions. The correction implemented by the software L1B in the ground data processing was based on an algorithm that did not include any a priori knowledge of the ionosphere, called the PGA (method of Phase Gradient Autofocus) originally developed for images of SAR [53]. The PGA was developed to obtain a reliable estimation of the gradient of the phase error directly from the complex SAR image. The process exploits the redundancy estimation information about the phase error contained in the image degraded regardless of the image scene [54].

II.2 MOLA

The Mars Orbiter Laser Altimeter (MOLA) is an instrument on the Mars Global Surveyor orbiter. The primary objective of MOLA is to map globally the topography of Mars at a level suitable for geophysical, geological, and atmospheric circulation studies of Mars. Secondary objective is to measure the heights of atmospheric reflections to better understand the three-dimensional structure of the Martian atmosphere; to measure 100 m scale surface roughness of Mars to contribute to geo-logical characterization of the surface and to assist in assessment of future potential landing sites; to measure the surface reflectivity of Mars to contribute to knowledge of surface composition and seasonal changes; and to attempt to measure the time-varying topography of the Martian polar caps to contribute to understanding seasonal cycles. With data collected in the capture orbit during the first 15 months of mapping orbits of the Mars Global Surveyor mission [55], all MOLA objectives, with the exception of

those relating to temporal changes, have been fully met. In addition, the status and major accomplishments of the MOLA investigation are reviewed as of June 1, 2000, at which time the instrument was turned off for a two-month period surrounding solar conjunction. MOLA measures the round trip time of flight of individual laser pulses between the MGS nadir deck and the Martian surface or atmospheric layer. Every 14 seconds, the laser fire time is compared to the MGS spacecraft time so that the location of the laser spot on the Martian surface can be reconstructed. The spacecraft time stamp has a resolution of 1/256 second, the range resolution is 36.5cm. The width of MOLA ' s backscattered laser pulse provides a measure of the target height variance or relief, which can be interpreted as footprint-scale slope or root mean square (RMS) roughness. Pulse width can be measured in two ways from MOLA, and the results represent the first quantitative measurements of the local vertical structure of the Martian surface and atmosphere at 160-m length scales.

II.3 SHARAD Data acquisition

SHARAD acquired a total of 12389 science observations up to Jul. 28, 2012 (RM149_b)

- 5567 observation during PSP
- 2393 observations during ESP
- 4429 observations during EM1 (79% of PSP Observations and 185% of ESP Observations and 56% of PSP+ESP Observations)

The Operation Center of SHARAD received ~2.69 TB of raw data up to Mar. 25, 2012 (RM140_b)

- ~1.21 TB during PSP
- ~0.59 TB during ESP

- ~0.89 TB during EM1

A total of ~7.38 TB of EDR + RDR products have been generated up to Jun. 16, 2012 (RM146_b) and 19707 EDR + RDR Products (about 6.554TB) delivered to PDS Node covering an acquisition period up to Feb. 11, 2012 (RM137-b)

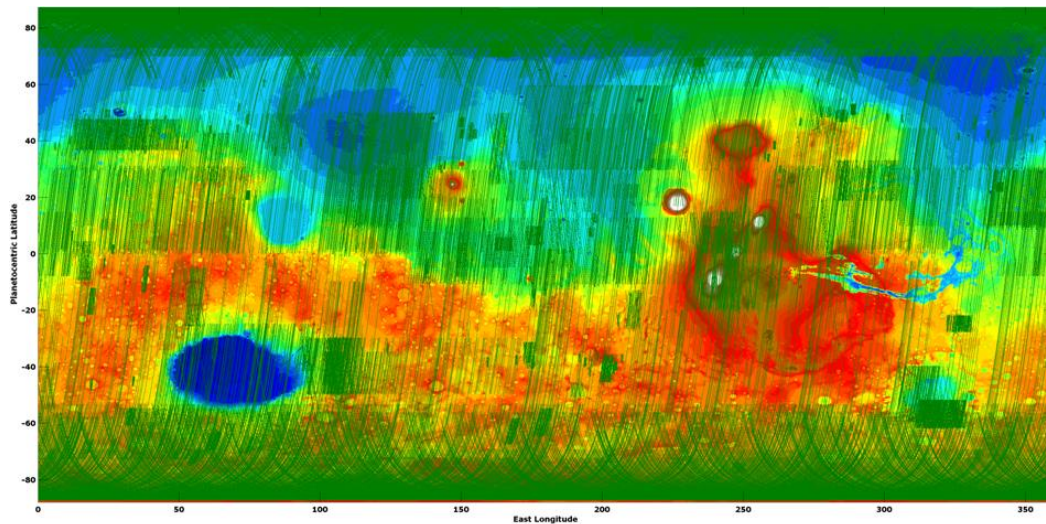


Figure II-11 Ground Track Coverage up to June 2, 2012 (observation 27431_01 – RM145_b)

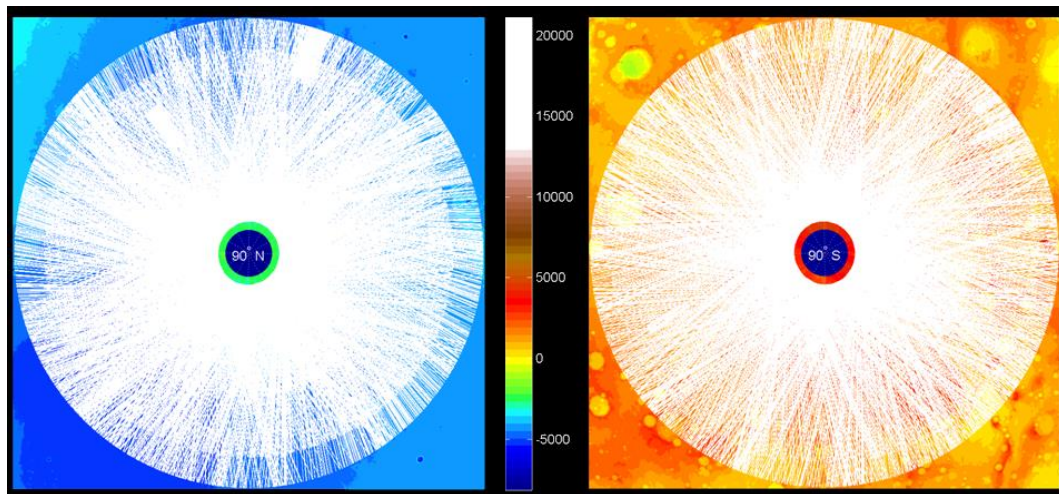


Figure II-12 North Pole Ground Track Coverage (Left Side) and South Pole Ground Track Coverage (Right Side)

II.3.1 Mola Data Product

Raw MOLA Experiment Data Records (EDRs) are transmitted from MGS to stations of the NASA Deep Space Network, after which they are transmitted to NAA/GSFC, where all processing occurs [6]. The Precision Experiment Data Records (PEDRs) are the processed EDR, they contain profiles of all MOLA's measured and derived parameters, as well as the value of the aeroid [56] at each shot location and a flag to indicate ground returns. The profile data are assembled into Experiment Gridded Data Products (EGDRs) of a resolution that depends on data density and distribution. When MOLA was turned off prior to Mars solar conjunction in June 2000, the laser had accumulated over 390 million pulses, making it by far the longest-lived laser ranging instrument that has so far flown in space [57]. The Figure II-13 shows the topographic model based on 333,689,830 MOLA ground shots. Data were corrected for spacecraft attitude, for pointing angles $< 6^\circ$ except where off-nadir ranging was performed to cover the North and South poles in areas not routinely sampled due to the 92.8° of

inclination of the MGS orbit[58]. To derive location coordinates and median heights, all ground shots were projected and binned on a $1/64^\circ$ latitude $1/32^\circ$ longitude global grid. The resolution of the global grid is currently approximately $1 \times 2000 \text{ km}^2$ at the equator, with longitudinal spacing decreasing with the cosine of latitude. More than half of the bins contained at least one observation, and usually more than three, while the remainder was interpolated by minimum-curvature-under-tension [59]. Planetary radii were then projected and similarly binned, and a spherical harmonic expansion was subsequently fit to the data [60].

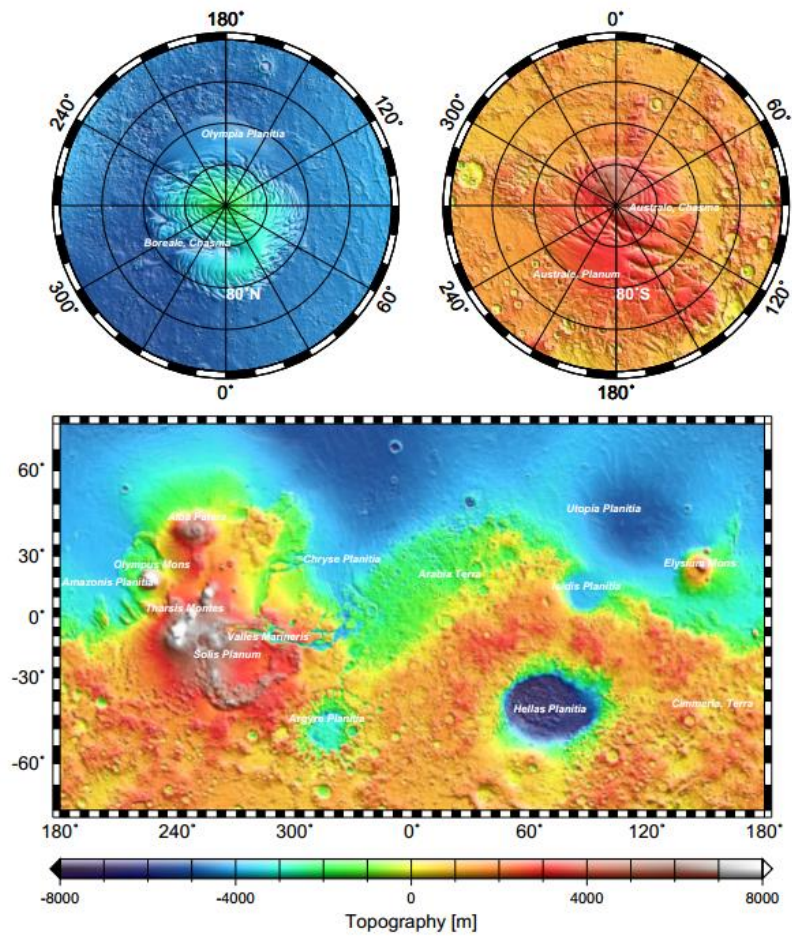


Figure II-13 Mars topography from MOLA [58]. Topography is shown as color coded elevation draped over shaded relief. The projection at mid-latitudes is Mercator and at high latitudes is polar stereographic. On Mars approximately 1° is 59 km.

CHAPTER III: INVERSION MODELS OF CERBERUS PALUS

The following chapter establishes the theoretical background of Inversion mathematical modeling and characteristics of the Cerberus Palus, which will be the area under investigation.

III.1 Scattering from Natural Surfaces: Fractal Geometry

Scattering problems arise whenever there is interaction of electromagnetic fields with materials. Scattering from natural surfaces plays a fundamental role in wave propagation and remote sensing. The mathematical models of the natural surfaces on Mars or other ones too are not made by man. The Euclidean geometry experimentally has been proved is not the appropriate one: a better match is obtained by employing the fractal geometry [61], [62]. The reason is that forces that model natural surfaces: gravity and microgravity, tensions, frictions, vibrations, erosions, thermal and freezing gradients, chemical reaction, etc.; and periodic and a-periodic happenings: seasons and vegetation changes, sun, wind, rain, snow, slides, subsidence, etc. generate surfaces whose topological dimension is larger than 2; i.e., larger than the Euclidean one [63]. The geometry of natural surfaces is surrounded by volumes; the topological dimension in the range from 2 for Euclidean surface to 3 for Euclidean volume. This topology and geometry is well described by the fractal geometry. Fractal

geometry brings to mathematical abstraction of fractal physics and electromagnetic field. The field scattered by the modeled surface illuminated by prescribed sources: it exhibits properties on all scales and does not allow the derivative operation at any point. Natural surfaces are observed, for their intrinsic nature, band limited and the mathematical fractals must be band limited [44]. When the natural surface is illuminated by an electromagnetic field, a scattered field is generated the electromagnetic scattering must be modeled by fractal natural surfaces theory.

III.1.1 The scattering

The electromagnetic incident field, radiated from a microwave emitter, is the incident field in the medium, usually homogeneous and called free-space medium; it is usually a plane wave. The scattered field is a solution of the source-free Maxwell equations, satisfying radiation conditions at infinity. Both incident and scattered fields including the conditions of tangential component continuity and of total fields on the natural surface constitute the electromagnetic field. In the case of natural surfaces, the modeling of the surface is achieved in two different coupled steps:

- Surface modeling which implies to make choices with subsequent mathematical elaborations.
- Development of Fractal method for evaluating the scattered field by the electromagnetic theory.

There are two ways of representing the geometric shape of natural surfaces:

- Deterministic function can be used to model the surface geometry in the case a specific natural surface is under study, the scattering from it will be considerate

- Stochastic process can be used to model the considered whole class of natural surfaces in the case of not a particular natural surface is under study, but a class of it, and only some significant parameters of the expected scattered field are desired.

Following will be taken in account the stochastic process modeling method as on Mars it is possible to refer to a class of backscattering geometric models. In the stochastic description of rough surfaces, the geometric shape may be modeled by means of a stochastic process of two independent space variables. In this case, a Cartesian coordinate system is employed

$$z(\vec{r}) = z(x, y) \quad \text{III-1}$$

Where $\vec{r} \equiv x\hat{x} + y\hat{y}$ and $z = 0$ is the mean plane and $z(x, y)$ describes its stochastic corrugations [44]. It is worth recalling that a stochastic process $z(\vec{r})$ is a rule for assigning to every outcome ζ of the statistical ensemble a function $z(r)$. Thus, a stochastic process is an ensemble of functions of the space variables depending on the parameter ζ . Alternatively, a stochastic process can be read as a function $z(x, y, \zeta)$ of three variables: the domain of (x, y) is \mathbb{R}^2 , the domain of ζ is the set of all the experimental outcomes. The field scattered from a natural surface can be analytically evaluated in a stochastic form if the surface description is provided in stochastic terms: in such a case, the problem consists of determining the stochastic characterization of the field scattered from a prescribed class of surfaces. In the pharos domain, the vector stochastic process $E(x, y, z)$ is a rule for assigning to each ensemble element ζ of the surface a function $E(\vec{r})$ of three independent space variables; at any space point, the scattered field is a vector random variable. Accordingly, fractal models, and in particular the fBm one, have been used recently in different disciplines to describe natural surfaces. Although use of fractal models in electromagnetic

scattering is not straightforward, some successful attempts have been reported recently. Such approaches can be roughly divided into two categories: the first one includes methods in which the fBm model is approximated by using the WM band-limited function; the second one includes methods that directly use the definition of the fBm process. A stochastic process is determined to the first order if, for each ζ and for each r , the first-order Cumulative-Distribution Function(CDF), $F(\zeta, r)$, is assigned:

$$\Pr\{z(r) \leq \zeta\} = F(\zeta, r) \quad \text{III-2}$$

Where $\Pr\{\cdot\}$ means probability, and ζ is an independent random variable.

The fBm is used to describe natural isotropic surfaces, defined in terms of the corresponding increment process. The stochastic process $z(x, y)$ describes an isotropic fBm surface if, for every x, y, x', y' , all belonging to R , the increment process $z(x, y) - z(x', y')$ satisfies the following relation [44]:

$$\Pr\{z(x, y) - z(x', y') < \zeta\} = \frac{1}{\sqrt{s\pi s\tau^H}} \int_{-\infty}^{\zeta} \exp\left(-\frac{\zeta^2}{2s^2\tau^{2H}}\right) d\zeta \quad \text{III-3}$$

$$\tau = \sqrt{(x-x')^2 + (y-y')^2}$$

where H is the Hurst coefficient, s is the standard deviation of surface increments at unitary distance measured in $[m^{1-H}]$ The value of z at a given point should be specified $z(0) = 0$ and it is defined so that the surface is self-affine.

The equation (III-3) exists if $0 < H < 1$, and that with probability 1, an fBm sample surface has a fractal dimension:

$$D = 3 - H \quad \text{III-4}$$

The equation (III-3) shows that if $\tau \rightarrow 0$, then $z(x, y) - z(x', y') \rightarrow 0$, that means any sample function z is continuous with respect to x and y . The fractal dimension D of the (III-4) can be considered as a “measure” of the surface

roughness [64]. The Topothesy is a characteristic length of the fBm surface expressed in meters; and defined as the distance over which chords joining points on the surface have a root mean square (RMS) slope equal to unity:

$$s = T^{(1-H)} \quad \text{III-5}$$

This has a relation with incremental standard deviation s .

The equation (III-3) can be rewritten using the (III-4) and (III-5) as follows:

$$\Pr\{z(x, y - z(x' - y')) < \zeta\} = \frac{1}{\sqrt{s\pi T^{(1-H)}}} \int_{-\infty}^{\zeta} \exp\left(-\frac{\zeta^2}{2T^{2(1-H)}\tau^{2H}}\right) d\zeta \quad \text{III-6}$$

$$\tau = \sqrt{(x - x')^2 - (y - y')^2}$$

Although a full stochastic characterization of the scattering surface is not achievable from the fBm fractal model represented by (III-3) and the prescription $z(0) = 0$, the presented fractal model is sufficient to evaluate the scattered-power density from such a surface[44], [63].

The expression of the NRCS of an fBm random rough surface can be obtained by using the Kirchhoff approach with the expression that follows:

$$\sigma_{pp}^0 = \frac{k^2 T^2 \cos^2 \vartheta}{H} \beta_{pq} \sum_{n=0}^{\infty} \frac{(-1)^n (2kT \sin \vartheta)^{2n}}{2^{2n} (n!)^2} \cdot \frac{\Gamma\left(\frac{n+1}{H}\right)}{(\sqrt{2kT \cos \vartheta})^{(2n+2)/H}} \quad \text{III-7}$$

With the limit of validity illustrated in literature[64]

III.2 Cerberus Palus

Cerberus Palus is located between 144.5°E and 152.5°E, and between 1°N and 8.9°N, is where the Mars Express High Resolution Stereo Camera acquired images of platy-ridged terrains that were interpreted as evidence for a frozen sea close to Mars' equator [65]. Athabasca Valles in Elysium Planitia is one of the best-preserved valley networks on Mars. Fluid emanating from the Cerberus Fossae, flowed Southwest through Athabasca Valles, and solidified ~300 km downstream in Cerberus Palus[66]. Cerberus Palus is a thoroughly studied region of Mars, characterized by evident platy textures that were interpreted either as evidence for a frozen sea close to Mars' equator or as being resultant of lava, mud or ice-flows coming from Cerberus Fossae through Athabasca Valles[65].



Figure III-1 Location on a map of Cerberus Palus (144.5° - 152.5°E, 1°N - 8.9°N)

III.2.1 Structure and Geology of the region

The area should consist of several layers of lava flows, many of which would be thinner than MARSIS resolution (i.e. MARSIS operates with a very high fractional bandwidth: 1 MHz bandwidth allows a vertical resolution of 150 m in vacuum which corresponds to 50-100 m in the subsurface, depending on the electromagnetic wave propagation speed in the crust [67]). Different lava flows made of the same material would still be discernible in SHARAD radargrams, as they would be separated by mechanical discontinuities (i.e. voids). If all layers were basaltic lava flows, however, very little penetration would be possible. Other studies of the Martian topography and images have focused on these platy features that are hundreds of meters to kilometers wide, interpreting them as being resultant of lava-flows, mud-flows, or ice-flows, with both lava and water erupting from Cerberus Fossae and reaching Cerberus Palus through Athabasca Valles [68]. The surface of the area is extremely young, perhaps less than 10 Ma old. The area is not uniform in age, however, as multiple events are testified by overlapping flows and variation in crater density. The stratigraphy of the area should consist of several layers of lava flows, many of which could be just a few tens of meters thick [67]. Determination of the real nature of the platy terrain will affect current understanding of the geologic history of the region, but will also have implications on the study of the history of water on Mars.

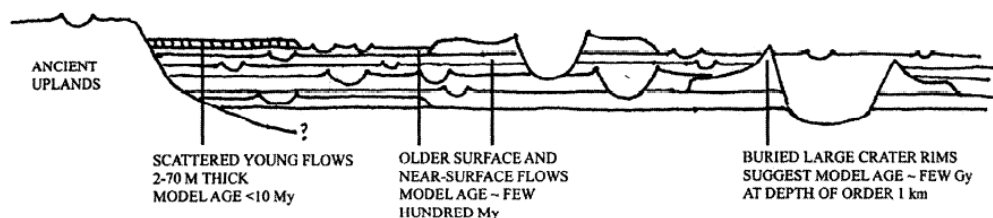


Figure III-2 A general stratigraphy of the area [67]

The Radargrams in the Figure III-3 provided by radar sounder SHARAD clearly show the presence of subsurface layers in the area.

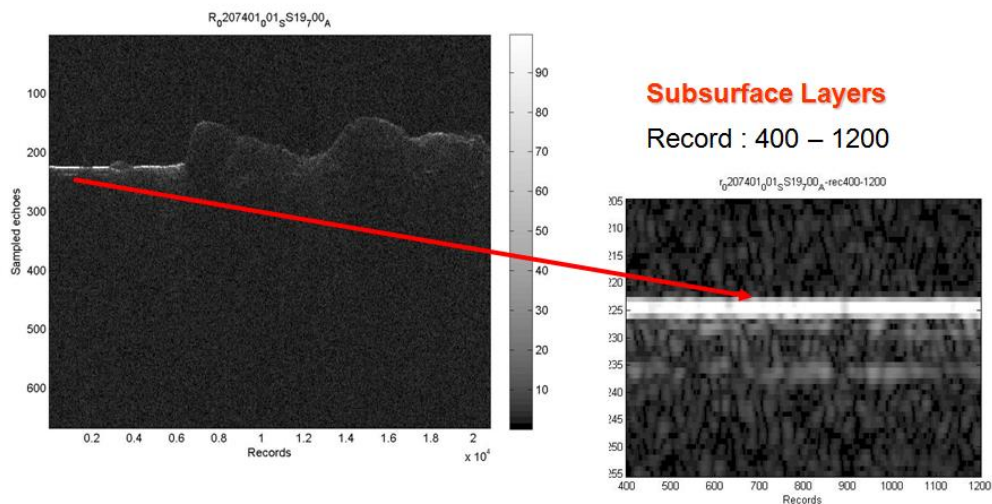


Figure III-3 level 1b image of R 0207401 001 SS19 700 which shows the first layer backscattering and a subsurface layer

III.3 SHARAD Backscattering

The SHARAD data have been used to study the stratigraphy of Cerberus Palus, and a mathematical method was developed to infer the dielectric properties of the platy terrains. These properties are then interpreted in terms of the material constituting the surface and subsurface of the area. SHARAD has a great amount of available data, on which it is possible to perform an accurate quantitative analysis aimed to estimate electromagnetic properties of surface and subsurface layers, in terms of permittivity and attenuation. Rough surfaces scatter the incident radar pulse in all directions, and echoes reflected towards the radar are thus weak because are summed incoherently, the scattering behavior depends

only on the Fresnel normal reflectivity ρ and a roughness parameter [69]. Horizontal and smooth surfaces and subsurface interfaces produce the strongest echoes.

The radar signal propagating in the subsurface is attenuated due to dielectric losses, to volume scattering and scattering off rough subsurface interfaces. Volume scattering is caused by random discontinuities of the dielectric properties within the first layer such as, for example, cracks or large rocks within a regolith.

For volume scattering to take place, dielectric discontinuities should have a characteristic size comparable to the wavelength of the radar, and would appear in radar data as a diffuse echo between the surface and the base of the first layer. We see no evidence of this in radargrams, which leads us to the conclusion that volume scattering can be neglected in modeling radar echoes for signal inversion. Subsurface scattering will be taken into account.

Because of the long (10-100 m) wavelength of radar pulses required in subsurface sounding, it is extremely challenging to produce an antenna that has both an acceptable gain and good directivity. SHARAD in fact transmits through a dipole, which has negligible directivity, with the consequence that the radar pulse illuminates the entire surface beneath the spacecraft and not only the near-nadir portion from which subsurface echoes are expected.

The electromagnetic wave can then be scattered by any roughness of the surface. If the surface of the body is being sounded is not smooth at the wavelength scale, i.e. if the R.M.S. of topographic heights is greater than a fraction of the wavelength, then part of the incident radiation will be scattered in directions different from the specular one. This means that areas of the surface

that are not directly beneath the radar can scatter part of the incident radiation back towards it, and thus produce surface echoes that will reach the radar after the echo coming from nadir, which can mask, or be mistaken for, subsurface echoes. This surface backscattering from off-nadir directions is called "clutter". Clutter can produce in a radargram the impression of subsurface structures where there are in fact none.

SHARAD processed data are usually displayed in the form of radargrams, which are produced by using echoes acquired at a rate of 700 Hz along the ground track. Radargrams are visualizations in which the vertical axis corresponds to time delay of the echo, the horizontal axis represents distance along the surface of Mars, and brightness is proportional to echo strength. The resulting image is a radar section of the Martian crust along the ground track of the spacecraft.

III.4 Mathematical Model

Radar echoes can be analyzed to retrieve the dielectric properties of the layers producing subsurface reflections, to constrain or even identify their composition. The so-called signal inversion of subsurface sounding radar data is an inverse problem for which different approaches have been presented over the years ([70], [71]).

Once it reaches the surface of a planet, an electromagnetic wave emitted by an orbiting spacecraft will be partly backscattered towards the radar, partly diffused by surface roughness, and partly transmitted into the subsurface. As the transmitted wave propagates into the subsurface, it can be scattered by inhomogeneity in the medium, until it reaches a dielectric discontinuity that causes it to be again partly backscattered, partly diffused and partly transmitted. Retrieving the dielectric properties of a subsurface layer thus requires that all

these phenomena are modeled, at least to some extent, so that the correct reflection coefficient of the subsurface layer can be determined and its dielectric properties inferred.

To this aim, realistic values can be obtained even by using simplified electromagnetic model for both surface scattering [72] and wave propagation. The selection of this approach is reinforced by the fact that the area under study shows very strong layers and it is very flat in topography.

Used model follows the simple sketch shown in Figure III-4 and it is based on the following main assumptions:

- Only two main interfaces are considered, i.e. the surface (subscript s) and the subsurface (subscript ss). Both interfaces are assumed to have negligible local slope values;
- the two layers in between the interfaces and after are supposed to be homogeneous and not dispersive media, characterized by different dielectric relative constants and (the real parts);
- the first layer is a low-loss medium with an attenuation factor and a depth d , that can be expressed as a function of the time delay between surface and subsurface as:

$$d = \frac{c\Delta\tau}{2\sqrt{\epsilon_s}} \quad \text{III-8}$$

- the two interfaces are rough, being characterized by a backscattering coefficient and depending on incidence angle;

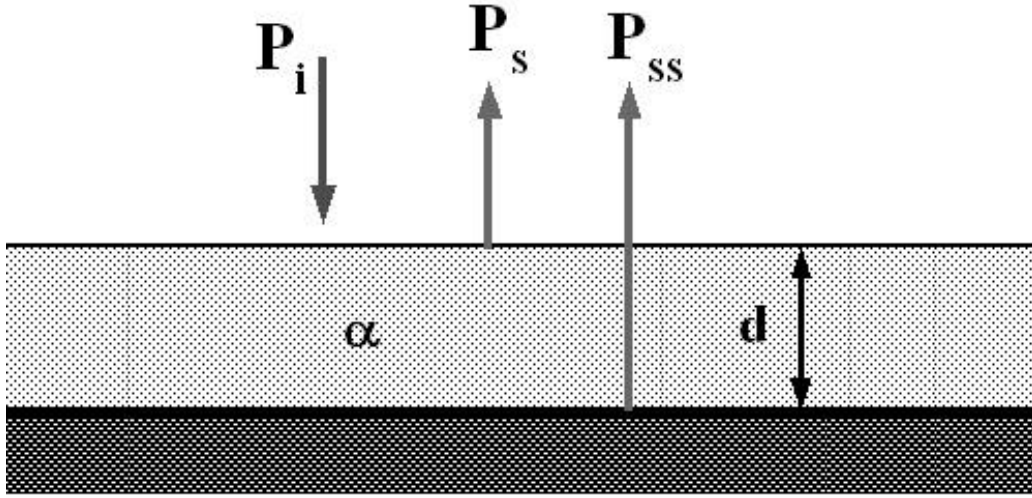


Figure III-4 Adopted electromagnetic model for SHARAD data inversion

With these assumptions, powers related to surface and subsurface can be evaluated by using classical “radar equation” [43], [72]. For the subsurface power the transmission coefficient of the surface and the attenuation of the first layer should also be taken into account.

By taking the ratio of the two powers and by eliminating common terms, it is possible to write:

$$\frac{P_{ss}}{P_s} = [1 - R_s^2(\theta)]_{\theta=0}^2 \exp(-2\alpha d) \frac{\sigma_{ss}^0(\theta)_{\theta=0}}{\sigma_{ss}^0(\theta)_{\theta=0}} \quad \text{III-9}$$

where the incidence angle is evaluated at nadir ($\theta = 0$) taking into account the looking geometry of the sounder and is the power Fresnel reflection coefficient at the first interface that, for the polarization used by SHARAD, can be written as:

$$R_s^2(\theta) = \left[\frac{\cos \theta - \sqrt{\epsilon_s - \sin^2 \theta}}{\cos \theta + \sqrt{\epsilon_s - \sin^2 \theta}} \right]^2 \quad \text{III-10}$$

and is the first layer attenuation factor that, in case of homogeneous low-loss medium, can be expressed as a function of material loss tangent such as [39]:

$$\alpha \approx \frac{\pi}{\lambda} \sqrt{\epsilon_s} \tan \delta \quad \text{III-11}$$

where the wavelength is considered as the free space wavelength.

It is worth noting that, even if the surface is supposed to be rough, expression (III-9) is used as the power transmission coefficient. This approximation, strictly valid only for flat interfaces, is well acceptable in the case of the area under study where the value of surficial roughness is expected to be much lower than the wavelength.

Moreover, the power Fresnel reflection coefficient at the second interface is:

$$R_{ss}^2(\theta) = \left[\frac{\sqrt{\epsilon_s} \cos \theta - \sqrt{\epsilon_{ss} - \epsilon_s \sin^2 \theta}}{\sqrt{\epsilon_s} \cos \theta + \sqrt{\epsilon_{ss} - \epsilon_s \sin^2 \theta}} \right]^2 \quad \text{III-12}$$

Evaluation of the backscattering coefficient is based on a fractal characterization of the Mars surface, since it is now widely recognized that fractal models are very useful in the description of natural surfaces because they properly account for the scale invariance property typical of such surfaces [61], [62].

The classical parameters usually employed to describe natural surfaces (i.e., standard deviation and correlation length) change when the scale at which the surface is observed changes [61]. Conversely, fractal parameters of a natural surface are independent of the observation scale. The most useful fractal model for natural surfaces is the fractional Brownian motion (fBm) [63] that has also the advantage of having an analytical evaluation of electromagnetic scattering. In fact, the mean-square value of the field scattered along an arbitrary direction by a surface illuminated by a plane wave can be evaluated in a closed form, with the Physical Optics (PO) solution under the Kirchhoff Approximation (KA) [63]. Therefore the backscattering coefficient can be written as:

$$\sigma^0(\theta) = 2k^2 \cos^2 \theta |R(\theta)|^2 \int_0^\infty J_0(2k\tau \sin \theta) \exp(-2k^2 s^2 \tau^{2H} \cos^2 \theta) \tau d\tau \quad \text{III-13}$$

where τ is generic distance between two points on the surface, is the zero-order Bessel function of first kind, is the generic power Fresnel coefficient and k is the wavenumber given by:

$$k = \frac{2\pi}{\lambda} \quad \text{III-14}$$

Previous expression involves the definition of the two characteristic fractal parameters; i.e. equations (III-4) and (III-5), at nadir, expression of backscattering coefficient (III-7) can be significantly simplified [44]:

$$\sigma^0(0) = \frac{k^2 |R(0)|^2 T^2}{H} \frac{\Gamma\left(\frac{1}{H}\right)}{(\sqrt{2kT})^{2/H}} \quad \text{III-15}$$

where Γ is the Gamma function. The last expression can be rewritten by isolating the factor G that accounts for geometric effects due to the fractal characteristics of surface, that is:

$$\sigma^0(0) = k^2 |R(0)|^2 G(H, T) \quad \text{III-16}$$

where:

$$G(H, T) = \frac{T^2}{H} \frac{\Gamma\left(\frac{1}{H}\right)}{(\sqrt{2kT})^{2/H}} \quad \text{III-17}$$

Coming back to equation (III-9), that can be considered as the basic relation involved by the envisaged inversion procedure and by taking the logarithm, we get:

$$\log\left(\frac{P_{ss}}{P_s}\right) = -2\alpha d + C \quad \text{III-18}$$

where:

$$C = 2 \log \left(\left[1 - R_s^2(0) \right] \frac{R_{ss}(0)}{R_s(0)} \sqrt{\frac{G_{ss}}{G_s}} \right) \quad \text{III-19}$$

with the position:

$$\begin{aligned} G_s &= G(H_s, T_s) \\ G_{ss} &= G(H_{ss}, T_{ss}) \end{aligned} \quad \text{III-20}$$

Therefore, both attenuation and subsurface dielectric constant can be estimated by linearly fitting logarithmic values of power subsurface/surface ratio as a function of depth. First value is just half the angular coefficient of the linear fit, while the second one is a function of the intercept C, according to:

$$\sqrt{\varepsilon_{ss}} = \frac{1 - M}{1 + M} \sqrt{\varepsilon_s} \quad \text{III-21}$$

where:

$$M = \pm \frac{1 - \varepsilon_s}{4\sqrt{\varepsilon_s}} \sqrt{\frac{G_s}{G_{ss}}} \exp(C) \quad \text{III-22}$$

It is worth noting that first layer depth d can be evaluated by means of (III-8) and by measuring the time delay between surface and subsurface returns directly from the radargram.

In other words, expression (III-18) states that, by performing a linear fit of the logarithm of power subsurface/surface ratio as a function of depth, it is possible to estimate both the relative dielectric constant of the subsurface (ε_{ss}) and attenuation of the surface (α) by knowing statistic properties of both interfaces (in term of fractal parameters) and their time delay ($\Delta\tau$).

III.5 Fractal parameter evaluation

Equations in the previous paragraph show that estimation of fractal parameters H and T is needed for evaluation the dielectric constant of subsurface layer. Suitable estimation of fractal parameters can be done by using topographic data provided by laser altimeter MOLA [7], [73], [74], that offers product data with a spatial resolution of about 460 m at the latitude of the analyzed site, that is smaller than SHARAD horizontal resolution (about 6 km in pulse-limited condition). Figure III-5 shows Digital Elevation Model (DEM) of the area as extracted by MOLA topographic database available on Planetary Data System nodes (PDS, <http://pds-geosciences.wustl.edu/missions/mgs/mola.html>).

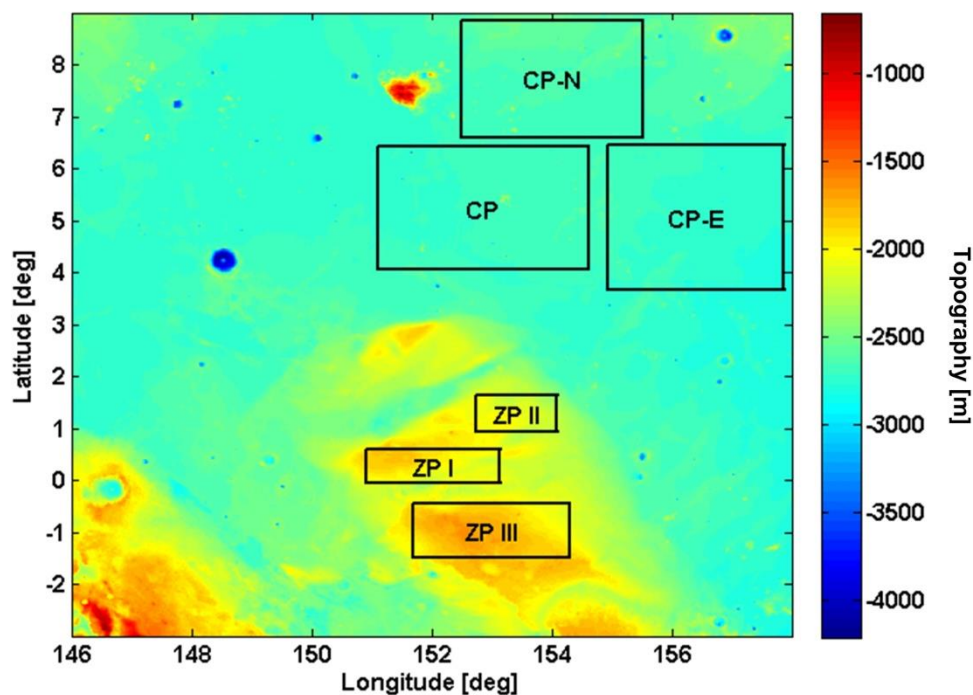


Figure III-5 MOLA Digital Elevation Model (DEM) of the area under study. Grey boxes represent zones where fractal parameters have been estimated (ZP is Zephyria Planum, CP is Cerberus Palus).

Grey boxes superimposed on DEM represent areas where fractal parameters estimation has been performed: one central for the flattest zone of Cerberus Palus (CP), two eastward (CP-E) and northward (CP-N) with respect the previous and three smaller for the hilly zone called Zephyria Planum (ZP-I, ZP-II and ZP-III). Estimation of H and T values has been done by using the periodogram method, i.e. by computing the standard deviation of height differences (σ) as a function space distance (τ). More specifically, H and T can be estimated by a linear fit of the log-log data [75], [76]:

$$\log(\sigma) = H\log(\tau) + (1 - H)\log(T) \quad \text{III-23}$$

Results for the previously mentioned areas are shown in Table 3 in which also the corresponding values of the geometric factor G have been computed following expression (III-17).

Table 3 Fractal parameter evaluation results

Zone	Latitude [°]	Longitude [°]	No. pixel	H	T	G	G mean
	I	0.000/0.563	150.797/153.172	305 x 74	0.80	3.6e-8	1.93e4
ZP	II	0.883/1.656	152.562/153.914	174 x 100	0.84	2.9e-10	2.25e4
	III	-1.469/-0.500	151.695/154.328	338 x 125	0.73	2.3e-5	1.19e4
CP-N		6.352/8.711	152.531/155.461	376 x 304	0.63	4.5e-4	6.24e4
CP-E		3.461/6.273	154.640/157.726	396 x 360	0.72	1.1e-6	2.77e5
CP		4.141/6.242	151.023/154.320	423 x 270	0.58	3.6e-4	7.57e5

In particular, for the inversion procedure described in the following paragraphs, three G values have been considered: 1) the value evaluated for CP area that, being the greatest, represents the flattest zone of Cerberus Palus, 2) the value averaged over CP-E and CP-N areas as representative of a “rougher” zone still within Cerberus Palus, 3) the value averaged over ZP-I, ZP-II and ZP-III areas as representative of Zephyria Planum area.

The averaged values are still shown in Table 3 the three values of geometric factor G will be associated to the three main interfaces (see color lines in Figure III-6) where inversion procedure has been applied, as described in the following paragraph.

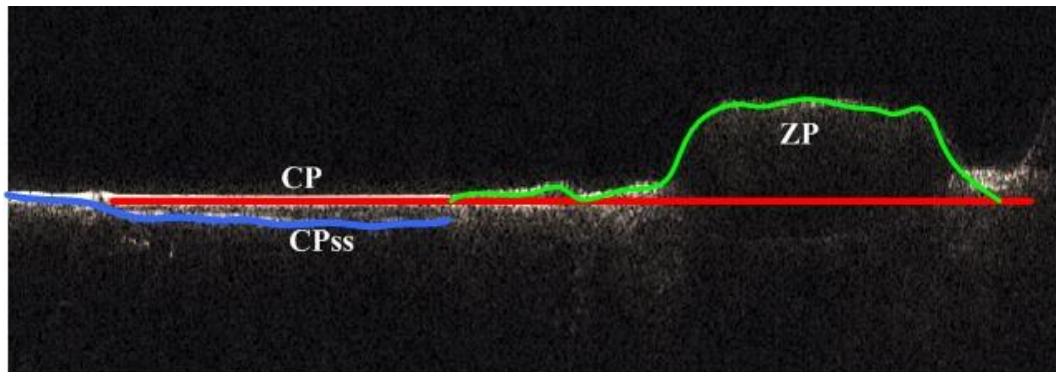


Figure III-6 Typical radargram of the area under study with a schematic indication of considered surface and subsurface interfaces.

III.6 Inversion results

All data products used hereafter have been downloaded from PDS node (<http://pds-geosciences.wustl.edu/missions/mro/SHARAD.html>). Analyzed radargrams have been produced by using the official focused processor [77] provided by the Italian Space Agency (ASI).

A typical radargram of the area under study is shown in Figure III-6 (observation no. 589803), where subsurfaces are clearly visible under either the flat area on the left (the Cerberus Palus, CP) and hilly zone of Zephyria Planum (ZP), where our analysis started.

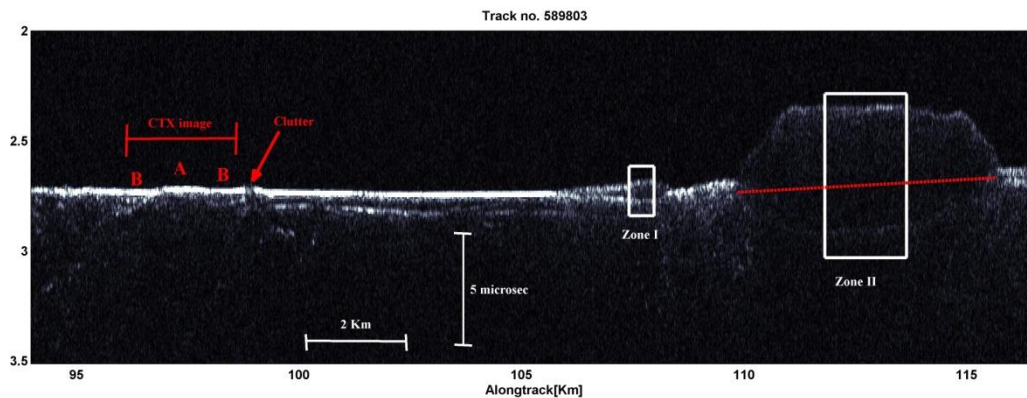


Figure III-7 Typical radargram image of the area under study (observation no. 589803): dotted red line represents the delay compensated subsurface over Cerberus Palus area, white boxes are the zones with different depth where attenuation value has been estimated. On the left side are indicated geological A and B units

Relative dielectric constant value of this area has been evaluated by compensating the time delay induced by the topography of the first large hill, under which the subsurface interface is visible.

Our analysis gives a relative dielectric constant value of 3 over the ZP area (Zone I in Figure III-5), and is in agreement with the results in literature [78]. It is difficult to assess the uncertainty of these values, since the compensation method is based on a visual analysis of the produced images. The corrected radargrams obtained in literature[78] with relative dielectric constant values of 2 and 4 suggest an overall precision of ± 0.5 , that corresponds to an uncertainty in positioning the subsurface interface of about ± 3 pixels.

At this stage, attenuation and subsurface dielectric constant can be estimated by linearly fitting logarithmic values of power subsurfaces/surface ratio as a function of depth, according to (III-18) and (III-21). It is worth noting that the previous mentioned uncertainty of the dielectric constant affects the evaluation

of depth values in (III-18), that only contributes to the estimation of the attenuation value α , by means of the fitting procedure. Therefore, since the depth is proportional to the root of dielectric constant, an additional relative uncertainty of 9% should be considered to the following estimated values of attenuation and corresponding precision.

Fitting error can be maintained low if data with a wide range of depth values are available. To this aim, the first two hills over ZP area (Zone I and Zone II of Figure III-5) can be exploited. Over these two zones a maximum local slope of 0.2° has been measured by using MOLA topographic data. Results are shown in Figure III-8-A that shows logarithmic values of power ratio (subsurface/surface) as a function of layer depth with the corresponding linear fit (red line corresponds to nominal fit, while black corresponds to variation of fitting parameters). In order to better assess fitting errors, colors representing power ratio values density have been added to Figure III-8-A.

Power values are evaluated by taking the square modulus of data samples directly extracted from radargrams by a dedicated software that is able to detect automatically surface and subsurface layers.

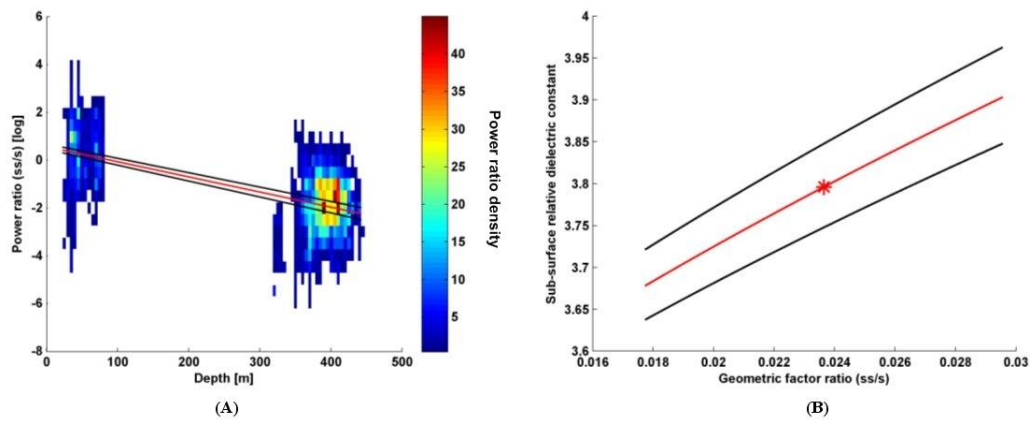


Figure III-8 ZP area: (A) logarithmic values of power ratio (subsurface/surface) as a function of subsurface interface depth and its linear fits (red line corresponds to nominal fit, black lines correspond to variation of fitting parameters). Colors represent power ratio values density. Power ratio values have been taken from Zone I and Zone II of Figure III-5 by using the products and the parametric values of Table 2; (B) subsurface relative dielectric constant as a function of the geometric factor (subsurface/surface). Red line has been obtained by using the nominal fitting parameter value (the C parameter of equation (III-18)); black lines correspond to variation of the fitting parameter. Star represents the nominal value obtained from the fitting procedure (dielectric constant of $ss=3.14$).

Table 4 Zephyria Planum area: products and parameters used for inversion procedure (symbols are those involved in equations (III-21) and (III-22)).

Product ID	03419-02-001	03419-02-001
	05898-03-001	05898-03-001
	20165-02-001	20165-02-001
	03208-02-001	03208-02-001
	03986-01-001	03986-01-001
	06254-03-001	06254-03-001
G ratio (G_s/G_{ss})	0.024	
Surface dielectric constant (ϵ_s)	3	

As far as the geometric factor is concerned, the schematic situation shown in Figure III-6 has been taken into account. The basic assumption is that ZP overlies an interface morphologically similar to CP (straight red line of Figure III-6). This allows us to apply fractal parameters estimated over CP area (see Table 3) for the subsurface interface under ZP, obtaining therefore a geometric factor ratio, as reported in Table 4.

The fitting procedure, performed on more than 6000 records of 12 level 1b products (see list reported in Table 4), gives the following values:

$$\alpha = 3.2e^{-3} \pm 5.3e^{-5} (1 \sigma)$$

III-24

$$\varepsilon_{ss} = 3.8 \pm 0.02 (1 \sigma)$$

For the relative subsurface dielectric constant, ambiguity of equation (III-22) has been solved by discarding non-physical solutions (near or less than 1).

For all calculations mentioned hereafter dedicated software has been developed in order to automatically detect the two interfaces. Time delay between these has been estimated by resampling the radargram in the range direction.

In addition, to evaluate the sensibility of the geometric factor variation, Figure III-8-B shows subsurface relative dielectric constant as a function of the geometric factor (subsurface/surface). Red line has been obtained by using the nominal fitting parameter value (the C parameter of equation (III-18)), while black lines correspond to variation of the fitting parameter. For example, by considering a relative variation of $\pm 25\%$ for the geometric factor ratio, it is possible to evaluate a maximum variation of in the range 3.6-4.0.

We used the same approach in Cerberus Palus area. In the CTX image shows the contact between two distinct terrains over Cerberus Palus. The geometry of these contacts can be tracked in the subsurface on the SHARAD radargram shown in Figure III-6, where it is evident how CP_{ss} (unit A in) outcrops along the radar section. The situation is also graphically depicted in Figure III-6 where the subsurface layer (CP_{ss}, the blue line) emerges in the zones around the flattest area of CP. Therefore, a geometric factor ratio of has been used that corresponds to the ratio of CP and the mean value of CP-N and CP-E areas of Table 3. In this case more than 22000 records has been used extracted from the 17 level 1b products listed in Table 5

Figure III-9 CTX image P03_002081_1866_XN_06N206W over the study area. Trace of radargram 05898 (Figure III-6) is shown as black line. Within this very flat area, we can distinguish the contacts between A and B units, that can be also observed along the radargram shown in Figure III-7

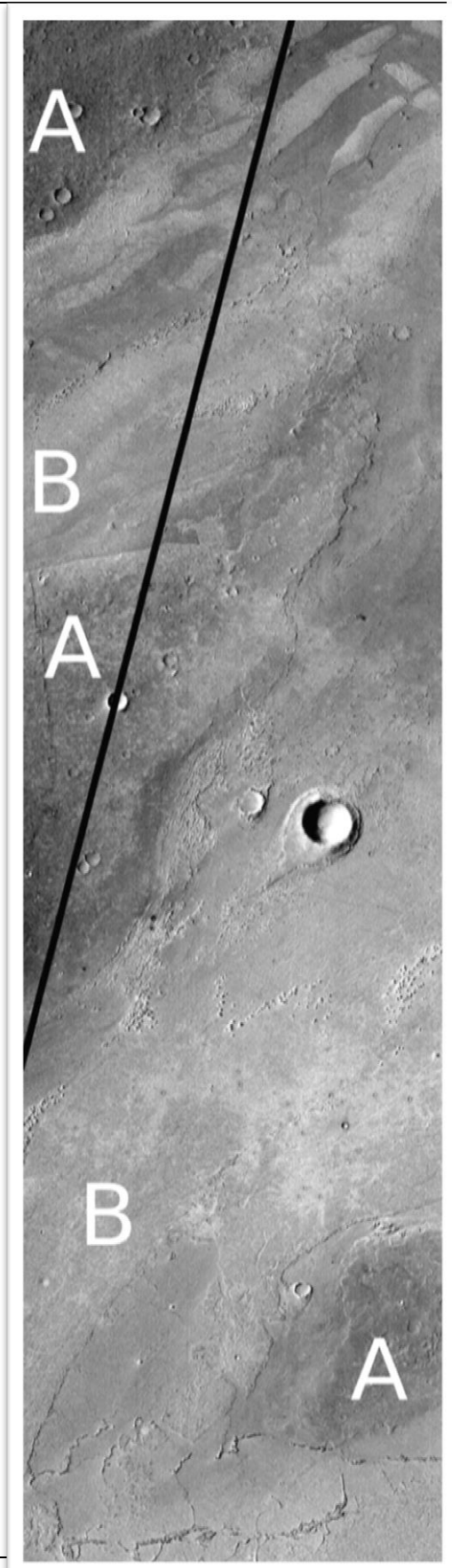


Table 5 Cerberus Palus area: products and parameters used for inversion procedure (symbols are those involved in equations (III-21) and (III-22)).

Product ID	0186301_001	0363001_001
	0207401_001	0398601_001
	0207401_001	0398601_001
	0264101_001	0440801_001
	0306301_001	0440801_001
	0320802_001	0518603_001
	0341902_001	0575303_001
	0341902_001	0625403_001
		0661003_001
G ratio (G_s/G_{ss})	4.453	
Surface dielectric constant (ϵ_s)	3.8	

Results of the fitting procedure, as plotted in Figure III-10-A, are the following:

$$\alpha = 1.1e^{-2} \pm 1.2e^{-3} (1 \sigma) \quad \text{III-25}$$

$$\epsilon_{ss} = 10.1 \pm 0.58 (1 \sigma)$$

Also in this case sensibility of the geometric factor variations have been studied. Results are shown in Figure III-10-B, where Red line has been obtained by using the nominal fitting parameter value (the C parameter of equation (III-18), while

black lines correspond to $\pm 3\sigma$ variation of the fitting parameter. For example, by considering a relative variation of $\pm 25\%$ for the geometric factor ratio ($G_s/G_{ss} = 4.453 \pm 1.113$), it is possible to evaluate a maximum variation of ε_{ss} in the range 8.4-12.3. A summary of all inversion results obtained is reported in Table 6.

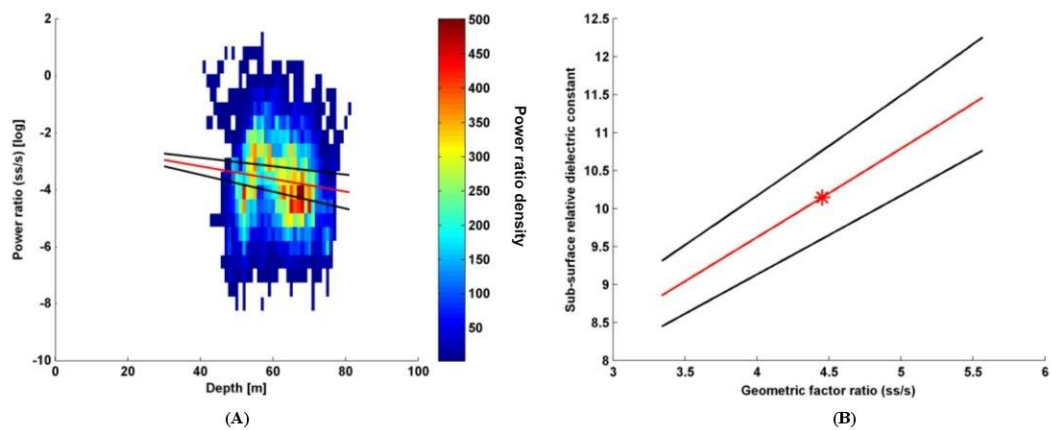


Figure III-10 CP area: (A) logarithmic values of power ratio (subsurface/surface) as a function of subsurface interface depth and its linear fits (red line corresponds to nominal fit, black lines correspond to $\pm 3\sigma$ variation of fitting parameters). Colors represent power ratio values density. Power ratio values have been evaluated by using the products and the parametric values of Table 5; (B) subsurface relative dielectric constant as a function of the geometric factor (subsurface/surface). Red line has been obtained by using the nominal fitting parameter value (the C parameter of equation (III-18)); black lines correspond to $\pm 3\sigma$ variation of the fitting parameter. Star represents the nominal value obtained from the fitting procedure ($\varepsilon_{ss} = 10.1$).

Table 6 Summary of inversion results

Area	Relative dielectric constant ε	Attenuation α and $\tan \delta$	Geometric factor ratio G_s/G_{ss}
ZP	$\varepsilon = 3 \pm 0.5$	$\alpha = 3.2e^{-3} \pm 5.3e^{-5} (1\sigma)$ $\tan \delta = 8.7e^{-3} \pm 1.5e^{-4} (1\sigma)$	$G_{ZP}/G_{CP} = 0.024$
CP	$\varepsilon = 3.8 \pm 0.02 (1\sigma)$ $\varepsilon = 3.6 - 4.0$ for $\pm 3\sigma$ variation of fitting parameter C of eq. (12) and 25% of relative variation of geometric factor ratio	$\alpha = 1.1e^{-2} \pm 1.3e^{-3} (1\sigma)$ $\tan \delta = 2.7e^{-2} \pm 3.0e^{-3} (1\sigma)$	
CPss	$\varepsilon = 10.1 \pm 0.19 (1\sigma)$ $\varepsilon = 8.4 - 12.3$ for $\pm 3\sigma$ variation of fitting parameter C of eq. (12) and 25% of relative variation of geometric factor ratio		$G_{CP}/G_{CPss} = 4.453$

III.7 Discussion of results

The origin of the area known as Cerberus Palus within Elysium Planitia has been debated for over 30 years, with interpretations varying from volcanic to sedimentary to lacustrine processes [68]. The analyzed area is centered around 152° E, 3°N and the values retrieved through the inversion of SHARAD data are tied to its structure and nature and can thus provide insight on the origin of the area. Natural materials expected to constitute the bulk of the layers sounded by SHARAD are water ice and rocks. Water ice has a relative permittivity of about 3.1 at the range of frequencies of the radar [71]. Rocks have a relative permittivity usually comprised between 4 and 10, with outliers caused by high porosity (lower end) or high metallic content (upper end) [71]. The main factor controlling the relative permittivity of dry rocks is porosity, with metal oxide content providing an important but not easily quantifiable contribution [78]. These findings lead us to conclude that any interpretation of the values of the dielectric constants found through the inversion procedure will not constraint the composition of the rock, but will give a sensible indication on its porosity, and, possibly, on the presence of a second material, such as ice, in the pores.

As shown in Figure III-6, the three geologic formations probed by SHARAD, for which the relative permittivity has been estimated, are the Cerberus plain (CP), the underlying bedrock (CPss) that is supposed to emerge northward and eastward with respect to CP, and the North Hill, belonging to Zephyria Planum (ZP) and thus part of the Medusae Fossae formation (MFF). Over the CP and ZP areas the attenuation values have also been retrieved.

The MFF has been previously studied through radar sounding using MARSIS [80] data and with SHARAD data [78]. Both the studies find evidence of a relative permittivity close to that of water ice, which they explain as resulting from a

lithic material with a high porosity, such as volcanic ash. Another interpretation of the MFF composition compatible with its dielectric properties, although not favored by those authors, is that its main component is water ice mixed with a relatively small amount of dust.

In the present work the relative permittivity value found for ZP area is similar to previous estimates, but further insight can be added by the retrieved attenuation value, that is linked to loss tangent by means of (III-11). Whereas relative permittivity for rocks and ice are not very distant, values of the loss tangent differ by orders of magnitude. In addition, for water ice the loss tangent is strongly dependent on temperature. By considering an average temperature of 210 K [13] for the Mars area under study and by applying the Mätzler model [81], it is possible to evaluate a loss tangent of 9×10^{-6} , value that will be used for the following considerations.

To determine if the additional information on the loss tangent can provide indications on the nature of the involved materials, a comparison with available mixing models has been performed in order to evaluate in what extent the retrieved dielectric properties could be obtained as a mixture of a plausible rock component with either the Martian atmosphere (here considered to be equivalent to vacuum) or ice. Many of these models exist in the literature [82], several of which are specialized for particular geometries within the mixture. Because of our complete lack of knowledge about the size and shape of pores or ice inclusions in the rock, one of the simplest and yet more widely used model has been used, the Polder-van Santen model.

This formula has the special property that it treats the inclusions and the hosting material symmetrically, i.e. it balances both mixing components with respect to the unknown effective medium, using the volume fraction of each component as a weight [82].

To this aim, it has been assumed that the relative permittivity of the rock without porosity, the hosting material, could range from 4 to 12, and that its loss tangent could independently vary between 10^{-3} and 10^{-1} . Then all possible combinations of relative permittivity, loss tangent and porosity (the volume fraction of intrusion material) that produce a complex dielectric constant as the one measured for ZP area (see Table 6), for both empty pores and ice-filled pores, have been evaluated by using the Polder-van Santen mixing rule. Results are shown in Figure III-11, from which possible combinations containing water ice in the pores have been considered unlikely, because they correspond to high values of ice volume fraction (80-90%) within high loss hosting material with low relative permittivity (4-5).

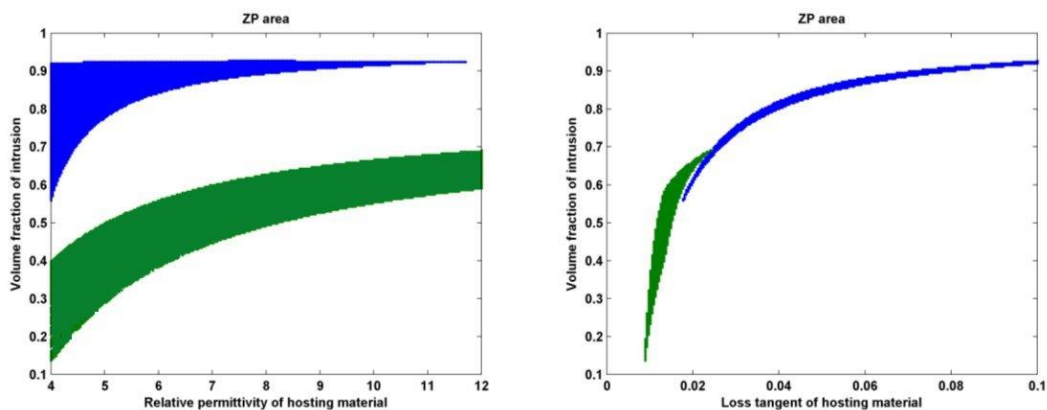


Figure III-11 Results from Polder-van Santen model on ZP area. Permittivity and attenuation values for the effective material (hosting + intrusion) are those reported in Table 6. Volume fraction of intrusion material as a function of relative permittivity (on the left) and loss tangent (on the right) of hosting material for ice-filled (blue area) and empty pores (green area). Water ice has a relative permittivity of 3.1 and a loss tangent of 9×10^{-6}

Therefore it is possible to conclude that the analyzed area of North Hill within ZP is most likely a very porous deposit of volcanic ash, in agreement with previous interpretations. In particular, with a relative permittivity in range 7-10 for the

hosting material, which would be typical for basalts of negligible porosity [79], it is possible to derive from Figure III-11 a porosity (void volume fraction) of about 50-60% and a tangent loss of the hosting material of about 0.015. The Cerberus plain, where the units CP and CPss are located, has been previously studied through radar sounding by two studies both using MARSIS data [83], [84]. The first study shows that the shape of MARSIS surface echoes has been compared to models of the expected echo decay as a function of subsurface composition, concluding that radar data favor a volcanic origin of the rafted plate terrain [83]. Although no number for the real dielectric permittivity is explicitly mentioned, values of epsilon for such a terrain would be higher than those for an ice-laden regolith. In the second study, there are calibrated MARSIS surface echoes which are compared to simulations, in order to determine the ratio between the real echo strength and the one computed for a given dielectric permittivity [84]. Although the area examined in this work is marginal with respect to the focus of their study, the map presented in Figure III-5 of their work allows us to infer that the estimated real dielectric permittivity for the Cerberus plains ranges between 6 and 7, a value compatible with literature results of the first study [83] results, and somehow intermediate between the values of epsilon for CP and CPss presented in Table 6. The difference between results obtained from MARSIS data and those presented here may be caused by many factors, including the different methods and assumptions behind them, but the very different resolution of the two radars might also play a role. MARSIS is incapable of detecting layers that are significantly thinner than its vertical resolution of about 100 m in a material with a dielectric permittivity close to 3, and would not discriminate between a low permittivity layer a few tens of meters thick and high permittivity bedrock beneath it. The power reflected by such a two-layer surface at MARSIS wavelengths would be determined by the combination of the properties of the two layers, weighted by their relative thickness within the vertical resolution of

the radar. With the same assumptions and input parameters (Table 6), the Polder-van Santen model has been also applied to CP area and the corresponding results are shown in Figure III-12.

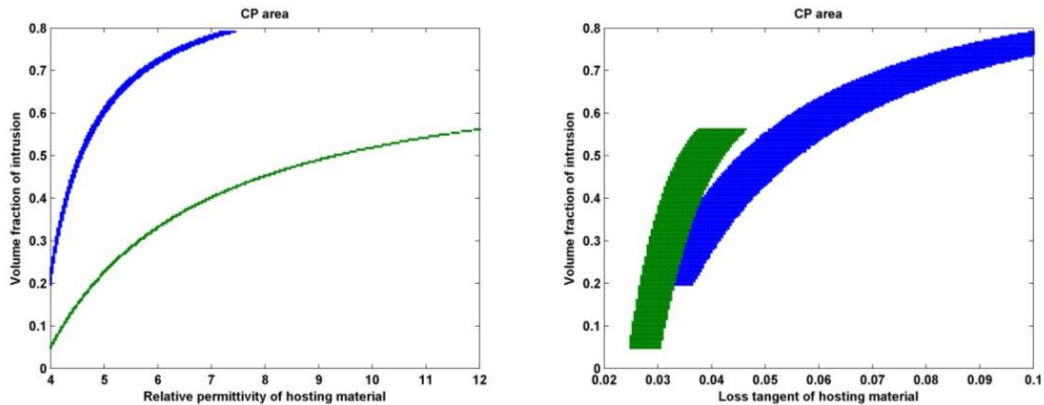


Figure III-12 – Results from Polder-van Santen model on CP area. Permittivity and attenuation values for the effective material (hosting + intrusion) are those reported in Table 6. Volume fraction of intrusion material as a function of relative permittivity (on the left) and loss tangent (on the right) of hosting material for ice-filled (blue area) and empty pores (green area). Water ice has a relative permittivity of 3.1 and a loss tangent of 9×10^{-6}

For Cerberus plains, no unambiguous explanation for the nature of the material within the pores could be obtained. The complex dielectric constant of the material could in fact be reproduced both using empty pores and ice-filled pores. In the case of ice intrusions, the fraction of ice required to match the measured value was well above 60% [about 80% with a relative permittivity of about 7 for the hosting material, from Figure III-12, and the required loss tangent [about 0.1 with a relative permittivity of about 7 for the hosting material] of the hosting rock was at or above the maximum value expected for basalts. Although this last fact would seem to make the presence of ice in the material less likely, the porosity required to match results for empty pores is also extremely high [in the range 40-50% with a relative permittivity in the range 7-10 for the hosting

material and a tangent loss of 0.05-0.06, from Figure III-12, contradicting the interpretation of authors that the entire surface of the plains is covered by lava flows [85]. Such high porosity is in fact typical of explosive, rather than effusive, volcanic rocks [86] and the high gas content required to produce such high porosity would greatly increase the viscosity of the lava and make its flow over long distances impossible.

III.8 6. Conclusions regarding Cerberus plains

The contradicting results obtained for both empty and ice-filled pores prevent us from drawing any conclusion. We can only note that evidence from other remote sensing experiments, such as cameras and spectrometers, is indicative of the nature of a layer a few microns thick, at most, while everything beneath such layer is essentially unknown. Even data from instruments such as the Neutron Spectrometer of the Mars Odyssey Gamma Ray Spectrometer [87] probe at most the first meter from the surface, a zone where has been estimated that ice is thermally unstable and would sublime in the atmosphere[13]. SHARAD on the contrary is insensitive to layers that are significantly thinner than its vertical resolution of about 10 m in a material with a dielectric permittivity close to 3, and would not discriminate between a thin, dry layer and a thicker, ice filled layer, providing an electromagnetic response that is a sort of weighted average of the dielectric properties of the two layers.

As far as the CPss layer, the value of 10.1 retrieved by the inversion procedure (see Table 6) most likely implies a composition of dense basalt, with at most a few percent of porosity.

To summarize, SHARAD radar echoes over the area centered on Cerberus Palus could be inverted to obtain estimates of the dielectric properties of three distinct

geologic formations, namely a part of Zephyria Planum (ZP), belonging to the Medusae Fossae formation, the Cerberus plains (CP) and the bedrock beneath the plains (CPss). The obtained results are reported in Table 6. These properties could be interpreted in terms of porosity and pore content of the material using mixing models to compare the measured complex dielectric constants with those resulting from a mixture of rock and vacuum or rock and ice. The properties of the bedrock are consistent with those of dense basalt, with at most a few percent of porosity. The ZP material is significantly porous [50-60%, with relative permittivity in range 7-10], and its attenuation properties [tangent loss of 0.015] are compatible with empty pores rather than with ice-filled pores. Ambiguous results were obtained for the plains material [80% of porosity, relative permittivity of 7 and loss tangent of 0.1 for the hosting material, in case of ice-filled pores, 40-50% of porosity, relative permittivity of 7-10 and loss tangent of 0.05-0.06 for the hosting material, in case of empty pores], but the resulting porosity is high both in the case of empty and of ice-filled pores. Such a large porosity is contradicting the common interpretation that the Cerberus plains are covered by lava flows produced from effusive volcanism and extending for hundreds of kilometers.

CHAPTER IV: MARS DATA MAPPING

In the following pages will be introduced a model used to make the map of the surface of Mars using the SHARAD Data.

IV.1 Mapping: introduction

One of the mission's main goals of Mars Reconnaissance Orbiter (MRO) is to map the Martian landscape in order to choose landing sites for future surface missions and to understand the geologic stratigraphy of the planet. MRO's Shallow Subsurface Radar i.e. SHARAD is designed to probe the structure of the Martian surface and subsurface. It is acknowledged that the surface of Mars will not be uniformly amenable to using radar sounding in the search for subsurface interfaces. Although the study of signal subsurface is in fact the most common application, the echo from the surface itself is useful to study the first layer of the Mars surface and it will be possible to find conditions of favourable radar viewing geometry, interface scattering, surface and volume scattering, and material properties, which may allow to have with a proper mathematical model the surface dielectric map, studying the reflectivity of the surface echo is a means to obtain information on the composition and geometry of the ground. When strong internal reflections do occur, they will be identifiable as aqueous only by contextual inferences drawn from the characteristic geological context of water habitats. Independent of any ability to directly detect water or ice, SHARAD is making significant new scientific data available toward addressing critical scientific problems on Mars, including the existence and distribution of buried paleochannels, subsurface layering, an improved understanding of the

electromagnetic properties of the “stealth” region, further insights into the nature of patterned ground, and other morphologies suggestive of the presence of water at present or in the past. In addition, it contributes to answer certain kinds of geologic questions, such as the character of the surface below the polar ice caps and the nature of some of the layered terrains [91].

SHARAD data gathering and processing should be transparent to the user, the first requirement, for the majority of users of SHARAD data, is that the data collection and processing techniques used to produce the images should be irrelevant, and scientific properties should be the main interest. A goal for the remote sensing scientist would be to model the relationship between some geophysical parameter and some set of radar backscatter measurements, so the scientific characterization of the data is needed to describe the data using an external calibration [89]. The classical method to calibrate the data i.e. checks of the form of the impulse response, point targets such as trihedral corner reflectors, with a large RCS (Radar Cross Section) [91] cannot be employed on Mars surface. SHARAD reflectivity should allow the study of Mars regions, but it requires the processing of more than 2 TB of data volume. An automatic method for locating echoes has been developed to be applied to the set of global Mars data, dedicated to the extraction of the surface echo. A mathematical method of calibration has been developed, making use of models of surface scattering in place of “ground truth”, to estimate the variation of geophysical parameter across the Martian surface. Several parameters affect the surface echo power: the dielectric constant, roughness, and slope. Most backscattering models separate the effect of the dielectric constant from the remaining parameters [90]. In the present work, a statistical model to take in account the effects of scattering due to surface roughness and slope has been developed using the theory of electromagnetic scattering from fractal surfaces and estimating the

parameters from topographic data provided by the MOLA laser altimeter [73, 92, 93].

IV.2 SHARAD Data Signal description

The ground penetration of SHARAD is expected to be around 1 km, depending on the nature of the soil [94]. The along-track resolution for the synthetic aperture radar processing along the ground track varies from 300 to 1000 m.

To handle the SHARAD data arises some problems which have to be overcome:

- Tracking of the surface echo position in recorded echoes, enough simple and fast, but also robust to minimize errors detections.
- estimation of the power losses due to the shape of the geometry

As a first step, has been taken advantage of oversampling of SHARAD range signal to improve the estimation of the Power Echo. In order to improve The S/N is provided a low-pass filtering operating in Azimuth and adopting a Local regression using weighted linear least squares and a 2nd degree polynomial model on the radargrams for the benefit of keeping better uniformity of the horizontal continuity of the echoes. The wavelength of the signal is greater than the plasma frequency of the ionosphere, allowing it to pass there through. However, during the propagation of the wave undergoes disturbances depending on SZA (solar zenith angle) of the Satellite and the position of Mars. In order to avoid filtering and compensation due to the Ionosphere distortion [95], only nocturnal data are used; a filter operating on the SZA data acquisition has been characterized to estimate the data in the nocturnal angles, i.e. angles between 95° and 175°. The echo generated by the surface is usually the first that arrives in time and it is generated by a high dielectric contrast. The surface echoes in a pulse echo is made by identifying the highest peak once the S/N has been

increased and the noise subtracted from the Echo, to avoid that the side echoes can match or exceed the true signal power from the ground to the nadir of the probe.

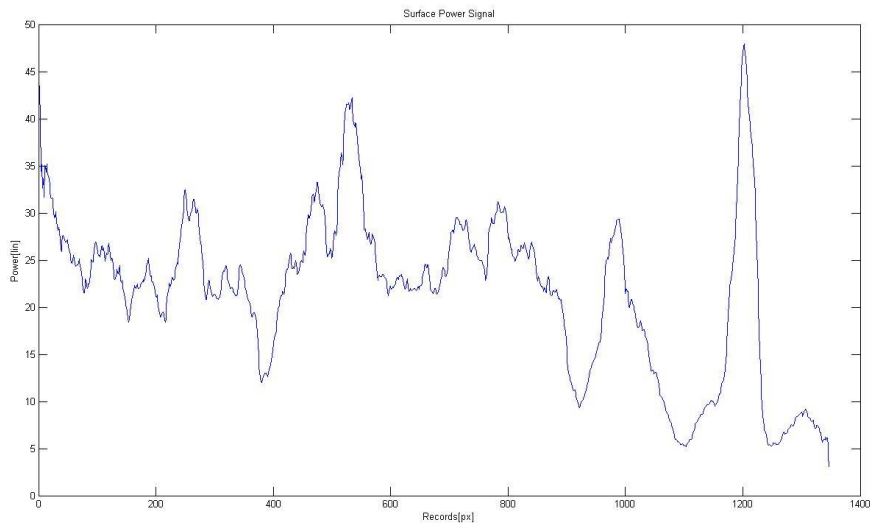


Figure IV-1 Surface Power Echo in linear scale extracted by the automatic routine from the observation 0659501 001 SS19 700A, low-pass filtered and weighted with linear least squares with a 2nd degree polynomial model

3D Electromagnetic model to estimate the backscattering from natural rough surface has been developed (96) in order to correct the variation of the Echo Power due to the geometry. The Fractal geometry model has been adopted as it is scale invariant and has high fidelity in surface backscattering estimation the data adopted for the fractal backscattering estimation are the Precision Experiment Data Records (PEDRs) are the processed EDR of MOLA following indicated as MOLA data, containing profiles of all MOLA's measured and derived parameters, as well as the value of the aeroid [97].

IV.3 SHARAD Data Signal correction

The signals extracted from the RDR need still several corrections in power in order to be comparable. These corrections show the influence of orbitographic phenomena (changes of altitude), technical issues (Satellite orientation, acquisition mode) geometry on the acquisition Signal.

IV.3.1 Orbitographic phenomena

Electromagnetic waves propagate with a geometric attenuation factor of $1 / h^2$. This means that, for the same reflective surface, the power intercepted by the Radar will decrease with increasing altitude. For comparing the signals received at altitudes, it is necessary to compensate this loss, can be easily estimated when is known the distance between the surface and the probe. For observation carried out at an altitude h the correction power due to the altitude must be:

$$H_a = \left(\frac{h}{h_{ref}} \right)^4 \quad \text{IV-1}$$

Where h_{ref} is the reference altitude.

IV.3.2 Technical Issues

In addition to the gain variations due to roll of the satellite which are corrected in pretreatment, each of the configuration involves disturbance variables on SHARAD signal. Four typical configurations have been identified and studied: SS04, SS05, SS11, and SS19. The corrections to be applied to the signal are provided with data and are related with magnitude of it [98]

IV.3.3 Geometry

The geometry is affecting the power that the antenna detects the effective aperture on the ground which takes into account that the power backscattered from the ground is incident on the antenna:

$$A_{eff} = \sqrt{\frac{c_0 H}{B}} \frac{\lambda}{\sin \theta_{3dB}} \quad \text{IV-2}$$

Where $\sqrt{\frac{c_0 H}{B}}$ is the half cross track resolution of the satellite, while $\frac{\lambda}{\sin \theta_{3dB}}$ represents the half along-track resolution which is from 300 m to 1000 m.

The along-track resolution is enhanced in SHARAD through what is called azimuth, Doppler, or synthetic aperture processing [99] this is another factor to take in account in the calculation of the normalized backscattered power:

$$P_{norm} \propto \frac{P_t H_a}{\sigma_0 A_{eff} A_z} \quad \text{IV-3}$$

Where A_z is the term that takes into account the broadening factor due to the non-ideal matched filter used in azimuth compression and also of the displacement in the sampling of data acquisitions for the operation mode used, σ_0 is the radar cross section estimated for linear polarizations, P_t the power backscattered, A_{eff} the effective aperture of the ground.

IV.4 Reference Area

The measured backscattered power does not allow a direct estimate of the Fresnel reflection coefficient of the surface, because topographic roughness also affects the backscattering coefficient. In order to achieve this result, the received power must be calibrated by comparing it to the reflection from a surface

characterized by a known reflectivity and nature [40]. To calibrate the signal, we used as reference the power backscattered by a Martian region that is homogeneous, smooth at the scales of the SHARAD wavelength, and has a known composition, making it possible to estimate with precision its permittivity and to measure its backscattered power without the contribution of a diffuse component of the signal. The radar backscatter for a known target is extracted from the data and used to test this hypothesis. The model it is based on the following main assumptions:

- Scattering takes place at the interface between two media, i.e. space and the Martian surface.
- The first medium is supposed to have the permittivity of open space.
- The second medium is supposed to be homogeneous and non-dispersive, and its surface is slightly rough, being characterized by a backscattering coefficient depending on incidence angle and on dielectric relative permittivity;

With these assumptions, power backscattered by the surface is directly measurable from radargrams and can be evaluated by using the classical “radar equation” [100]. The flatter areas of the Martian surface are on the polar ice caps [101], but the possible presence of CO₂ just below the surface of Planum Australe [102] introduces uncertainties in the determination of the dielectric permittivity of the area, and directs the choice over the North Polar cap. The chosen calibration area is located inside the North Polar cap, between 82°N and 84°N, and between 180°E and 200°E. The area consists primarily of water ice with a few percent of dust [103]. Over this area the radargrams show the minimum recorded noise. The MOLA data show that this area is essentially smooth at the scale of SHARAD wavelength, and thus the estimation of the

surface echo power can be made avoiding clutter noise. The real part of the dielectric constant is known from the literature.

IV.5 Constant Extraction

The calibration of the signal requires the determination of a constant that takes in to account the backscattering gain due to the radar system and the surface, to compensate the power losses due to the orbitographic phenomena. The determination of this constant is obtained using the reference area over Mars. For which the real part of the dielectric constant has been estimated through other means (i.e. 3.14). The constant has been calculating starting from the power backscattered on this area and taking care to neglect all the terms depending on the geometry, ground and orbit. The slope has been estimated considering the geometry of the area: the point target has been individuating in the MOLA data and from it the zone that contributes to the backscattering, a mean plane has been calculated and for each point the angle has been evaluated. The backscattering is evaluated using the statistical parameters estimated along the orbit with the fractal theory for a monostatic radar configuration [96]. Taking care that the backscattering in the specular direction occurs only in the case of normal incidence, $\vartheta = 0$; in this case, results are polarization independent as shown:

$$\sigma_0 = \frac{|R_0|^2 k^2 T^2}{H} \frac{\Gamma\left(\frac{1}{H}\right)}{(\sqrt{2kT})^{(1/H)}} \quad \text{IV-4}$$

Where H and T are respectively the Hurst and Topothesis coefficients, Γ is the gamma function, k is the wave vector and R0 is the Fresnel reflection coefficient of the mean plane. The topography has been characterized by fractal processes

[104] using the MOLA data and estimating Topothesy and Hurst coefficients over the whole of Mars.

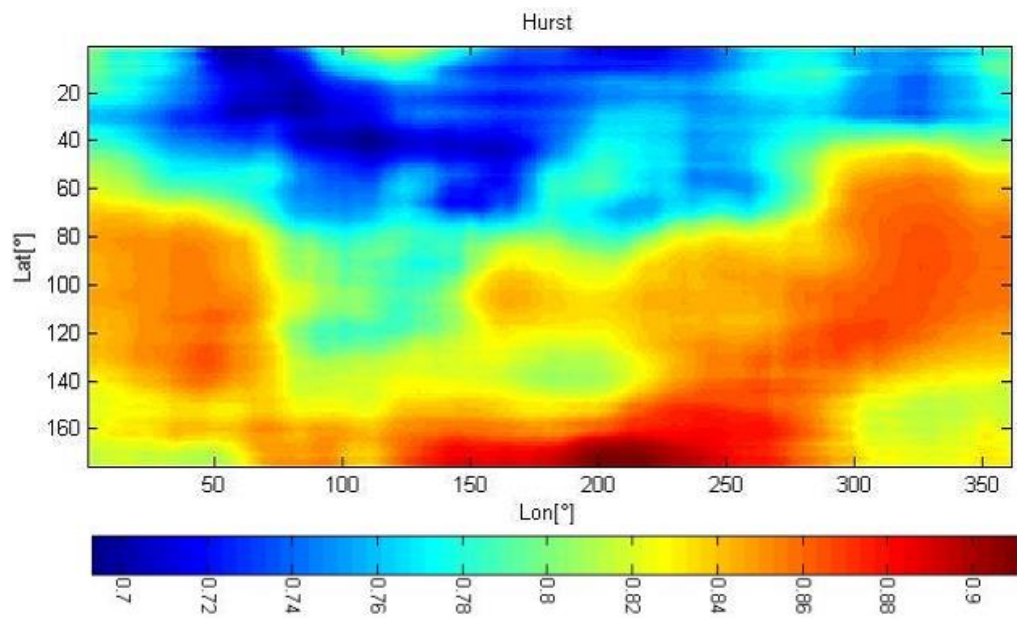


Figure IV-2 Mars Hurst calculated on Mars MOLA data

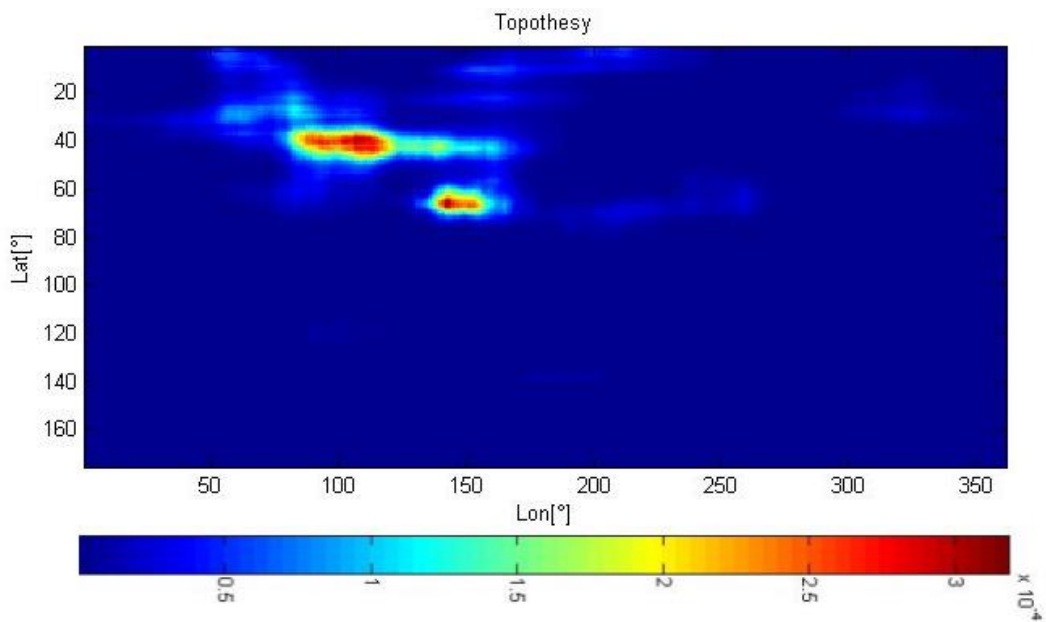


Figure IV-3 Mars Topothesy calculated on Mars MOLA data

The surface power echo is extracted from Level 1B data, as showed in Figure IV-1, it is now necessary to model the surface backscattered power measured by the radar using the fractal geometry of the area [105]. The calibration constant is needed also to compensate for the power losses due to altitude changes; moreover calibration constant must be valid over the whole dataset. Following is the formulation the calibration constant:

$$K_{ice} = \frac{G_{ice} \sigma_0 A_{eff} A_z}{P_r H^4} \quad \text{IV-5}$$

Where G_{ice} is the antenna gain on the ice, P_r is the received power, H is the altitude of the spacecraft, A_{eff} is the antenna effective area at 3dB of the ground, A_z is the azimuth factor, σ_0 is the radar cross section estimated for linear polarizations with fractal geometry.

IV.6 Data Calibration

The calculation of the calibration constant K_{ice} brings to the analysis of the surface power echo extracted from the Level 1B data, where the surface power measured by the radargram is modeled using the fractal geometry of the area [105], again the slope and radar footprint needs to be estimated using the MOLA data. The radar cross σ_0 is estimated in the specular direction in the case of normal incidence, the altitude of the spacecraft extracted from the Level 1B data, A_{eff} and A_z are estimated from the MOLA data, compensating also the power losses due to altitude changes. The Fresnel reflection coefficient at normal incidence at the plane interface between two media with refractive indexes and respectively, is defined as follows:

$$\Gamma = \frac{\sqrt{(\varepsilon_i)} - \sqrt{(\varepsilon_j)}}{\sqrt{(\varepsilon_i)} + \sqrt{(\varepsilon_j)}} \quad \text{IV-6}$$

Has been developed and automatic procedure which using the equations (IV-5) and (IV-6), is able to estimate the dielectric constant from the following equation:

$$\Gamma = \frac{K_{ice} G P_r H^4}{\sigma_0 A_{eff} A_z} \quad \text{IV-7}$$

in this case G is the two ways gain of the antenna on the surface.

IV.7 Discussion Results

In this section, we present the results obtained through the proposed calibration method using the full dataset of SHARAD in all available operational modes, highlighting the results for a particular area of interest, Argyre Planitia. As discussed above, the calibration method uses as calibration set of data the RDR located on the North Polar Cap. Figure IV-4 shows the occurrences of the dielectric constant after calibration of that area: it shows a consistent set of results from the model, as the highest occurrence of the dielectric constant it is near 3.14 which is the input data for the calculation of the calibration constant.

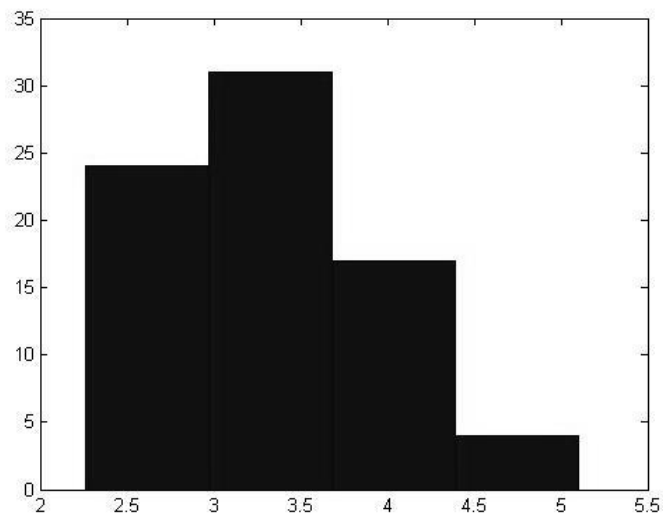


Figure IV-4 Occurrences of the dielectric constant in the calibration area after calibration

In Figure IV-5 and Figure IV-6 are showed respectively the dielectric constant map of Mars and the power map of the RDR. The effect of the correction of backscattered power due to the model: is evident, there is no direct relation between the two maps because the model operates by taking out the effect on the backscattering caused by the topography of Mars. The model thus reveals the contribution due to the dielectric properties of the surface material.

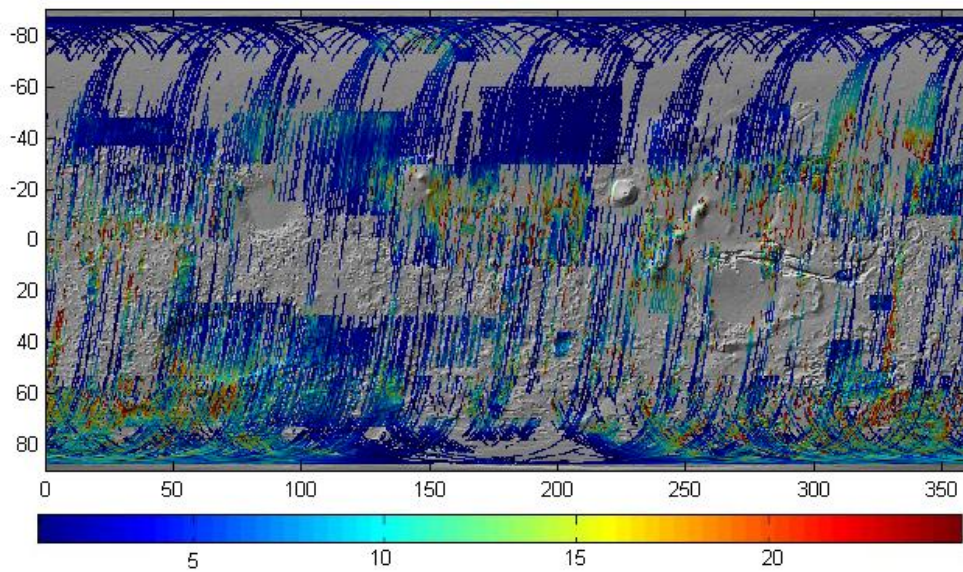


Figure IV-5 Map of Mars dielectric constant

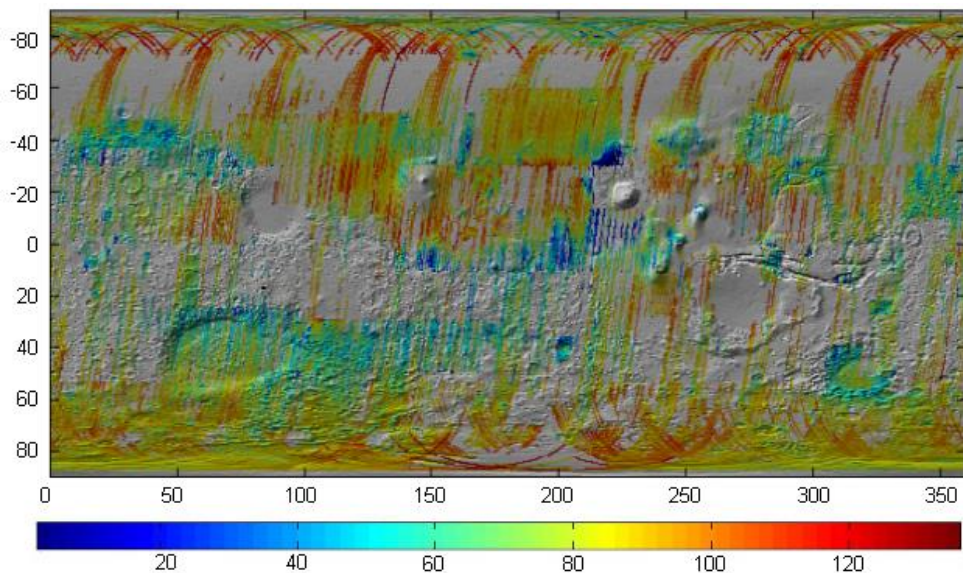


Figure IV-6 Map of the SHARAD RDR data surface extracted power (linearly scaled)

Figure IV-7 shows a particularly interesting area of the map which is located around 320°E, 50°S. The area is called Argyre Planitia. These preliminary results show that this area has in some parts a low dielectric constant. This could be due to the presence of ice near the surface.

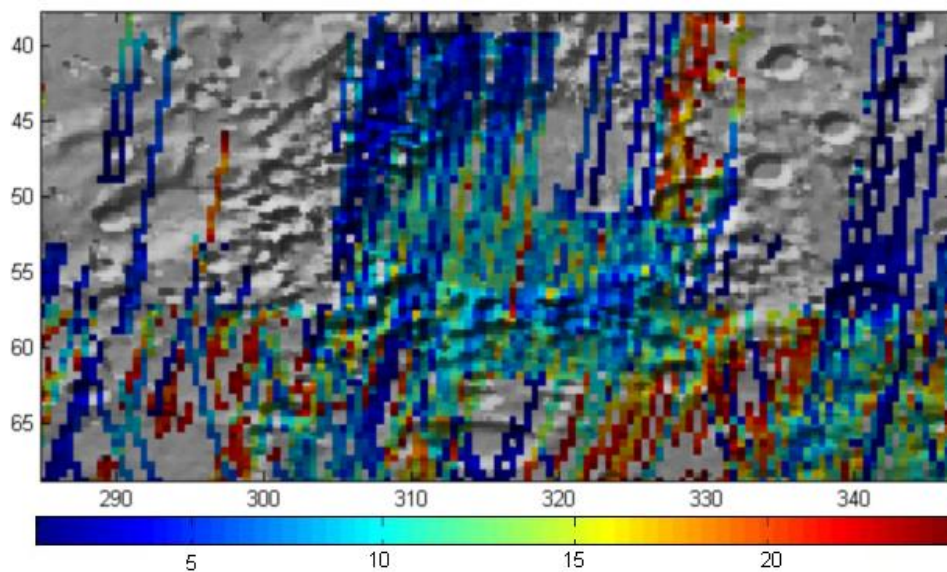


Figure IV-7 Map of the Dielectric constant of Argyre Planitia

IV.8 Conclusions related to the obtained maps

The description of the method to extract the dielectric constant of the surface of Mars from the echoes of the subsurface sounding radar SHARAD is made giving also a brief description SHARAD data signal and MOLA data peculiarity. The relative strength of the surface echo is equated to the reflectivity, and the effects of surface roughness are modeled using the MOLA topographic dataset. The resulting information provides insight on the nature of the materials constituting the Martian surface. In particular, low values of surface permittivity indicate either a very loose, porous regolith or an ice-rich terrain, whereas high values are characteristic of solid rock. The last part of this work focuses on the area of Argyre Planitia. The area is a large impact basin centered at 320°E, 50°S whose rim is very rugged and ancient. It has been found that the southern half of the rim has a high dielectric constant, as expected, while the northern half, which is extremely similar from the geologic point of view, exhibits a much lower permittivity. This fact points to the possibility that the northern part of Argyre

Planitia contains large quantities of ice in the ground, perhaps a relic of a past ice age such as the lobate debris aprons found elsewhere at similar latitudes on Mars [106].

CHAPTER V: SYNOPSIS AND OUTLOOK

The present PhD thesis is focused on the elaboration and interpretation of SHARAD data, the radar sounder currently in orbit around Mars. This instrument has greatly contributed to explore Mars surface and sub-surface also in view of future human exploration of the planet. The research work done deals with the estimation of dielectric parameters of the soil and subsoil and with the detection and interpretation of subsurface morphologies in order to understand the formation of the Martian landscape.

The work has been developed in two subsequence steps. First, a detailed study has been conducted over a specific geological area of Mars, the Cerberus Palus, with the aim of estimating the dielectric characteristic of the strong subsurface layer present in the zone. Secondly, the analysis has been extended to the whole Mars surface, by exploiting the full coverage of SHARAD data and by modelling the relationship between surface scattering and signal power received by the instrument.

V.1 Technological approach

Synthetic Aperture Sounding is an important advancement over conventional sounder, and it can be used to directly resolve the stratigraphy of the subsurface and to determine the composition of the first meters of the surface. Radar echoes can be analysed to retrieve the dielectric properties of the layers producing surface and subsurface reflections, to constraint or even identify their composition. The signal inversion of subsurface-sounding radar data is an inverse

problem for which different approaches have been presented over the years [39], [65], [92], [96]

V.2 Cerberus Palus

After the introduction and the description of radar data used in this study, Chapter 3 describes the use of SHARAD data to determine the composition of the subsurface. The first analysis has been done on an area known as Cerberus Palus, located between 144.5°E and 152.5°E, and between 1°N and 8.9°. Over this area the Mars Express High Resolution Stereo Camera acquired images of platy-ridged terrains that were interpreted as evidence for a frozen sea close to Mars' equator [65]. Cerberus Palus is a deeply studied region of Mars for its interesting geological features and for the presence of sub-surface layers. Radargrams provided by the SHARAD radar sounder clearly show the presence of subsurface layers in the area. SHARAD is the subsurface sounding radar provided by the Italian Space Agency (ASI) as a facility instrument on NASA's Mars Reconnaissance Orbiter (MRO) mission [107]. The science objective of SHARAD is to map, in selected regions, dielectric interfaces to depths of up to one kilometre in the Martian subsurface and to interpret these interfaces in terms of the occurrence and distribution of materials such as rock, regolith, and ice or water [108]. The area, being essentially flat and surrounded by simple geological structures, is well suited for a sub-surface investigation by using data provided by low-frequency radars like SHARAD [65], [67]. SHARAD transmits a low-frequency radar pulse capable of penetrating the Martian surface with a vertical resolution of 15 m in vacuum, thanks to its central frequency of 20 MHz and transmitted bandwidth of 10 MHz. SHARAD data consist of radar echoes continuously acquired along the ground track of the spacecraft during observations. Rough surfaces scatter the incident radar pulse in all directions, and echoes reflected towards the radar are thus weak. Flat surfaces and subsurface interfaces produce

the strongest echoes. The radar signal propagating in the subsurface is attenuated due to dielectric losses, and subsurface echoes are thus generally much weaker than surface echoes [77]. The Fractal approach has been used to model the roughness and the geometry of the observed scene [44]. The analysis of the radar data in order to make the inversion of subsurface sounding radar data is an inverse problem for which different approaches have been presented over the years [70], [71]. By exploiting the great amount of available SHARAD data, it has been possible to perform an accurate quantitative analysis aimed at estimating electromagnetic properties of surface and subsurface layers, in terms of permittivity and attenuation. To this aim, the electromagnetic approach must take into account effects of scattering due to surface roughness, for avoiding overestimated results. All data products used have been downloaded from PDS node (<http://pds-geosciences.wustl.edu/missions/mro/sharad.html>). Analysed radargrams have been produced by using the official focused processor [77] provided by the Italian Space Agency (ASI). This has been done by using theory of electromagnetic scattering from fractal surfaces and by estimating needed parameters from topographic data provided by MOLA. Three distinct geologic formations have been analysed, namely a part of Zephyria Planum, the Cerberus plains and the bedrock beneath the plains. The retrieved electromagnetic parameters have been interpreted as a mixture of volcanic rocks with either ice or air [108]. The Zephyria Planum material was found to be significantly porous [50-60%] with attenuation more likely compatible with empty pores. Ambiguous results were obtained for the plains material, being the resulting porosity high in both the cases of empty [40-50%] and of ice-filled [80%] pores [108]. The obtained results do not allow giving evidence of a frozen sea in the Cerberus Palus area.

V.3 Mars Mapping procedure

Chapter 4 is focused on the study of radar signal backscattered from the Mars surface. This signal is highly dependent on physical parameters (permittivity and roughness) characterizing the near surface (0-10 m deep) and we can therefore potentially learn about its composition. A robust automatic method to extract the power of the surface backscattered echo from SHARAD radargrams has been used to build and present maps of overall reflectivity [109]. A calibration procedure has been devised in order to derive a relationship between the geophysical parameters, dielectric constant, and a set of radar backscatter measurements. The model to extract the dielectric constant of the surface of Mars from the echoes of the radar takes into account the signal distortion source. The relative strength of the surface echo is equated to the reflectivity, and the effects of surface roughness are modelled using the MOLA topographic dataset. The resulting information provides insight on the nature of the materials constituting the Martian surface. The results are the production of dielectric constant maps of the Martian surface. In particular, low values of surface permittivity indicate either a very loose, porous regolith or an ice-rich terrain, whereas high values are characteristic of solid rock. In the end the analysis of a restricted area has been made. Argyre Planitia is a large impact basin centred at 320°E, 50°S whose rim is very rugged and ancient. It has been found that the southern half of the rim has a high dielectric constant, as expected, while the northern half, which is extremely similar from the geologic point of view, exhibits a much lower permittivity [110]. This fact points to the possibility that the northern part of Argyre Planitia contains large quantities of ice in the ground, perhaps a relic of a past ice age such as the lobate debris aprons found elsewhere at similar latitudes on Mars [106]

V.4 Future works

The developed analysis method can be further improved in the next future:

- it can be applied to different areas of interest, to understand the composition of both surface and subsurface (for example, Valles Marineris, the giant valley system that stretches along the Martian equator, was entirely glaciated during Late Noachian to Early Hesperian times and still contains huge volumes of fossil ice[111]);
- it can exploit the most accurate High Resolution Stereo Camera (HRSC) images the entire planet in full color, 3D and with a resolution of about 10 meters, it is on board of Mars Express Orbiter [112] which has 50 m of space resolution while the MOLA resolution is of $1/128^\circ$ about 500 m [73]
- it can be optimized by using more accurate DEM resolution
- it can be applied to future SAR sounder mission for planetary exploration;

V.5 Short form biography

Luigi Castaldo October 2013

PERSONAL DATA

First Name: Luigi

Last Name: Castaldo

Date of Birth: January.25.1976

Place of Birth: Napoli

Nationality: Italian

Address: via A de Gasperi 73, 80021 Afragola(Na) Italy

Phone: (+39) 339 4975011

Phone: (+48) 690 130815

E-mail: luigi.castaldo@gmail.com

E-mail: luigi.castaldo2@unina2.it

Present Position: Researcher

CO.RI.S.T.A

Viale Kennedy

80125 Naples

Italy

TRAINING

Education

XVI cycle of the PhD in Electronic Engineering from 2010 at the
Seconda Università degli studi di Napoli Aversa (Ce)

Master Graduate Electronic Engineering in 2005 at the Seconda
Università degli studi di Napoli Aversa (Ce)

Master Thesis: 'Development of an interferometric SAR simulator'

Courses and events

- 2005 operational and installation for corner reflector and transponder ,
held at DLR
- 2011 " Electro - Optical Sensing Applications in Aerospace Systems " held
by Tim Howard , Technical Chair AIAAConference edition of 2012 , at the
Faculty of Engineering of Federico II , Naples
- 08/06/2011 to 01/07/2011, Inglese scientific and academic course,
doctor. Nicola Borrelli
- 12/04/2011 , SHARAD Joint Science and MARSIS team meeting
- 27/04/2011, Seminar: Correlations and probability maps for seismic
occurrence , Prof. Lucilla de Arcangelis
- 25/05/2011,HIGH PERFORMANCE computing , Marco Briscolini , Senior
Consultant , Deep Computing , IBM Italy , Piero Sguazzero
- 04/05/201, Embedding Capacity of Information Flows Prof. Stefano

Marano, Department of Electrical Engineering and Information Engineering (DIEII), University of Salerno

- 11/05/2011, BEHAVIOR -BASED ROBOTICS AND attentional mechanisms , Prof. Ernesto Puppets, Department of Physical Sciences , PRISCA Lab, University of Naples Federico II
- 27/05/2011, Some connections between Electromagnetism and Theory of Information, prof. Mark Donald Best
- 07/06/2011, Micron Technology, Italy and the educational program, Campus @ microns , 2011, Dr. V. Martial and Eng. M. Lucianelli
- 08/06/2011, Robot Interaction Control Using Force and Vision, Prof. Bruno Siciliano PRISMA Lab, Department of Computer Science and Systems Engineering University of Naples Federico II
- 05/06/2011, Applying SCRUM: Practices and Challenges Eng.Stefania Marinelli, Intecs Rome
- 15/06/2011, Controlled Thermonuclear Fusion and High Performance Computing, Sergio Briguglio, Gregorio Vlad, CR Frascati ENEA
- 20/06/2011, The SAP system: main features and design experiences - Systems Planning & Reporting : Platform Enterprise Performance - Management, features and design experiences , Stefania Bonifacio , Project Manager , Accenture Italy, Marco Passera, Senior Manager, Accenture Italy
- 27-28/06/2011, GSA 2011(Days Scientific University 2011)
- 01/07/2011, Electromagnetism : the point of view of " ELECTRONIC " , Mr. Antonio Manna , Satellite Dept. Elettronica SpA
- 09/07/2011, The University: A Finmeccanica's strategic partner in the field of applied research. Lorenzo Flowers Technical Director (CTO) Finmeccanica, Attilio Di Giovanni and Ennio Giaccari Technical Direction Finmeccanica.

- 09/11/2011, Alternative Energy : Global Perspectives Prof. Mark Halpin \ Presentation activities doctorate
- • 01/02/2012, Frustration, frailty, aging , from materials science to engineering information , Dr. Mauro Sellitto
- 15/02/2012, New Perspectives Green ICT sector : Towards Energy -Aware model for economic and environmental sustainability , Dr. Francesco Palmieri
- • 29/02/2012, Seminar HIGH PERFORMANCE COMPUTING , Mr. Nino Guranacci
- 18/04/2012, Seminar: Smart Meter to Smart Grid , Dr. Daniel Gallo ;
- 18/04/2012, Seminar :HIGH PERFORMANCE COMPUTING , Mr. Marco Briscolini
- 18/04/2012, Seminar :The five imperatives of the ' Application Lifecycle Management according to IBM , Mr. Marco Balazarotti
- 20/04/2012, Seminar: What Every Engineer Should Know about Electrical Nonlinear Circuits and Systems, Dr. Michael Peter Kennedy
- 21/04/2012 - 27/04/2012, Conference and courses EGU2012 Wien
- 09/05/2012 Seminar on Alternative Energy : Global Perspectives Prof. Mark Halpin
- 16/05/2012 Seminar: Dr. Briguglio and Vlad ENEA
- 23/05/2012 Seminar: Eng. Luigi Grassia
- 28/05/2012 Seminar (DDrr. Russian Paolucci and Oracle)
- 28/05/2012 Seminar HIGH PERFORMANCE COMPUTING (Prof. Xhafa Polytechnic University of Barcelona) killing Oracle)
- 29/05/2012 Seminar Prof. Barolli FIT Japan
- 06/06/2012 Seminar Services to Agents for Negotiation and Resource Management Cloud- Dr. S. twenty-five
- 14/06/2012 Seminar High Performance Computing with GPU:

Performance , Libraries , Applications

- 20/06/2012 Seminar Eng. Emanuele Martelli
- 10/07/2012 Conference: Scientific University days 2012

Curses and Seminars abroad

- Professor Hermann Rohling Technical University
Hamburg-Harburg "Automotive Radars" 2013.January 15-20., Warszawa
Polytechnic
- Course: Professor Paulo Marques Instituto Superior de Engenharia de
Lisboa "SAR imaging radars" 2013.March.20-28, Warszawa Polytechnic

Languages

- Excellent knowledge of the English Languages, excellent capability to
read and communicate due to courses and living abroad for over 4
years.
- Knowledge of the Polish language, level M4
- Basic knowledge of German.

RESEARCH EXPERIENCE

1. Research scientist at DLR (German Aerospace Center) in Monaco of
Bavaria , Germany, Pol-InSAR Team, Microwaves and Radar Institute,
Title of research project : **Development of an Interferometric Sar
Simulator, from 2005 to 2006**

Web page: http://www.dlr.de/hr/desktopdefault.aspx/tabid-2312/3439_read-5200/

2. Participating Scientist of SHARAD Science Team and Research scientist at Co.Ri.Sta, viale Kennedy, Napoli; from September 2009 to present
Web page: <http://www.corista.unina.it/>

Main research activities

- Surface and Subsurface Modeling of backscattering
- Modeling of Calibration data SHARAD
- Writing and evaluation of documents
- Design development and implementation in Matlab of tools for scientific data analysis
- Development of algorithms for SAR Processing and Post Processing
- Sar and InSAR Imaging
- Development of models for Range Filtering
- Development of Polarimetric Sar Interferometric and analysis tools
- Development of Phase Unwrapping Algorithms
- Development of tools for the removal of the Flat Earth
- Study of models for estimating forest biomass

ADDITIONAL KNOWLEDGE

- Radar signal and image processing, SAR and InSAR, modeling and testing data
- MATLAB, PDL2 for Robot, C
- Corner Reflector & Transponder installation

AREAS OF INTEREST

Electromagnetic wave propagation and scattering, Inversion techniques and modeling, Radar, SAR, SAR interferometry, RAR Sounders, SAR Sounders, Mathematical modeling of different aspect of electromagnetic fields paying particular attention to the radar.

WORK OBJECTIVES

Development of simulation models for analyzing the performance of the radar, analysis and development of mathematical models to understand the composition of the materials in a scenario. Development of new mathematical methods to model scenario as much as can be near the reality.

RECENT SCIENTIFIC PROJECT

Analysis of data from the instrument SHARAD, Shallow Radar, the radar mounted on board the Italian mission, MRO (Mars Reconnaissance Orbiter) NASA, with particular reference to implementation of algorithms for discernment of the scientific data. These studies have recently led to a modeling of the Martian surface in some areas of considerable interest to physical and abiotic characteristics.

Research project on the calibration of radar data to be transparent to the scientist, software development to collect data and process: The scientist will be able to extract geophysical parameters from backscattering measurements using multitemporal observations over large areas.

Collaborative filter modeling to decrease the speckle in SAR images.

Webpages: http://www.corista.unina.it/Docs/towards_a_calibrationi.pdf

http://www.corista.unina.it/Docs/the_frozen_sea.pdf

V.6 Publications

ARTICLES SUBMITTED

- Castaldo L., G. Alberti, R. Orosei, G. Cirillo, **Calibration of Martian SHARAD Data**

ARTICLES IN JOURNALS WITH REFEREES

- Alberti G., L. Castaldo, R. Orosei, A. Frigeri, and G. Cirillo (2012), **Permittivity estimation over Mars by using SHARAD data: the Cerberus Palus area**, J. Geophys. Res., doi:10.1029/2012JE004047
ISSN 0148-0227

CONTRIBUTIONS TO CONFERENCES WITH REFEREES

- Castaldo L., G. Alberti, G. Cirillo, R. Orosei, **Scientific Calibration of SHARAD Data over Martian Surface**, SIGNAL PROCESSING SYMPOSIUM - 4-7 June 2013, Jachranka Village, Poland, 978-1-4673-6319-8/13/S31.00 c 2013 IEEE /ISBN COPYRIGHT REG. NO. ISBN 978-1-4673-6318-1
- Gromek A., L. Castaldo, **Collaborative filtering technique for SAR image speckle noise suppression**, SIGNAL PROCESSING SYMPOSIUM - 4-7 June 2013, Jachranka Village, Poland, 978-1-4673-6319-8/13/S31.00 c 2013 IEEE/ISBN COPYRIGHT REG. NO. ISBN 978-1-4673-6318-1
- L. Castaldo et al, **Calibration over North Polar Caps of SHARAD data**, 2012 Geophysical Research Abstracts, Egu Wien 22 - 28 April 2012,

Vol. 14, EGU2012-10155, EGU General Assembly 2012 ISSN 1607-7962

- Orosei R., G. Alberti, L. Castaldo, **Radar Subsurface Sounding over the Putative Frozen Sea in Cerberus Palus Mars**, European Planetary Science Congress 2010, EPSC Abstracts Vol. 5, **EPSC2010-723**, 2010

CONTRIBUTIONS TO CONFERENCES

- Castaldo L., G. Alberti, R. Seu, **SHARAD Data inversion over Ceberus Palus**, Joint MARSIS and SHARAD Science Team Meeting; 2011 April 11-13, Rome
- webpage: <http://www.corista.unina.it/news.html>
- Castaldo L., L. Zeni, G. Alberti, **Inversione Dati SHARAD in Cerberus Palus area**, GSA meeting, **Seconda Università degli Studi di Napoli SUN, 2011 June 27-28, Capua**
- *Alberti G., L. Castaldo, G. Cirillo, R. Seu, R. Orosei, **The Frozen sea area: a reference case of study for inversion problem**, Joint MARSIS-SHARAD Science Team Meeting, 2010 September 8-10, Pasadena, CA, USA*
- webpage: <http://www.corista.unina.it/docse.html>
- *Alberti G., L. Castaldo, G. Cirillo, R. Seu, R. Orosei, **Estimation of Mars surface dielectric constants by means of SHARAD data**, Joint MARSIS-SHARAD Science Team Meeting, 2010 April 28-30, Naples, Italy*
- webpage: <http://www.corista.unina.it/docse.html>
- *Alberti G., L. Castaldo, G. Cirillo, R. Seu, R. Orosei, **Sub-surface dielectric constants estimation on Medusae Fossae formation by means of SHARAD data**, Joint MARSIS-SHARAD Science Team*

Meeting, 2010 April 28-30, Naples, Italy

- webpage: http://www.corista.unina.it/att_SHARAD_mro.html

BIBLIOGRAPHY

- [1] Coradini, A., R. Orosei, The exploration of Mars: past and future, Mem. S.A.It. Vol. 82, 321,SAIt 2011 Memories of the Italian Astronomical Society.
- [2] Sagan, C., 1980, London: Macdonald Futura, Publishers, and New York: Random House and Wings Books
- [3] G. von Dardel, et al., STATUS REPORT ON THE LUND VIDICON SYSTEM, August 1965, IEEE TRANSACTIONS ON NUCLEAR SCIENCE,II. 4.
- [4] Wilhelms, D. E., and Squyres, S. W. 1984, Nature, 309, 138
- [5] Frey, H., and Schultz, R. A. 1988, Geophys. Res. Lett., 15, 229
- [6] Smith, D. E., et al. 1999, Science, 284, 1495
- [7] David E. Smith; Maria T. Zuber; Herbert V. Frey; James B. Garvin; James W. Head; Duane O. Journal of Geophysical Research: Planets (1991–2012). Volume 106, Issue E10, pages 23689–23722, 25 October 2001.
- [8] Withers, P., and Neumann, G. A. 2001, Nature,410, 651
- [9] Golombek, M. P. 2005, GSA Abstracts with Programs, 37, 312
- [10] Lucchitta, B. K. 1979, J. Geophys. Res., 84, 8097
- [11] Lucchitta, B. K., McEwen, A. S., Clow, G. D., Geissler, P. E., Singer, R. B., Schultz, R. A., & Squyres, S. W. 1992, Mars, 453
- [12] Hartmann, W. K., and Neukum, G. 2001, Space Science Systems. Rev., 96, 165

- [13] Mellon, M. T., Feldman, W. C., & Prettyman, T. H. 2004, *Icarus*, 169, 324
- [14] Pelletier J.D.,2004, *Geology* 32, 365–367 & 384
- [15] Carr, M. H. 1996, New York: Oxford, University Press
- [16] Owen, T. 1992, *Mars*, 818
- [17] Malin, M. C. & Edgett, K. S. 2000, *Science*, 288, 2330
- [18] Acuna, M. H. et al. 1998, *Science*, 279, 1676
- [19] Malin, M. C. and Edgett, K. S. 2003, *Science*, 302, 1931
- [20] Boynton, W. V. et al. 2002, *Science*, 297, 81
- [21] Bibring, J. P., et al. 2004, *Nature*, 428, 627
- [22] Plaut, J. J. et al. 2007, *Science*, 316, 92
- [23] Formisano, V., Atreya, S., Encrenaz, T.,Ignatiev, N., Giuranna, M. 2004, *Science*,306, 1758
- [24] Stern, W., 1929, Versuch einer elektrodynami, schen Dickenmessung von Gletschereis: *Ger. Beitr. zur Geophysik*, v.23, p. 292-333.
- [25] Stern, W., 1930, Uber Grundlagen,Methodik und bisherige Ergebnisse, elektrodynamischer Dickenmessung von Gletsc hereis: *Z. Gletscherkunde*, v.15, p. 24-42.
- [26] Olhoeft, G.R.,1996, Application of Ground Penetrating Radar: in Proceedings of the 6th Int'l. Conf. on Ground Penetrating Radar, GPR'96, Sept 30-Oct 3, 1996, Sendai, Japan, p.1-4.(invited keynote).
- [27] Porcello, L. J. et al. 1974, *Proceedings of the IEEE*, 62, 769
- [28] Picardi, G. et al. 2005, *Science*, 310, 1925

-
- [29] Seu, R., et al., 2007, SHARAD sounding radar on the Mars Reconnaissance Orbiter, J. Geophys. Res.,112, E05S05, doi:10.1029/2006JE002745.
- [30] Muhleman, D.O. (1995). Earth-based remote sensing of solar system objects. Reviews of Geophysics 33: doi: 10.1029/95RG00555. issn: 8755-1209.
- [31] Seu R., Phillips, R. J., Workshop on Radar Investigations 2005, SHARAD: RADAR SOUNDER ON THE 2005 MARS RECONNAISSANCE ORBITER.
- [32] Croci, R., F. Fois, D. Calabrese, E.M. Zampolini, R. Seu, G. Picardi, E. Flamini, Geoscience and Remote Sensing Symposium, 2007. IGARSS 2007. IEEE International; 08/2007
- [33] Seu, R., D. Biccari, R. Orosei, L.V. Lorenzoni, R.J. Phillips, L. Marinangeli, G. Picardi, A. Masdea, E. Zampolini, SHARAD: The MRO 2005 shallow radar, Planetary and Space Science. 01/2004
- [34] Alberti G., Salzillo G., " Raw signal simulator for SHARAD", 23rd EARSeL Symposium "Remote Sensing in Transition", 2-5 June 2003, Gent (Belgium), Proc. pp.299-305.
- [35] Moreira, J. R. (1992), "Bewegungsextraktionsverfahren für Radar mit synthetischer Apertur", PhD thesis TU München, DLR research report DLR-FB 92-31.
- [36] Olmsted, C. (1993), "Alaska SAR facility – scientific SAR user's guide", <http://www.asf.alaska.edu/>.
- [37] Reigber, A. (2002), "Airborne polarimetric SAR tomography", PhD thesis Univ. of Karlsruhe, DLR research report, 2002-02, ISSN 1434-8454.
-

- [38] Croci, R., Seu, R. Flamini, E. Russo, E., The SHALLOW RADAR (SHARAD) Onboard the NASA MRO Mission, Proceedings of the IEEE, May 2011, pages 794 - 807, ISSN: 0018-9219
- [39] Daniels, D.J. (1996), Surface Penetrating Radar. IEE Radar, Sonar, Navigation And Avionics, Series 6, pp. 165 - 182.
- [40] Ulaby F.T., M.G.Dobson, 1989, Radar Scattering Statistics for Terrain, Artech
- [41] Biccari, D, A. Masdea, G. Picardi ,R. Seu, SHARAD radar sounder for the Mars Reconnaissance Orbiter Mission, Geophysical Research Abstracts, Vol. 7, 08889, 2005, SRef-ID: 1607-7962/gra/EGU05-A-08889
- [42] Elachi, C., (1988), "Spaceborne radar remote sensing applications and techniques", New York: IEEE Press.
- [43] Curlander, J.C. and McDonough, R.N., (1991), 'Synthetic Aperture Radar'. John Wiley & Sons Inc.
- [44] Franceschetti, G., D. Riccio, Scattering, Natural Surfaces, and Fractals, ISBN: 978-0-12-265655-2, 2007 Elsevier Inc.
- [45] Evans, J.V., and Hagfors, T., 1964, On the interpretation of radar reflections from the Moon: Icarus, v. 3, p. 151-160.
- [46] Simpson, R.A., and G.L. Tyler, Radar scattering laws for the lunar surface, IEEE Trans. Ant. Prop., 30, 438-449, 1982.
- [47] Farina, A., F. Gini, M.V. Greco, P.H.Y. Lee, Improvement factor for real sea-clutter Doppler frequency spectra, IEE PPOC-R adar Sonar Navig Vol 141 No 5 October 1996
- [48] Picardi, G. & Sorge, S. (1999). Adaptive Compensation of Mars Ionosphere

Dispersion: A Low Computational Cost Solution for MARSIS, Infocom Technical

Report MRS-002/005/99, October 1999.

[49] Slavney S., R. Orosei, SHALLOW RADAR EXPERIMENT DATA RECORD SOFTWARE INTERFACE SPECIFICATION,2008 ,PDS Geosciences Node

[50] Hanson, W. B., S. Sanatani, and D.R. Zuccaro, The Martian ionosphere as observed by the Viking retarding potential analyzers, *J. Geophys. Res.*, 82, 4351, 1977.

[51] Safenili, A., W. Kofman, J.-F. Nouvel, A. Herique, and R. L. Jordan, "Impact of Mars ionosphere on orbital radar sounder operation and data processing," *Planetary and Space Science*, Vol. 51, No. 7, June 2003.

[52] Chapman, S., The absorption and dissociative or ionizing effect of monochromatic radiation of an atmosphere on a rotating Earth, 1931,*Proc.Phys. Soc.*, 43, 26–45

[53] Wahl, D. E., P. H. Eichel, D. C. Ghiglia, C. V. Jakowatz, "Phase Gradient Autofocus. A robust tool for high resolution SAR phase correction", *IEEE log.N°T-AES/30/3/16653*, April 1993

[54] Alberti, G., D. Biccari, S. Dinardo, S. Mattei, R. Orosei, C. Papa, R. Phillips, G. Picardi, A. Safaenili, R. Seu, Mars Ionosphere preliminary impact analysis on SHARAD radar signal, *Geophysical Research Abstracts*, Vol. 9, 08754, 2007 SRef-ID: 1607-7962/gra/EGU2007-A-08754

[55] Albee, A. L., Arvidson, R.E., Palluconi, F. and Thorpe, T. (2001). Overview of the Mars Global Surveyor mission. *Journal of Geophysical Research* 106: doi: 10.1029/2000JE001306. issn: 0148-0227.

- [56] Smith, D. E., W. L. Sjogren, G. L. Tyler, G. Balmino, F. G. Lemoine, and A. S. Konopliv, The gravity field of Mars: Results from Mars Global Surveyor, *Science*, 286, 94–96, 1999a.
- [57] Smith, D. E., M. T. Zuber, G. A. Neumann, and F. G. Lemoine, Topography of the Moon from the Clementine lidar, *J. Geophys. Res.*, 102, 1591–1611, 1997.
- [58] Smith D.E., et. al., Mars Orbiter Laser Altimeter: Experiment summary after the first year of global mapping of Mars, *JOURNAL OF GEOPHYSICAL RESEARCH*, VOL.106, NO. E10, PAGES23,689-23,722, OCTOBER 25, 2001
- [59] Smith, W., and Wessel, P. (1990). "Gridding with continuous curvature splines in tension." *GEOPHYSICS*, 55(3), 293–305. doi: 10.1190/1.1442837
- [60] Smith, D.E., et. al., The Global Topography of Mars and Implications for Surface Evolution, *SCIENCE* VOL 284 28 MAY 1999, pag 1495 – 1502
- [61] Mandelbrot, B. B., *The fractal geometry of nature*, Editor Freeman, San francisco 1983,
- [62] Brown, S. R., C.H. Scholz, Broad bandwidth study of the topography of natural rock surfaces, Article first published online: 20 SEP 2012, DOI: 10.1029/JB090iB14p12575
- [63] Franceschetti G., A. Iodice, M. Migliaccio, and D. Riccio, 1999, Scattering from natural rough surfaces modeled by fractional brownian motion two-dimensional processes, *IEEE Trans. Antennas Propag.*, vol. 47, no. 9, pp. 1405–1415.
- [64] Franceschetti, G., A. Iodice, D.Riccio, Scattering from Dielectric Random Fractal Surfaces via Method of Moments, *IEEE TRANSACTIONS ON GEOSCIENCE AND REMOTE SENSING*, VOL. 38, NO. 4, JULY 2000

-
- [65] Murray, J. B., J.-P. Muller, G. Neukum, S. C. Werner, S. van Gasselt, E. Hauber, W. J. Markiewicz, J. W. Head, B. H. Foing, D. Page, K. L. Mitchell, G. Portyankina, and the HRSC Co-Investigator Team, "Evidence from the Mars Express High Resolution Stereo Camera for a frozen sea close to Mars' equator," *Nature*, Vol. 434, pp. 352-356, 2005.
- [66] Williams, R. M., and M. C. Malin, "Evidence for late stage fluvial activity in Kasei Valles, Mars," *J. Geophys. Res.*, Vol. 109, CiteID E06001, 2004.
- [67] Hartmann, W. K., and D. C. Berman, "Elysium Planitia lava flows: Crater count chronology and geological implications," *J. Geophys. Res.*, Vol. 105, pp. 15011-15026, 2000.
- [68] Page, D. P. 2010. Resolving the Elysium Controversy: an open invitation to explain the evidence. *Planetary and Space Science* 58, 1406-1413.
- [69] Campbell, B.A., N.E.Putzig,SURFACE ROUGHNESS MAPS OF MARS BASED ON SHARAD ECHOES,42nd Lunar and Planetary Science Conference 2001
- [70] Picardi, G., and 19 colleagues (2007), MARSIS Data Inversion Approach. Proceedings of the 4th International Workshop on Advanced Ground Penetrating Radar, Proc. IEEE, 256.
- [71] Zhang, Z., Hagfors, T., Nielsen, E., Picardi, G., Masdea, A., Plaut, J.J. (2008), Dielectric properties of the Martian south polar layered deposits: MARSIS data inversion using Bayesian inference and genetic algorithm. *Journal of Geophysical Research (Planets)* 113, 5004.
- [72] Ulaby, F. T., Moore, R. K., Fung, A. K. (1986) *Microwave Remote Sensing: Active and Passive*, Vol. III - Volume Scattering and Emission Theory, Advanced
-

Systems and Applications. Artech House, Inc., Dedham, Massachusetts, 1100 pages.

[73] Kreslavsky, M.A., Head, J.W. (1999), Kilometer-scale slopes on Mars and their correlation with geologic units: initial results from Mars Orbiter Laser Altimeter (MOLA) data. *J. Geophys. Res.* 104, pp. 21911–21924.

[74] Orosei, R., Bianchi, A. Coradini, S. Espinasse, C. Federico, A. Ferriccioni, A. I. Gavrishin, (2003), Self-affine behavior of Martian topography at kilometer scale from Mars Orbital Laser Altimeter data, *J. Geophys. Res.* 108, Issue E4, pp. GDS 4-1, CiteID 8023, DOI 10.1029/2002JE001883.

[75] Feder, J. S. (1988), *Fractals*, Plenum, New York.

[76] Flandrin, P. (1989), On the spectrum of fractional brownian motions, *IEEE Trans. Inf. Theory*, vol. 35, no. 1, pp. 197–199.

[77] Alberti, G., S. Dinardo, S. Mattei, C. Papa, M.R. Santovito. 2007, SHARAD radar signal processing technique, 4th International Workshop on Advanced Ground Penetrating Radar, doi: 10.1109/AGPR.2007.386564

[78] Carter, L. M., Campbell, B. A., Holt, J. W., Phillips, R. J., Putzig, N. E., Mattei, S., Seu, R., Okubo, C. H., Egan, A. F. (2009) Dielectric properties of lava flows west of Asraeus Mons, Mars. *Geophysical Research Letters* 362, 23204.

[79] Rust, A. 1999. Dielectric constant as a predictor of porosity in dry volcanic rocks. *Journal of Volcanology and Geothermal Research* 91, 79-96.

[80] Watters, T. R., B. Campbell, L. Carter, C. J. Leuschen, J. J. Plaut, G. Picardi, R. Orosei, A. Safaeinili, S. M. Clifford, W. M. Farrell, A. B. Ivanov, R. J. Phillips and E. R. Stofan, Radar Sounding of the Medusae Fossae Formation Mars: Equatorial Ice or Dry, Low-Density Deposits?, *Science*, Nov. 2007, Vol. 318 no. 5853 pp. 1125-1128 DOI: 0.1126/science.1148112

[81] Mätzler C., Microwave properties of ice and snow, in Schmitt, B., et al. (eds.) "Solar System Ices", Astrophys. and Space Sci. Library, Vol. 227, Kluwer Academic Publishers, Dordrecht, pp. 241-257 (1998).

[82] Sihvola, A. (2000) Mixing Rules with Complex Dielectric Coefficients. Subsurface Sensing Technologies and Applications 1, 393-415.

[83] Boisson, J., and 10 colleagues (2009), Sounding the subsurface of Athabasca Valles using MARSIS radar data: Exploring the volcanic and fluvial hypotheses for the origin of the rafted plate terrain. Journal of Geophysical Research (Planets) 114, 8003.

[84] Mouginot, J., Pommerol, A., Beck, P., Kofman, W., Clifford, S. M. 2012. Dielectric map of the Martian northern hemisphere and the nature of plain filling materials. Geophysical Research Letters 39, 2202. Brown S. R. and C. H. Sholz (1985), Broad band study of the topography of natural rock surfaces, J. Geophys. Res., vol. 90, pp. 12575–12 582.

[85] Jaeger, W. L., and 10 colleagues 2010. Emplacement of the youngest flood lava on Mars: A short, turbulent story. Icarus 205, 230-243.

[86] Mueller, S., Scheu, B., Kueppers, U., Spieler, O., Richard, D., Dingwell, D. B. 2011. The porosity of pyroclasts as an indicator of volcanic explosivity. Journal of Volcanology and Geothermal Research 203, 168-174.

[87] Feldman, W.C., 12 colleagues, 2002. Global distribution of neutrons from Mars: results from Mars Odyssey. Science 297, 75-78.

[88] Seu, R., D. Biccari, R. Orosei, L.V. Lorenzoni, R.J. Phillips, L. Marinangeli, G. Picardi, A. Masdea, E. Zampolini, SHARAD: The MRO 2005 shallow radar,

Planetary and Space Science Volume 52, Issues 1–3, January–March 2004, Pages 157–166

[89] Currie, N. C., Ed., *Techniques of Radar Reflectivity Measurement*. Norwood, MA Artech House, 1984.

[90] Ulaby, F., Moore, T.R., Fung, A., 1986. *Microwave Remote Sensing*. Artech House Publishers

[91] Gray, L., P. W. Vachon, C. E. Livingstone, and T. I. Lukowski, “Synthetic aperture radar calibration using reference reflectors,” *IEEE Trans. Geosci. Remote Sensing*, vol. 31, pp 374-383, May 1990

[92] Smith, D.E., et al. (1999), The global topography of Mars and implications for surface evolution, *Science* 284, pp. 1495–1503.

[93] Seu, R. J. Phillips, D. Biccari, R. Orosei, A. Masdea, G. Picardi, A. Safaeinili, B. A. Campbell, J. J. Plaut, L. Marinangeli, S. E. Smrekar, D. C. Nunes, SHARAD sounding radar on the Mars Reconnaissance Orbiter, *JOURNAL OF GEOPHYSICAL RESEARCH*, VOL. 112, E05S05, doi:10.1029/2006JE002745, 2007

[94] Seu, R., D. Biccari, R. Orosei, L.V. Lorenzoni, R.J. Phillips, L. Marinangeli, G. Picardi, A. Masdea, E. Zampolini, SHARAD: The MRO 2005 shallow radar, *Planetary and Space Science* Volume 52, Issues 1–3, January–March 2004, Pages 157–166, *Exploring Mars Surface and its Earth Analogues*

[95] Nèmec, F., Morgan, D. D., Gurnett, D. A., Duru, F. 2010. Nightside ionosphere of Mars: Radar soundings by the Mars Express spacecraft. *Journal of Geophysical Research (Planets)* 115, E12009, doi:10.1029/2010JE003663.

[96] Franceschetti, G., D. Riccio, *Scattering, Natural Surfaces, and Fractals*, BURLINGTON (MA) ACADEMIC PRESS 2007

-
- [97] Smith, D.E., et al (2001)., Mars Orbiter Laser Altimeter (MOLA): Experiment Summary after the First Year of Global Mapping of Mars, *Journal of Geophysical Research* Volume 106, Issue E10, pages 23689–23722, 25 October 2001, DOI: 10.1029/2000JE001364
- [98] Slavney S., R. Orosei, SHALLOW RADAR REDUCED DATA RECORD SOFTWARE INTERFACE SPECIFICATION, 2008, PDS Geosciences Node
- [99] Alberti, G., S. Dinardo, S. Mattei, C. Papa, M.R. Santovito, SHARAD radar signal processing technique, unpublished. (2009)
- [100] Albee, A.L., Arvidson, R.E., Palluconi, F. and Thorpe, T. 2001. Overview of the Mars Global Surveyor mission. *Journal of Geophysical Research* 106: doi: 10.1029/2000JE001306. issn: 0148-0227.
- [101] Aharonson, O., Zuber, MT and Rothman, DH (2001). 'Statistics of Mars' topography from the Mars Orbiter Laser Altimeter: Slopes, correlations, and physical Models'. *Journal of Geophysical Research-Planets*, 106 (E10) :23723-23735.
- [102] Phillips, R.~J., and 17 colleagues 2011. Massive CO₂ Ice Deposits Sequestered in the South Polar Layered Deposits of Mars. *Science* 332, 838.
- [103] Grima, C., W. Kofman, J. Mouginot, R. J. Phillips, A. Hérique, D. Biccari, R. Seu, and M. Cutigni (2009), North polar deposits of Mars: Extreme purity of the water ice, *Geophysical Research Letters*, 36(3), 2-5, doi:10.1029/2008GL036326
- [104] Orosei., R., Bianchi, A. Coradini, S. Espinasse, C. Federico, A. Ferriccioni, A. I. Gavrishin, (2003), Self-affine behavior of Martian topography at kilometer scale from Mars Orbital Laser Altimeter data, *J. Geophys. Res.* 108, Issue E4, pp. GDS 4-1, CiteID 8023, DOI 10.1029/2002JE001883.
-

- [105] Franceschetti, G, A. Iodice, D. Riccio, G. Ruello, Fractal Surfaces and Electromagnetic Extended Boundary Conditions, IEEE TRANSACTIONS ON GEOSCIENCE AND REMOTE SENSING, VOL. 40, NO. 5, MAY 2002
- [106] Holt, J. W., Safaeinili, A., Plaut, J. J., Head, J. W., Phillips, R. J., Seu, R., Kempf, S. D., Choudhary, P., Young, D. A., Putzig, N. E., Biccari, D., Gim, Y. (2008), Radar Sounding Evidence for Buried Glaciers in the Southern Mid-Latitudes of Mars. *Science* 322, 1235.
- [107] Orosei R., G. Alberti, L. Castaldo, Radar Subsurface Sounding over the Putative Frozen Sea in Cerberus Palus Mars, European Planetary Science Congress 2010, EPSC Abstracts Vol. 5, EPSC2010-723, 2010
- [108] Alberti G., L. Castaldo, R. Orosei, A. Frigeri, and G. Cirillo (2012), Permittivity estimation over Mars by using SHARAD data: the Cerberus Palus area, *J. Geophys. Res.*, doi:10.1029/2012JE004047 ISSN 0148-0227
- [109] Castaldo L., G. Alberti, G. Cirillo, R. Orosei, Calibration over North Polar Caps of SHARAD data, 2012 Geophysical Research Abstracts, Egu Wien 22 - 28 April 2012, Vol. 14, EGU2012-10155, EGU General Assembly 2012 ISSN 1607-7962
- [110] Castaldo L., G. Alberti, G. Cirillo, R. Orosei, Scientific Calibration of SHARAD Data over Martian Surface , SIGNAL PROCESSING SYMPOSIUM - 4-7 June 2013, Jachranka Village, Poland, 978-1-4673-6319-8/13/S31.00 c 2013 IEEE /ISBN COPYRIGHT REG. NO. ISBN 978-1-4673-6318-1
- [111] Gourronc, Marine, Bourgeois, Olivier, Mège, Daniel, Pochat, Stéphane, Bultel, Benjamin, Massé, Marion, Le Deit, Laetitia, Le Mouélic, Stéphane, Mercier, Denis, One million cubic kilometers of fossil ice in Valles Marineris: relicts of a 3.5 Gy old glacial landsystem along the Martian equator, *Geomorphology* (2013), doi:10.1016/j.geomorph.2013.08.009.

- [112] Jaumann, R., G. Neukum, T. Behnke, T.C. Duxbury, K. Eichentopf, J. Flohrer, The high-resolution stereo camera (HRSC) experiment on Mars Express: Instrument aspects and experiment conduct from interplanetary cruise through the nominal mission, *Planetary and Space Science* 55 (2007) 928–952